

**Theory of quantum transport in
nano scale structures**

Bader Alharbi

Ph.D. Thesis in Physics

Department of Physics, Lancaster University, UK



**This thesis is submitted for the degree of Doctor of
Philosophy 2023**

Declaration

I confirm that the content presented in this dissertation represents the author's authentic and self-directed efforts during the period from January 2020 to August 2023 at the Department of Physics, Lancaster University, UK, under the supervisor of Professor Colin J. Lambert and Songjun Houe with the support of Prince Sattam Bin Abdulaziz University, KSA. Furthermore, I assert that this thesis has not been previously submitted, either partially or in its entirety, for the acquisition of any higher degree in any other academic institution. All information derived from existing literature has been appropriately credited within the text, and a comprehensive list of references has been provided.

Bader Alharbi

August 2023

Dedication

I dedicate this work to my beloved parents,

Ali Alharbi and Modhi Alharbi

whose love, unwavering support, encouragement, and sacrifices have been the driving force behind my journey.

Acknowledgement

First and foremost, I extend my heartfelt gratitude to ALLAH for His boundless mercy and blessings.

Next, I wish to express my sincere acknowledgment and deepest appreciation to my supervisor, Professor Colin J. Lambert. His exceptional guidance and unwavering dedication have been invaluable throughout my journey in molecular electronics. The time and effort he devoted to providing excellent supervision and conducting tutorials to share his vast knowledge in this field are truly commendable. I am truly grateful for his kindness and patience in addressing any questions I had, and I feel privileged to be part of his research group, benefiting from his extensive experience, which continues to inspire and motivate me.

Additionally, I wish to extend my gratitude to my Deputy Supervisor, Dr. Songjun Hou, whose generous assistance played a crucial role in the completion of this thesis. His exceptional guidance, patience, and constructive discussions have been invaluable. The feedback he provided was instrumental in refining my work. The tutorials he conducted enabled me to gain a profound understanding of SIESTA and GOLLUM, which will undoubtedly prove beneficial for my future studies and research. I would also like to express my appreciation to all my friends and colleagues in Colin's group for their unwavering cooperation and support throughout this journey. Their assistance has been invaluable in making this thesis possible.

I express my heartfelt gratitude to my sponsor, the Saudi Ministry of Higher Education, the Saudi Cultural Mission in London, and Prince Sattam Bin Abdulaziz University in Saudi Arabia, for providing me with the invaluable opportunity to pursue a Ph.D. program in the United Kingdom. Their support has been instrumental in making my academic journey possible.

Lastly, I wish to extend my heartfelt appreciation and gratitude to my father, mother, brothers, and sisters, as well as to my beloved family: my wife Shaykhah, my daughter Ward, and my son Ziyad. Words cannot adequately express how thankful I am for all that you have done for me. Your unwavering support, patience, and understanding have been the pillars that have enabled me to reach this stage in my journey. I am deeply grateful for your love and encouragement.

Abstract

In the pursuit of future nano-scale applications within the field of molecular electronics, extensive investigations into electron transport through single molecules hold significant importance. As single or multiple molecules serve as crucial building blocks for designing and constructing molecular electronic devices, comprehending their electronic and transport properties becomes imperative. Countless theoretical and experimental studies have been conducted to create molecular junctions and explore their electrical performance. This thesis focuses on fundamental aspects of transport theory, employing theoretical and mathematical approaches to investigate electron transport through junctions, particularly involving a scattering region formed by a single molecule connected to metal electrodes. The research methods used are based on a combination of density functional theory, implemented within the SIESTA code, and non-equilibrium Green's function, realized using the GOLLUM code, to delve into electrical conductance on a molecular scale.

The objective of this chapter is to address a puzzling paradox concerning meta connectivity, which exhibits destructive quantum interference (DQI) in a tight binding model. However, in certain instances, DQI does not manifest in a DFT calculation on the same system. To shed light on this inconsistency, a selection of molecules is examined, focusing on the distinction between meta and para connectivity. Two different types of linkers, thiol (-SH) and methyl sulphide (-SMe), are employed to couple different molecules to Au electrodes. Through this investigation, we aim to gain

insights into the underlying factors that lead to the observed quantum interference behaviors.

In project two, we conducted a comprehensive study, combining experimental and theoretical approaches, to explore charge transport in stacked graphene-like dimers. Our findings revealed that the interaction between room-temperature quantum interference and stacking significantly influences their highly non-classical electrical conductance. Notably, for the molecule CQI-L, the electrical conductance of the dimer exceeds that of the monomer by a remarkable factor of 25, attributed to the most energetically favorable stacking interactions. Conversely, for the molecule CQI-H, the dimer's conductance is approximately 40 times lower than that of the monomer. These results unequivocally demonstrate that precise control of connectivity to molecular cores, coupled with stacking interactions between their systems, provides a versatile avenue for modifying and optimizing charge transfer between molecules. This discovery is expected to inspire further vigorous research at both macroscopic and microscopic levels.

Contents

1. The fundamentals of molecular-scale electronics	13
1.1. Molecular electronics	13
1.2. Molecular Junctions	16
1.3. Quantum interference	18
1.4. Tight-binding model	19
1.5. Molecular junctions with graphene electrodes	19
1.6. Conclusion	20
1.7. Thesis outline	20
Bibliography:	22
2. Density Functional Theory	29
2.1. Introduction	29
2.2. The Schrödinger Equation	30
2.3. Born-Oppenheimer approximation:	31
2.4. Hohenberg-Kohn theorem approximation:	32
2.5. The Kohn-Sham Approach	33
2.5.1. Exchange and correlation functional	36
2.5.1.1. Local Density Approximation (LDA)	37
2.5.1.2. Generalized Gradient Approximation (GGA)	37
2.6. SIESTA	38
2.6.1. The Pseudopotential Approximation	39
2.6.2. Calculating binding energies using the counterpoise method (CP)	40
2.7. Calculations in Practice	43
2.8. Conclusion	47

Bibliography:	48
3. Transport theory	51
3.1. Introduction:	51
3.2. The Landauer formula	52
3.3. Scattering matrix	57
3.4. Green's Function	63
3.4.1. Green's function of a doubly infinite chain	64
3.4.2. Green's function of a semi-infinite one-dimensional chain	67
3.4.3. One-dimensional scattering region	69
3.5. Conclusion	73
Bibliography:	74
4. Quantum interference in polycyclic aromatic molecules.	77
4.1. Introduction	77
4.2. Quantum interference	78
4.3. Tight binding calculation	79
4.4. DFT calculation	83
4.5. Theory of room-temperature QI effects	87
4.6. Frontier molecular orbitals and green's function	91
4.7. Transmission coefficient	92
4.7.1 Transmission coefficient for the benzene core with different linkers connected to gold electrodes	93
4.7.2 Transmission coefficient for the benzene core with an increasing number of central rings	98
4.7.3 Transmission coefficient for the benzene core with oligoynes linkers of different lengths	103
4.7.4 Transmission coefficient for the benzene core with increasing number of central rings connected to gold via SMe- anchor	104
4.8. Conclusion	109

Bibliography	110
5. Quantum Interference-controlled conductance enhancement in stacked graphene-like dimers	113
5.1. Introduction	113
5.2. Studied molecules	115
5.3. Finding and discussing	116
5.4. Transmission function calculations of the molecule CQI-L based on AB2 stacking	123
5.5. Transmission function calculations of the molecule CQI-H based on AB2 stacking	128
5.6. Comparison of DFT results with experimental results for molecule CQI-L	130
5.7. Comparison of DFT results with experimental results for molecule CQI-H	133
5.8. Transmission function calculations oh the molecule CQI-L connecting to the electrode on both side	135
5.9. Conclusion	136
Bibliography	137
6. Conclusions and Future works	142
6.1. Conclusions	142
6.2. Future works	143
Bibliography	146

List of abbreviations

ICs	Integrated Circuits
CMOS	Complementary Metal-Oxide Semiconductor
SAMs	Self-Assembled Monolayers
MCBJ	Mechanically Controllable Break Junctions
STM	Scanning Tunnelling Microscopy
EBJ	Electromigration Break Junctions
DFT	Density Functional Theory
PAHs	Polycyclic Aromatic Hydrocarbons
QI	Quantum Interference
CQI	Constructive Quantum Interference
DQI	Destructive Quantum Interference
LDA	Local Density Approximation
GGA	Generalized Gradient Approximation
SCF	Self-Consistent Field
vdW-DF	Van Der Waals Density Functional

SIESTA Spanish Initiative for Electronic Simulations with
Thousands of Atoms

HOMO Highest Occupied Molecular Orbitals

LUMO Lowest Unoccupied Molecular Orbitals

SMJs Single-Molecule Junctions

OPEs Oligophenylene ethynylenes

1. The fundamentals of molecular-scale electronics

1.1 Molecular electronics

A single molecule or self-assembled monolayer (SAM) connected to nanoscale electrodes (also known as ‘leads’) made from various materials such as metals (e.g., Au, Ag, Cu or and Ni)[3,4], semiconductors (e.g., Si)[5] or carbon (e.g., graphene [6,7] or carbon nanotubes[8]) are the focus of the scientific field known as molecular electronics. The number of transistors used in chips doubles every 18 months and their size shrinks by a factor of two, according to Gordon Moore's 1965 observation. Moore's Law [52] states that the rate of reduction on a logarithmic scale is exponential. More than fifty years later, the exponential growth is still present and as components get closer to the sub-10nm length scale, Moore's Law is beginning to reach its limit. By substituting the conventional semiconductor with a single molecule, the field of single-molecule electronics has the potential to provide an alternative to silicon-based devices by enabling the production of smaller, quicker and more energy-efficient devices. Since Aviram and Ratner presented the first molecular rectifier [10] as an alternative to silicon chips in the 1970s, single molecules as building blocks to design and produce molecular electronic nanoscale devices have been investigated and developed in the intervening period [1,9,29]. Numerous experimental and theoretical advances in the area of molecular electronics over recent decades have sparked multidisciplinary research in chemistry, engineering and physics.

Fundamentally, the field has been developing quickly, because it is thought likely to offer several benefits relative to the more established complementary metal-oxide semiconductor (CMOS) technology. The first benefit is the possibility to reduce the size of two electronic components to less than 10nm, which could enhance circuit integration

and result in faster and more energy-efficient performance. The range of their capabilities as a result of quantum interference, such as conducting wires [11,12] switches [13,14,6], thermoelectric materials [15,16,17], and negative differential resistance devices [18,19,20] are their second advantage. Another advantage that could lead to low-cost manufacturing is the capacity to create molecular devices using specialised intermolecular interactions. Single-molecule electronics may therefore be a useful addition to current silicon-based electronics.

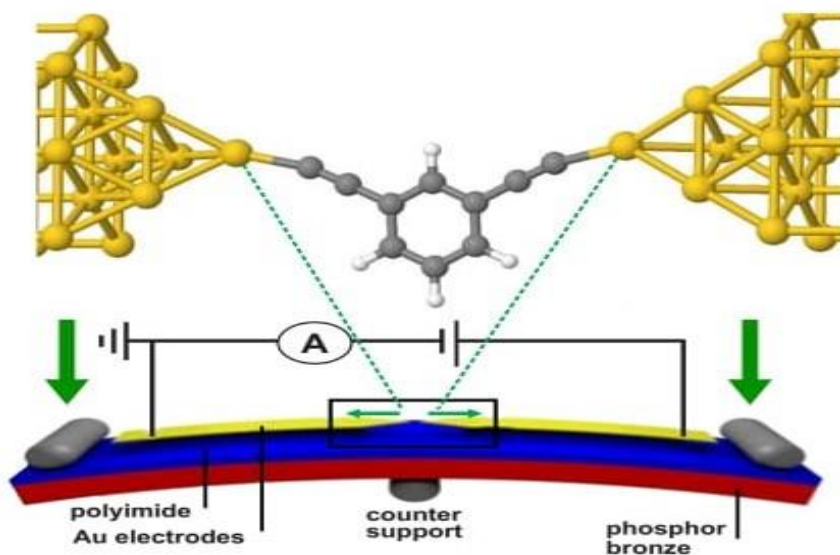


Fig (1.1): Schematic of a mechanically controllable break junction on a bulk substrate. In the top panel, a molecule sandwiched between a source and drain electrode is shown [26].

How to bridge a single molecule between nanoscale electrodes to examine the electronic characteristics of systems is one of the main experimental hurdles when creating single-molecule electronics. Metal-molecule-metal junctions have been constructed for this purpose using a variety of techniques such as scanning tunnelling microscope break junctions (STMBJ) [21,22,23], atomic force microscopes (AFM)[29], mechanically controllable break junctions (MCBJ, Figure 1.1.1), [24,25,26], electro-migration breakdown [27] and electrochemical depositions [28, 29]. Alongside these experimental developments, theoretical methods for computing the electronic assembly of atomic structures such as density functional theory (DFT) have also been developed. One DFT implementation program that permits the investigation of finite and periodic systems is the Spanish Initiative for Electronic Simulations with Thousands of Atoms (SIESTA) [30]. The transport characteristics of molecular devices can be predicted by combining DFT with the Green's function formalism. The Gollum code [32] which is utilised in the current study is one way to implement the Green's function formalism. Researchers are able to create a quantitative picture to comprehend transport features and make predictions to direct more experimental studies by combining experimental methods with this theoretical framework. Although there has been a significant increase in experimental progress regarding molecular electronics, certain issues remain to be solved and there are areas requiring further research such as robustness, solvent effects and electric system noise.

1.2. Molecular junctions

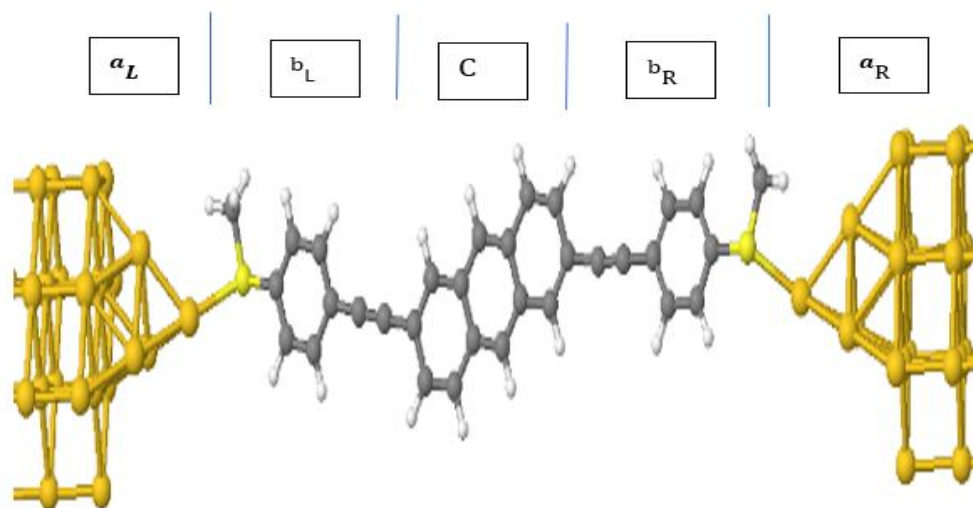


Fig (1.2): Diagram of a single-molecule junction: a_L and a_R are the left and right gold electrodes. b_L and b_R are the left and right SMe anchor groups. C is central functional unit (in this case an anthracene) coupled to phenyl rings on both sides.

Molecular junctions (see Figure 1.2) are sensitive to even the smallest adjustments to their atomic arrangement. Direct contact between the metallic electrode surfaces and the molecular unit is made possible, for instance, by anchor groups. Practically speaking, several investigations have shown the impact of various anchor groups on molecular transport and underlined the significance of their mechanical stability and their electronic transparency (i.e., weak or strong coupling). Thiol (-S) is the most widely used anchor group experimentally [33], because of its strong binding energy to gold, silver and copper electrodes [34]. Aside from thiol terminal groups, which are more stable and have a higher likelihood of forming junctions, other anchor groups investigated to date include amines (-NH₂), SMe and pyridyl. In addition to anchoring

groups, the type of electrode material (which may be metallic or non-metallic) has a significant effect on molecular transport. The most popular metallic electrodes are Au [37], Ag [4], Pd and Pt [38]. Due to its qualities as a noble metal, including exceptional chemical stability, high conductivity and readily obtainable clean surfaces and tips, gold has been the most commonly employed electrode material to date.

However, there are a number of disadvantages associated with the use of gold electrodes, including the mobility of surface atoms at room temperature, which results in thermal fluctuations and instabilities [39]. It is therefore crucial to find alternative materials. Researchers have sought to develop non-metallic electrodes such as carbon-based materials [40][41], graphene [42][49] and silicon [5], because they may be able to take accurate single-molecule electrical measurement using these kinds of electrodes. These display a variety of intriguing characteristics such as high charge mobility, stability, mechanical strength and the flexibility of their conjugated structure [41][42]. Recently, the use of superconducting electrodes has also been considered [50], because these electrodes have their own interference phenomena [51], which when combined with molecular-scale constructive quantum interference (CQI) and destructive quantum interference (DQI) can produce unusual interference effects. The fact that molecules can adopt a multitude of configurations within a junction [17] necessitates consideration of their molecular conformation [43], which also plays a significant role in molecular transport. Because of their small size (often as small as one nanometre), the molecules at the nanoscale device effectively function as an electronic circuit which is extremely desirable. Additionally, the ability to self-assemble on surfaces enables the molecular units to spontaneously form ordered structures through non-covalent interactions. Another crucial element in defining an effective molecular junction is the length dependency of electron transport via molecules. The current study primarily focuses on investigating molecules with desirable features, including aromatic chemical

compounds. The benzene ring, whose carbon atoms are connected by alternating double and single bonds, is an example of an archetypal aromatic compound.

In conclusion, anchor groups, molecular wire topologies, length dependency, and conformation variations are all important elements governing electron transport and present a multitude of potential regarding the chemical design of single-molecule devices. However, in electron transport experiments, the conductance of a molecular junction depends not only on the molecule itself, but also on the molecule's environment (such as solvents, vacuum or air), as well as on the molecule's contact geometry with the electrodes, all of which cause significant sample-to-sample fluctuations [44].

1.3. Quantum interference

The regulation of quantum transport across molecular-scale structures is significantly influenced by quantum interference (QI) [33][45]. Through constructive or destructive QI, this phenomenon can increase or decrease conductance, respectively [46]. Recently, academics have investigated QI both theoretically and experimentally [33][47]. The conductance of benzene rings is a straightforward illustration of QI; meta connectivity shows in DQI, resulting in low conductance, whereas para connectivity results in CQI and high conductance. Single-molecule junctions' electrical and thermoelectrical properties can be controlled by adjusting the connectivity of external electrodes to the centre rings of carbon-based molecules. To build molecular electrical devices by chemical alterations, QI therefore offers new potential. One of these consequences the DQI (described in depth in Chapter 5) is the subject of Chapter 4's discussion. By markedly lowering the transmission probability compared to junctions that exhibit constructive interference (CQI) [17,31,45,46,48], this phenomenon has a significant impact on molecular conductance.

1.4. Tight-binding model

The tight-binding model (TBM) [12] is an analytical method, which describes a structure based on the wave function of an electron as a linear combination of atomic orbitals (LCAO) of localised states. It investigates electronic transport properties through the Hamiltonian of a finite set of atomic orbitals. This approach assumes that electrons in a molecule form tightly bound interactions with only their nearest neighbouring sites. The exact solution to the Schrödinger equation is obtained by computing the eigenstates and eigenvalues.

1.5. Molecular junctions with graphene electrodes

Recently, certain researchers have achieved the creation of molecular junctions by substituting metal electrodes with graphene counterparts. This substitution is attributed to the notable dispersive density of states close to the Fermi energy E_F in graphene [43], along with its robust mechanical stability. Moreover, graphene electrodes exhibit the capability to establish secure connections with individual molecules through covalent bonds, such as the amide bond [44, 45], and non-covalent interactions, including van der Waals interactions [46-48] and p-p interactions [49-52]. Owing to the aforementioned benefits, the utilization of two-dimensional planar graphene electrodes enables the examination of the inherent characteristics of molecules via non-covalent interactions with graphene electrodes.

1.6. Conclusion

This chapter offers a concise overview of the molecular electronics domain, encompassing a historical perspective and an exploration of advancements in both experimental and theoretical methodologies. Key determinants affecting charge transport in molecular junctions are examined. Additionally, the discussion delves into single-molecule junctions established with graphene electrodes, highlighting their merits through illustrative examples. Lastly, the chapter provides an examination of quantum interference effects within molecular devices.

1.7. Thesis outline

The goal of the current study is to investigate theoretical approaches for dealing with electron transport in two-terminal molecular junctions utilising gold electrodes. As discussed in Chapter 2, one of the primary theoretical approaches employed in the current study to investigate and comprehend the electrical characteristics of single-molecule junctions is density functional theory (DFT), which is primarily implemented in the SIESTA code [32]. The second approach to single-particle transport theory is described in Chapter 3 and is encoded in the quantum transport code GOLLUM, which is a program that computes transport and thermal properties based on the theoretical foundation of Green's functions for a doubly infinite chain and semi-infinite 1D chains and the transmission coefficient equations. It explores how charges move within

individual molecules. Recently, there has been considerable interest in how to facilitate charge transport using quantum interference phenomena. The electrical and thermoelectrical properties of the structures under examination, which are depicted in Chapters 4 and 5, are the two main results that are theoretically investigated within this framework.

Bibliography:

- [1] M. Kiguchi, *Single-Molecule Electronics*. Springer, 2016.
- [2] J. C. Love, L. A. Estroff, J. K. Kriebel, R. G. Nuzzo, and G. M. Whitesides, “Self- assembled monolayers of thiolates on metals as a form of nanotechnology,” *Chem. Rev.*, vol. 105, no. 4, pp. 1103–1170, 2005.
- [3] S. V Aradhya and L. Venkataraman, “Single-molecule junctions beyond electronic transport,” *Nature Nanotechnology.*, vol. 8, no. 6, pp. 399–410, 2013.
- [4] T. Kim, H. Vázquez, M. S. Hybertsen, and L. Venkataraman, “Conductance of molecular junctions formed with silver electrodes,” *Nano Lett.*, vol. 13, no. 7, pp. 3358–3364, 2013.
- [5] Q. Wu, S. Hou, H. Sadeghi, and C. Lambert, “A single-molecule porphyrin-based switch for graphene nano-gaps,” *Nanoscale*, vol. 10, pp. 6524–6530, 2018.
- [6] Q. Wu, H. Sadeghi, V. M. García-Suárez, J. Ferrer, and C. J. Lambert, “Thermoelectricity in vertical graphene-C60-graphene architectures,” *Sci. Rep.*, vol. 7, p. 11680, 2017.
- [7] S. H. Choi, B. Kim, and C. D. Frisbie, “Electrical resistance of long conjugated molecular wires,” *Science (80-.)*, vol. 320, no. 5882, pp. 1482–1486, 2008.
- [8] L. Lafferentz, F. Ample, H. Yu, S. Hecht, C. Joachim, and L. Grill, “Conductance of a single conjugated polymer as a continuous function of its length,” *Science (80-.)*, vol. 323, no. 5918, pp. 1193–1197, 2009.

- [9] M. Del Valle, R. Gutiérrez, C. Tejedor, and G. Cuniberti, “Tuning the conductance of a molecular switch,” *Nat. Nanotechnol.*, vol. 2, no. 3, pp. 176–179, 2007.
- [10] M. Paulsson and S. Datta, “Thermoelectric effect in molecular electronics,” *Phys. Rev. B*, vol. 67, no. 24, p. 241403, 2003.
- [11] Q. Wu, H. Sadeghi, and C. J. Lambert, “MoS₂ nano flakes with self-adaptive contacts for efficient thermoelectric energy harvesting,” *Nanoscale*, vol. 10, no. 16, pp. 7575–7580, 2018.
- [12] R. Almughathawi, S. Hou, Q. Wu, Z. Liu, W. Hong, and C. Lambert, “Conformation and Quantum-Interference-Enhanced Thermoelectric Properties of Diphenyl Diketopyrrolopyrrole Derivatives,” *ACS Sensors*, vol. 6, no. 2, pp. 470–476, 2021.
- [13] J. Chen, W. Wang, M. A. Reed, A. M. Rawlett, D. W. Price, and J. M. Tour, “Room-temperature negative differential resistance in nanoscale molecular junctions,” *Appl. Phys. Lett.*, vol. 77, no. 8, pp. 1224–1226, 2000.
- [14] N. P. Guisinger, M. E. Greene, R. Basu, A. S. Baluch, and M. C. Hersam, “Room temperature negative differential resistance through individual organic molecules on silicon surfaces,” *Nano Lett.*, vol. 4, no. 1, pp. 55–59, 2004.
- [15] J. Chen, M. A. Reed, A. M. Rawlett, and J. M. Tour, “Large on-off ratios and negative differential resistance in a molecular electronic device,” *Science* (80-

- .), vol. 286, no. 5444, pp. 1550–1552, 1999.
- [16] B. Xu and N. J. Tao, “Measurement of single-molecule resistance by repeated formation of molecular junctions,” *Science* (80-.), vol. 301, no. 5637, pp. 1221–1223, 2003.
- [17] C. Li, I. Pobelov, T. Wandlowski, A. Bagrets, A. Arnold, and F. Evers, “Charge transport in single Au vertical bar alkanedithiol vertical bar Au junctions: Coordination geometries and conformational degrees of freedom,” *J. Am. Chem. Soc.*, vol. 130, no. 1, pp. 318–326, 2008.
- [18] M. Teresa González, S. Wu, R. Huber, S. J. Van Der Molen, C. Schönenberger, and M. Calame, “Electrical conductance of molecular junctions by a robust statistical analysis,” *Nano Lett.*, vol. 6, no. 10, pp. 2238–2242, 2006.
- [19] M. A. Reed, C. Zhou, C. J. Muller, T. P. Burgin, and J. M. Tour, “Conductance of a molecular junction,” *Science* (80-.), vol. 278, no. 5336, pp. 252–254, 1997.
- [20] H. Park, A. K. L. Lim, A. P. Alivisatos, J. Park, and P. L. McEuen, “Fabrication of metallic electrodes with nanometer separation by electromigration,” *Appl. Phys. Lett.*, vol. 75, no. 2, pp. 301–303, 1999.
- [21] C. Z. Li, H. X. He, and N. J. Tao, “Quantized tunneling current in the metallic nanogaps formed by electrodeposition and etching,” *Appl. Phys. Lett.*, vol. 77, no. 24, pp. 3995–3997, 2000.
- [22] D. Xiang, X. Wang, C. Jia, T. Lee, and X. Guo, “Molecular-Scale Electronics: From Concept to Function,” *Chem. Rev.*, vol. 116, no. 7, pp. 4318–4440, 2016.
- [23] C. J. Lambert, *Quantum Transport in Nanostructures and Molecules*. IOP

- Publishing, 2021.
- [24] C. J. Lambert, “Basic concepts of quantum interference and electron transport in single-molecule electronics,” *Chemical Society Reviews*. pp. 875–888, 2015.
- [25] N. B. Luque and E. Santos, “Ab Initio Studies of Ag–S Bond Formation during the Adsorption of l-Cysteine on Ag (111),” *Langmuir*, vol. 28, no. 31, pp. 11472–11480, 2012.
- [26] F. Schwarz and E. Lörtscher, “Break-junctions for investigating transport at the molecular scale,” *J. Phys. Condens. Matter*, vol. 26, no. 47, pp.1-21, 2014.
- [27] V. M. García-Suárez, A. R. Rocha, S. W. Bailey, C. J. Lambert, S. Sanvito, and J. Ferrer, “Single-channel conductance of H₂ molecules attached to platinum or palladium electrodes,” *Phys. Rev. B*, vol. 72, no. 4, p. 45437, 2005.
- [28] J. C. Cuevas and E. Scheer, *Molecular electronics: an introduction to theory and experiment*. World Scientific, 2010.
- [29] X. H. Zheng, G. R. Zhang, Z. Zeng, V. M. García-Suárez, and C. J. Lambert, “Effects of antidots on the transport properties of graphene nanoribbons,” *Phys. Rev. b*, vol. 80, no. 7, p. 75413, 2009.
- [30] C. M. Finch, S. Sirichantaropass, S. W. Bailey, I. M. Grace, V. M. García-Suárez, and C. J. Lambert, “Conformation dependence of molecular conductance: Chemistry versus geometry,” *J. Phys. Condens. Matter*, vol. 20, no. 2, pp. 22203, 2008.
- [31] Y. Selzer and D. L. Allara, “Single-molecule electrical junctions,” *Annu. Rev. Phys.*

- Chem., vol. 57, pp. 593–623, 2006.
- [32] C. J. Lambert, H. Sadeghi, and Q. H. Al-Galiby, “Quantum-interference-enhanced thermoelectricity in single molecules and molecular films,” *Comptes Rendus Phys.*, vol. 17, no. 10, pp. 1084–1095, 2016.
- [33] J. Liu, X. Huang, F. Wang, and W. Hong, “Quantum interference effects in charge transport through single-molecule junctions: detection, manipulation, and application,” *Acc. Chem. Res.*, vol. 52, no. 1, pp. 151–160, 2018.
- [34] F. Evers, R. Korytár, S. Tewari, and J. M. Van Ruitenbeek, “Advances and challenges in single-molecule electron transport,” *Rev. Mod. Phys.*, vol. 92, no. 3, 2020.
- [35] R. Frisenda, V. A. E. C. Janssen, F. C. Grozema, H. S. J. Van Der Zant, and N. Renaud, “Mechanically controlled quantum interference in individual π -stacked dimers,” *Nat. Chem.*, vol. 8, no. 12, pp. 1099–1104, 2016.
- [36] S. Bailey, D. Visontai, C. J. Lambert, M. R. Bryce, H. Frampton, and D. Chappell, “A study of planar anchor groups for graphene-based single-molecule electronics,” *J. Chem. Phys.*, vol. 140, no. 5, 2014.
- [37] N. L. Plaszkó, P. Rakyta, J. Cserti, A. Kormányos, and C. J. Lambert, “Quantum interference and nonequilibrium Josephson currents in molecular Andreev interferometers,” *Nanomaterials*, vol. 10, no. 6, p. 1033, 2020.
- [38] V. C. Hui and C. J. Lambert, “Andreev scattering, universal conductance fluctuations and phase periodic transport,” *Epl (Europhysics Lett.)*, vol. 23, no. 3, pp. 203–209, 1993.
- [39] G. E. Moore, Cramming more components onto integrated circuits. *Electronics*,

- vol. 38, no. 8, 1965.
- [40] Orientation preference control: a novel approach for tailoring molecular electronic functionalities. Wang, X., Li, X., Ning, S., Ismael, A. *Journal of Materials Chemistry C*, 2023, 11(36), pp. 12348–12355
- [41] 20-State Molecular Switch in a Li@C60 Complex. Ismael, A.K. *ACS Omega*, 2023, 8(22), pp. 19767–19771
- [42] Influence of Charge Transfer on Thermoelectric Properties of Endohedral Metallofullerene (EMF) Complexes Alshammari, M., Alotaibi, T., Alotaibi, M., Ismael, A.K. *Energies*, 2023, 16(11), 4342
- [43] Impact of the terminal end-group on the electrical conductance in alkane linear chains. Alshehab, A., Ismael, A.K. *RSC Advances*, 2023, 13(9), pp. 5869–5873
- [44] Orientational control of molecular scale thermoelectricity. Alshammari, M., Al-Jobory, A.A., Alotaibi, T., Lambert, C.J., Ismael, A. *Nanoscale Advances*, 2022, 4(21), pp. 4635–4638
- [45] Assembly, structure and thermoelectric properties of 1,1'-dialkynylferrocene 'hinges'. Wilkinson, L.A., Bennett, T.L.R., Grace, I.M., Robinson, B.J., Long, N.J. *Chemical Science*, 2022, 13(28), pp. 8380–8387
- [46] Interference Controls Conductance in Phthalocyanine Molecular Junctions. González, M.T., Ismael, A.K., García-Iglesias, M., Lambert, C.J., Agrait, N. *Journal of Physical Chemistry C*, 2021, 125(27), pp. 15035–15043
- [47] Interference Controls Conductance in Phthalocyanine Molecular Junctions. González, M.T., Ismael, A.K., García-Iglesias, M., Lambert, C.J., Agrait, N. *Journal of Physical Chemistry C*, 2021, 125(27), pp. 15035–15043.

- [48] Zhao S, Deng ZY, Albalawi S, Wu Q, Chen L, Zhang H, Zhao XJ, Hou H, Hou S, Dong G, Yang Y, Shi J, Lambert CJ, Tan YZ, Hong W. Charge transport through single-molecule bilayer-graphene junctions with atomic thickness. *Chemical Science* 2022; 13:5854-5859.
- [49] Max Roemer AG, David Jago, David Costa-Milan, Jehan Alqahtani, Juan Hurtado-Gallego, Hatf Sadeghi, Colin J Lambert, Peter R Spackman, Alexandre N Sobolev, Brian W Skelton, Arnaud Grosjean, Mark Walkey, Sven Kampmann, Andrea Vezzoli, Peter V Simpson, Massimiliano Massi, Inco Planje, Gabino Rubio-Bollinger, Nicolás Agrait, Simon J Higgins, Sara Sangtarash, Matthew J Piggott, Richard J Nichols, George A Koutsantonis. 2, 7-and 4, 9-Dialkynyldihydropyrene molecular switches: syntheses, properties, and charge transport in single-molecule junctions. *Journal of the American Chemical Society* 2022; 144.
- [50] Liljeroth SJvdMaP. Charge transport through molecular switches. *Journal of Physics: Condensed Matter* 2010; 22.
- [51] Zi-Zhen Chen S-DW, Jin-Liang Lin, Li-Chuan Chen, Jing-Jing Cao, Xiangfeng Shao, Colin J. Lambert, Hao-Li Zhang. Modulating Quantum Interference Between Destructive and Constructive States in Double N-Substituted Single Molecule Junctions. *Advanced Electronic Materials* 2023; 9.
- [52] Juan Hurtado-Gallego RD, Iain M Grace, Laura Rincón-García, Andrei S Batsanov, Martin R Bryce, Colin J Lambert, Nicolás Agrait. Quantum interference dependence on molecular configurations for cross-conjugated systems in single-molecule junctions. *Molecular Systems Design & Engineering* 2022; 7.

2. Density Functional Theory

2.1. Introduction

To elucidate the electronic behavior of molecular electronic devices, theoretical approaches to resolve electronic interaction problems are of fundamental importance. The interacting many-body Schrödinger equation can be described using several theoretical methods such as quantum Monte Carlo, wave function methods. Density Functional Theory (DFT) is one method that physicists and chemists use repeatedly. This section presents a complete presentation of the Hohenberg-Kohn theorem (1964) and the Kohn-Sham equation [1,2] which underlie the DFT estimation of the ground state of organic molecules. The main purpose of this chapter is to briefly introduce the DFT computational code SIESTA [3], research on the development of molecular structures, the calculation of charge densities, binding energies, band structures, and the generation of Hamiltonian operators for subsequent charge transport calculations.

DFT techniques can be used to solve the non-relativistic many-body time-independent Schrödinger equation (TISE). Important formats are described at the beginning of this section. This is so that electron density can be used to find properties of multi-electron systems. Part 2 provides a brief introduction to numerical applications and their DFT fundamentals, clarifying the challenges and performing accurate calculations of molecular structures, despite these systems being large. DFT has therefore become one of the most important techniques in theoretical physics.

2.2 The Schrödinger Equation

In general, all many-particle systems can be described using the Hamiltonian operator via a given nonrelativistic Schrödinger equation as follows:

$$H\Psi_i = E_i\Psi_i \quad (2.1)$$

where Ψ_i is the wavefunction of the state of the i^{th} system, E_i is the numerical representation of the energy of the i^{th} state described by Ψ_i , and the variable H is the system consisting of N -electrons and M -nuclei representing the time-independent Hamiltonian. The details of the Hamiltonian operator for such a system are given by the notation:

$$= \frac{-\hbar^2}{2m_i} \sum_{i=1}^{N_e} \nabla_i^2 - \frac{\hbar^2}{2M_I} \sum_{I=1}^{N_{nuc}} \nabla_I^2 + \frac{1}{2} \sum_{i \neq j} \frac{e^2}{|r_i - r_j|} - \sum_{i,I} \frac{Z_I e^2}{|r_i - R_I|} + \frac{1}{2} \sum_{I \neq J} \frac{Z_I Z_J e^2}{|R_I - R_J|} \quad (2.2)$$

Where \hbar denotes Planck's constant, m_i and M_i represent the masses of the electron and nucleus, respectively. Z_I is the atomic number of the I^{th} atom, e signifies the charge of the electron, r_i and R_i represent the positions of the i^{th} electron and I^{th} nucleus.

In equation 2.2, the first two terms depict the kinetic energies of the electron and nucleus. Subsequently, there are representations for electron-electron interactions, electron-nucleus interactions, and nucleus-nucleus interactions, in that order. Hence, equation (2.2) can be alternatively expressed as follows:

$$\hat{H} = \hat{T}_e(r) + \hat{T}_N(R) + V_{ee}(r) + V_{eN}(r, R) + V_{NN}(R) \quad (2.3)$$

2.3. Born-Oppenheimer approximation

The Schrödinger equation (2.1) can only be solved analytically for systems with a few electrons, like the simple hydrogen atom problem. Based on the fact that the mass of nucleons is at least three orders of magnitude larger than that of electrons [5] [6], nuclei can be treated as classical particles that generate a constant external potential and electrons can be treated as quantum particles sensitive to this potential (i.e., their kinetic energy is neglected). Therefore, the electron position does not affect the nucleon wave function.

Assuming that the nucleon wave function is independent of electron position, this is called the Born-Oppenheimer approximation [5]. In Formula 2.2, the classical interacting components of the core potential do not contribute intrinsically to the electronic description structure. As a result, the electronic Hamiltonian component is simplified because the electron position does not affect the nucleon wave function.

$$\hat{H}_e(r, R)\psi_e(r, R) = E_e\psi_e(r, R) \quad (2.4)$$

In this context, the electronic Hamiltonian can be formulated as follows:

$$\hat{H} = \frac{-\hbar^2}{2m_i} \sum_{i=1}^{N_e} \Delta_i^2 + \frac{1}{2} \sum_{i \neq j} \frac{e^2}{|r_i - r_j|} - \sum_{i,l} \hat{V}_{ext}(r_i) \quad (2.5)$$

where the variable $v_{ext}(r_i)$ is the external potential due to the interaction between the nucleus and the electron. This approximation makes it possible to separate the degrees of freedom coming from the electron and nucleon. Solving Equations 2.5, even on modern supercomputers, is still challenging despite the reduced system size due to the Born-Oppenheimer approximation. Therefore, additional DFT methods are needed such as Hartree, Hartree-Fock or other quantum-mechanical methods. DFT theory solves this problem by defining the physical quantity in terms of the ground state density $n(r)$ [7]. Hartree-Fock captures exchange energy but ignores electronic correlation.

2.4 Hohenberg-Kohn theorem approximation

Developed in 1964, the Hohenberg-Korn theorem [1] is a fundamental aspect of the DFT because it makes it possible to characterise the ground state by the density of electrons $n(r)$. A multi-electron system interacting with an applied external potential $V_{ext}(r)$ can employ this quantity to determine the minimum total energy. The first HK theorem states that the energy of an atomic system, as well as all other observables, is unambiguously determined by the electronic density of the system, $n(r)$.

$$\hat{H} = \frac{-\hbar^2}{2m_i} \sum_{i=1}^{N_e} \nabla_i^2 + \frac{1}{2} \sum_{i \neq j} \frac{e^2}{|r_i - r_j|} - \sum_{i,l} \hat{V}_{ext}(r_i) \quad (2.6)$$

According to this theorem, density $n(r)$ is a function of the total energy of a multi-electron system and is given by:

$$E_{HK}[n] = F_{HK}[n] + \int V_{ext}(r) n(r) dr \quad (2.7)$$

$$F_{HK}[n] = T_{int}[n] + \underbrace{E[n]}_{\substack{=zero, \text{ for} \\ \text{non-interacting} \\ \text{system}}} \quad (2.8)$$

The potential energy of a multi-electron interacting system is noted as F_{HK} . This theorem is supported by two strong claims:

The ground state density $n(r)$ of each interacting multi-particle system is uniquely specified concerning the external potential $V_{ext}(r)$. This equation shows that two external potentials produce the same ground state density distribution [1,4,8,9]. The electron density that minimizes the energy of the overall functional is the true electron density corresponding to the full solutions of the Schrödinger equation. A global function of energy $E[n(r)]$ can be defined with density $n(r)$. Furthermore, the global minimum of this function and the density $n(r)$ that minimises the function and represents the exact ground state density $n(r)$ are known as the exact ground state energies of the existing system. Outside the perinatal period ($V_{ext}(r)$) [1,4,8,9].

2.5. The Kohn-Sham approach

Kohn and Sham's strategy [2,10,11] offered a solution to Kohn and Sham's many-body problem (1965) using independent particle equations for non-interacting electron systems. For any system of interacting particles, the proposed method produces the same ground-state density [2][12]. Kohn and Sham proposed that it is possible to replace the original Hamiltonian of the system with the effective Hamiltonian of the non-interacting system (H_{eff}) in the effective external potential $V_{eff}(r)$. Therefore,

$$F_{HK}[\mathbf{n}] = T_{int}[\mathbf{n}] + V_{eff}(r)[\mathbf{n}] \quad (2.9)$$

Becomes

$$F_{KS}[\mathbf{n}(r)] = T_{non}[\mathbf{n}(r)] + E_{Hart}[\rho(r)] + \int V_{ext}(r) \mathbf{n}(r) dr + E_{xc}[\mathbf{n}(r)] \quad (2.10)$$

In 2.8. the quantity T_{non} refers to the kinetic energy of non-interacting systems, as opposed to T_{int} (for interactive systems), and E_{Hart} , which is associated with the density $\mathbf{n}(r)$, refers to the classical static electron energy or classical self-interaction energy of electronic gases. The last term, $E_{xc}[\mathbf{n}(r)]$, the exchange-correlation energy functional, gives the difference in kinetic energy between the interacting and non-interacting systems. The formula is as follows:

$$E_{xc}[\mathbf{n}(r)] = F_{HK}[\mathbf{n}(r)] - \frac{1}{2} \int \frac{\overbrace{\mathbf{n}(r_1)\mathbf{n}(r_2)}^{E_{Hart}[\mathbf{n}(r)]}}{|r_1 - r_2|} dr_1 dr_2 - T_{non}[\mathbf{n}(r)] \quad (2.11)$$

In this variational equation, both the interacting and non-interacting electron systems have the same $\mathbf{n}(r)$ ground state energy and density. In recent decades, considerable effort has been made to improve the accuracy of $E_{xc}[\mathbf{n}(r)]$.

This capability can now be used to study and predict the physical properties of multiple molecules and solid-state systems. Therefore, the effective single-particle potential $V_{eff}(r)$ is computed for the last three terms in Equation (1). 2.10. Use of function

derivatives.

$$V_{eff}(r) = V_{ext}(r) + \frac{\partial E_{Hart}[n(r)]}{\partial n(r)} + \frac{\partial E_{xc}[n(r)]}{\partial n(r)} \quad (2.12)$$

Significantly, the single particle's Hamiltonian can be obtained from the potential $V_{eff}(r)$ as:

$$H_{KS} = T_{non} + V_{eff} \quad (2.13)$$

The Schrödinger equation changes to:

$$[T_{non} + V_{eff}] \Psi_{KS} = E \Psi_{KS} \quad (2.14)$$

This is called the Kohn-Sham equation. The Kohn-Sham approach shows that a complex many-particle interacting system can be correctly mapped to a set of simple non-interacting equations if the exchange-correlation function is known. However, because the exchange-correlation function is unknown, an approximation must be made.

2.5.1. Exchange and correlation functional

Although DFT is still used on the basis of an approximation of the kinetic energy function and the exchange-correlation function defined by electronic density, it is a very reliable and well-established method used in the analysis. Another benefit of DFT is that the Kohn-Sham equation can reduce the quantum mechanical ground-state many-body problem to a self-consistent one-electron problem [8]. Although this approach is technically correct, there is not an exact formula for calculating the exchange-correlation energy as a function of density. Local density approximation (LDA) is a long-preferred option among the various forms proposed for exchange and correlation [13]. Despite its simplicity, LDA predictions provide accurate descriptions of the atomic structure, elastic and vibrational properties of various systems. However, LDA generally overestimates the binding energies of molecules and solids. This is because they do not accurately describe the energetics of chemical reactions (e.g., heat of the reaction and activation energy barrier). In addition, LDA often places molecular conformations and crystalline bulk phases in even more imprecise energy orders [14]. Compared to LDA, the Generalized Gradient Approximation (GGA) largely eliminates these shortcomings [8][15]. For example, it provides a more detailed representation of the energy barriers in the dissociative adsorption of hydrogen onto metal and semiconductor surfaces [16]. Local densities and spatial variations in densities are key components of the gradient correction (GGA) function. Therefore, the two most commonly used exchange-correlation functional approximations are LDA [13] and GGA which are based on density and local density, respectively, and use advanced techniques that incorporate density derivatives. The following sections briefly describe LDA and GGA.

2.5.1.1. Local density approximation

The LDA approximation developed by Kohn and Sham [2][10] assumes that the exchange-correlation function depends only on the local density. The simplest approximation of this exchange-correlation formula is as follows:

$$E_{xc}^{LDA}[n] = \int n(r) e_{xc}^{homo}[n(r)] dr \quad (2.15)$$

The exchange-correlation energy of a homogeneous electron gas with a density of n is referred to as $E_{xc}^{homo}[n(r)]$. It is helpful to separate the contribution into two parts from

$E_{xc}^{homo}[n]$

$$E_{xc}^{homo}[n] = E_x^{homo}[n] + E_c^{homo}[n] \quad (2.16)$$

In this situation, the first term $E_x^{homo}[n]$ is related to the exchange energies, whereas the second term $E_c^{homo}[n]$ is related to the correlation energies.

In homogeneous systems such as graphene and carbon nanotubes where the electron density does not change rapidly, the LDA functional is still considered to be correct. For atoms with d or f orbitals, errors are to be expected because LDA handles homogeneous systems.

2.5.1.2. Generalized Gradient Approximation

For truly heterogeneous systems where the electron density varies rapidly at the point (r^{\rightarrow}), the LDA approximation is inaccurate. Therefore, an alternative approximation is required which probes the electron density gradient, the so-called GGA. Therefore, the higher spatial derivatives of the total charge density ($|\nabla n(r)|$, $|\nabla^2 n(r)|$, ...) enter the

functional form of the exchange and correlation energies of the GGA approximation. The functional exchange term, which does not have a closed form in the GGA approximation, was numerically estimated along with the correlation contribution. As a result, this fitting process uses a large number of parameterisations. This section examines one of them, the PBE functional form, proposed by Perdew Burke and Ernzerhof [15]. The correlation energy is given by:

$$E_x^{GGA}[n(r)] = \int n(r) \varepsilon_x^{GGA}[n(r), |\nabla n(r)|] dr \quad (2.17)$$

2.6. SIESTA

A Spanish acronym for electron simulation with thousands of atoms (SIESTA) [3] is able to perform efficient computations in a self-consistent manner in density functional theory using a linear combination of norm-conserving pseudopotentials and atomic orbital basis sets (LCAOBs). All of the calculations provided in this work are based on the SIESTA code, including the electronic properties of the optimal structure of target molecules such as charge density, binding energy and other aspects.

2.6.1. The pseudopotential approximation

A pseudopotential or effective potential is an example of an approximation beyond those of DFT. This is because the SIESTA code requires approximations to produce reliable calculations. As a result, fewer electrons are used in the simulation, which helps solve the many-body Schrödinger equation. This approximate concept suggests that atomic electrons can be classified into two groups. Core electrons occupy filled atomic orbital shells and valence electrons occupy partially filled atomic orbitals. As a result, pseudopotentials are created using the non-valence electrons (also known as core electrons) of atoms and the complex effects of nuclear motion as a surrogate. This is supported by the observation that core electrons in most molecules are not involved in chemical bonds that lead to the development of molecular orbitals. Fermi made this assumption in 1934 [18] and uses a particular kind of pseudopotential in the calculations. Most chemical properties are primarily determined by valence electrons. Due to their fast interaction with the nucleus, an approximation can be made by treating only the valence electrons and removing the core electrons. In general, valence electrons should be taken into consideration when constructing molecular orbitals because their states overlap other valence states of neighbouring atoms.

2.6.2. Calculating binding energies using the counterpoise method

By using the DFT approach to determine the ground state energies of various molecules and the binding energies of various system components, the optimal energies can be determined. The core-focused localised set of basic functions makes these calculations error-prone when using the SIESTA code. If the atoms are close together, their basis functions may overlap, thereby artificially strengthening the connections of the atoms and giving an erroneous reading of the overall energy of the system. This kind of error is usually resolved with counterpoise (CP) correction [20] or basis function convolution error correction (BSSE) [19]. The binding energy of the interaction can be defined as follows, assuming two molecular systems denoted by the letters **A** and **B**:

$$\Delta E = E^{AB} - (E^A + E^B) \quad (2.18)$$

where E^{AB} is the combined system's total energy and E^A and E^B are the isolated components' total energies respectively. The superscript in the above statement indicates the basis set that was used in each computation; i.e., **A** stands for the basis set of system **A**, **B** stands for the basis set of system **B**, and **AB** stands for the combined basis set of systems **A** and **B**. Energy calculations should be made using the same total basis set of the **AB** system to reduce numerical errors.

$$\Delta E = E_{AB}^{AB} - (E_A^{AB} + E_B^{AB}) \quad (2.19)$$

where E_A^{AB} and E_B^{AB} represent the energies of systems **A** and **B**, respectively, as determined by the

supersystem. To provide trustworthy and accurate outcomes, this is a vital notion that has been applied in numerous systems [21,22].

The illustration of the origin of the basis used in a CP calculation is depicted in the figure below:

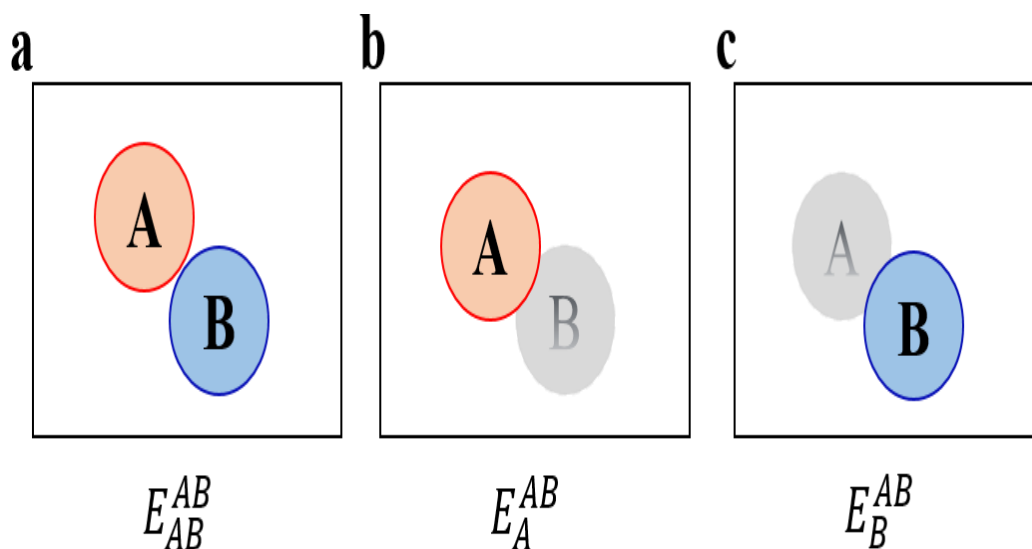


Fig (2.1): Utilizing the counterpoise approach for determining binding energy, wherein symbols A and B represent the molecule and the lead, respectively.

The calculation of binding energy is shown in Figure 2.1 (a) Basis functions for the entire system AB , where atoms are represented by red and blue circles. (b) Basis functions for a single system A . System B is the ghost state represented by the blue dashed circle. (c) Basis functions for a single system B . Here, system A is in the ghost state represented by the red dashed circle. In practice, setting the nuclear charge of the relevant system to zero makes it easier to specify the basis set for the counterweight calculation.

2.7 Calculations in practice

In the current study, many steps of transportation calculation are performed using the SIESTA code. The atomic configuration of the system must be constructed first. Subsequently, each element requires the correct pseudopotential specific to each exchange-correlation functional. Regarding computations, accurate computations require a large amount of memory, so choosing an appropriate basis set is important to reduce the amount of memory and time required. Including convergence tolerances for screen frequencies and densities is an alternative way to ensure the accuracy of the calculations. Furthermore, the Pulay parameter describes the control parameter for the convergence of SIESTA which accelerates or keeps the convergence of the charge density stable.

Assuming no interatomic interactions, the next step is to create the desired initial charge density. With a known pseudopotential, the total charge density is the sum of the individual charge densities. The self-consistent calculation shown in Fig. 2.8 begins with the calculation of Hartree and exchange-correlation potentials. Therefore, the Kohn-Sham equation is solved to obtain the new charge density. The next iteration is then initiated and repeated until a critical convergence criterion is achieved. This indicates that the Kohn and Sham ground state orbitals and energies are achieved for specific atom combinations.

This is another loop managed by the conjugate gradient method [23][24] for geometry optimisation (i.e., relaxing the atomic coordinates to allow the shape and volume of the periodic cell to be changed). This gives the equilibrium lattice parameter of the system

and the minimum atomic ground state energy. Density matrices and Hamiltonian operators are computed after applying this self-consistent method. This is important because the quantum transport calculations in the next chapter are based on these.

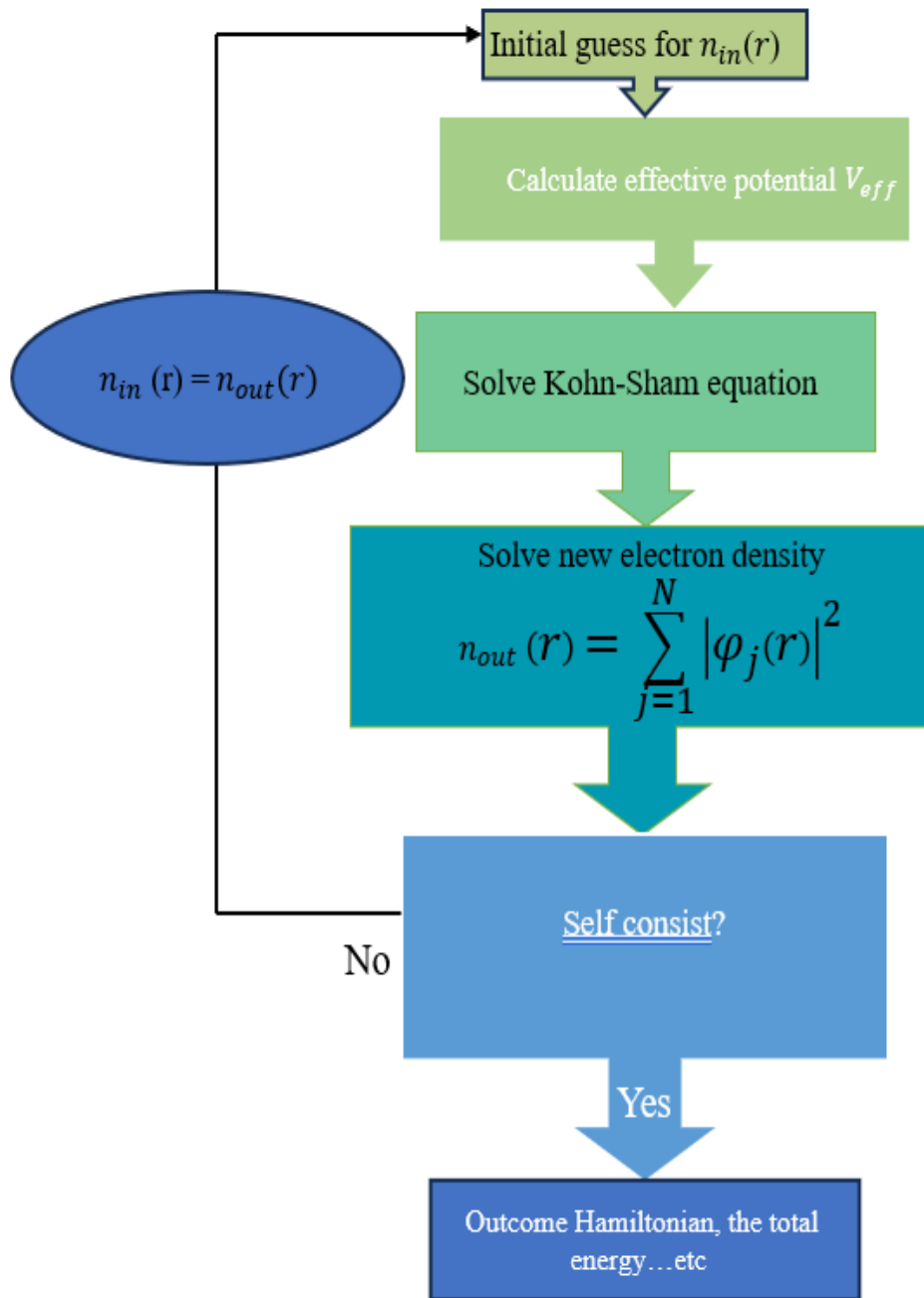


Fig (2.2): Schematic of the self-consistency process within SIESTA

First, an initial electron density, $n_{in}(r)$, is assumed (iteration 0). Then, the effective potential $V_{eff}(r)$ is constructed using equation (2.13). After that, equation (2.12) will be solved to find $\varphi_i(r)$. Finally, the new output density $n_{out}(r)$ is obtained, which should be the same as the initial one or smaller than a certain small value called tolerance. If it is not the new electron density will be used and iterated until it is. By the end of the process, the converged eigenvalues, energies, and eigenfunctions will be determined, as well as the final density.

2.8 Conclusion

The many-body Schrödinger equation for the ground state density can only be solved from the basic ideas of the DFT and SIESTA codes. This includes the Hohenberg-Kohn theorem and the Kohn-Sham equations considered in this section. Some approximations, such as the Born-Oppenheimer approximation, are necessary to find the eigenvalues and eigenstates of the Hamiltonian of the system of nuclei and electrons as a solution to many-body problems. Because it is difficult to know exactly the shape of the Kohn-Sham exchange-correlation function (the energy difference between interacting and non-interacting systems), approximations are unavoidable.

These are essential for the quantum transport calculations in the next chapter. The two most common approximations for exchange and correlation energies are the LDA and The GGA. Finally, technical elements such as pseudopotential approximation and basis functions were introduced into the SIESTA DFT algorithm as a means of performing all electronic structure calculations, including simulations of binding energies.

Bibliography:

- [1] P. Hohenberg and W. Kohn, “Inhomogeneous electron gas,” *Phys. Rev.*, vol. 136, no. 3B, p. B864, 1964.
- [2] W. Kohn and L. J. Sham, “Self-consistent equations including exchange and correlation effects,” *Phys. Rev.*, vol. 140, no. 4A, p. A1133, 1965.
- [3] SHOLL DS, STECKEL JA. Density functional theory-a practical introduction. John Wiley & Sons, Inc., Hoboken, New Jersey 2009.
- [4] R. M. Martin, Electronic structure: basic theory and practical methods. Cambridge University Press, 2004.
- [5] M. Born and J. R. Oppenheimer, “On the quantum theory of molecules,” *Ann.Physik*, vol. 84, no. 20, pp. 457–484, 1927.
- [6] A. Bartók-Pirtay, The Gaussian Approximation Potential: an interatomic potential derived from first principles quantum mechanics. Springer Science & Business Media, 2010.
- [7] V. Sahni, “The Hohenberg-Kohn Theorems and Kohn-Sham Density Functional Theory,” in *Quantal Density Functional Theory*, Springer, pp. 99–123, 2004.
- [8] W. Kohn, A. D. Becke, and R. G. Parr, “Density functional theory of electronic structure,” *J. Phys. Chem.*, vol. 100, no. 31, pp. 12974–12980, 1996.
- [9] W. Kohn, “Nobel Lecture: Electronic structure of matter—wave functions and density functionals,” *Rev. Mod. Phys.*, vol. 71, no. 5, p. 1253, 1999.
- [10] R. M. Dreizler and E. K. U. Gross, *Density functional theory: an approach to the quantum many-body problem*. Springer Science & Business Media, 2012.
- [11] W. Yang, “Direct calculation of electron density in density-functional theory,”

Phys. Rev. Lett., vol. 66, no. 11, p. 1438, 1991.

[12] R. G. Parr, “Density functional theory of atoms and molecules,” in *Horizons of quantum chemistry*, Springer, pp. 5–15, 1980.

[13] R. O. Jones and O. Gunnarsson, “The density functional formalism, its applications and prospects,” *Rev. Mod. Phys.*, vol. 61, no. 3, pp. 689–746, 1989.

[14] J. C. Grossman, L. Mitas, and K. Raghavachari, “Structure and stability of molecular carbon: importance of electron correlation,” *Phys. Rev. Lett.*, vol. 75, no. 21, p. 3870, 1995.

[15] J. P. Perdew, K. Burke, and M. Ernzerhof, “Generalized gradient approximation made simple,” *Phys. Rev. Lett.*, vol. 77, no. 18, p. 3865, 1996.

[16] E. Penev, P. Kratzer, and M. Scheffler, “Effect of the cluster size in modeling the H₂ desorption and dissociative adsorption on Si (001),” *J. Chem. Phys.*, vol. 110, no. 8, pp. 3986–3994, 1999.

[17] D. Sánchez-Portal, P. Ordejon, E. Artacho, and J. M. Soler, “Density-functional method for very large systems with LCAO basis sets,” *Int. J. Quantum Chem.*, vol. 65, no. 5, pp. 453–461, 1997.

[18] E. Fermi, “Motion of neutrons in hydrogenous substances,” *Ric. Sci.*, vol. 7, no. 2, pp. 13–52, 1936.

[19] H. B. Jansen and P. Ros, “Non-empirical molecular orbital calculations on the protonation of carbon monoxide,” *Chem. Phys. Lett.*, vol. 3, no. 3, pp. 140–143, 1969.

[20] S. F. Boys and F. Bernardi, “The calculation of small molecular interactions by the differences of separate total energies. Some procedures with reduced errors,” *Mol. Phys.*, vol. 19, no. 4, pp. 553–566, 1970.

[21] P. D. Haynes, C.-K. Skylaris, A. A. Mostofi, and M. C. Payne, “Elimination of basis set superposition error in linear-scaling density-functional calculations with local orbitals optimised in situ,” *Chem. Phys. Lett.*, vol. 422, no. 4–6, pp. 345–349, 2006.

[22] A. D. Boese, G. Jansen, M. Torheyden, S. Höfener, and W. Klopper, “Effects of counterpoise correction and basis set extrapolation on the MP2 geometries of hydrogen bonded dimers of ammonia, water, and hydrogen fluoride,” *Chem. Phys.*, vol. 13, no. 3, pp. 1230–1238, 2011.

[23] M. C. Payne, M. P. Teter, D. C. Allan, T. A. Arias, and ad J. D. Joannopoulos, “Iterative minimization techniques for ab initio total-energy calculations: molecular dynamics and conjugate gradients,” *Rev. Mod. Phys.*, vol. 64, no. 4, p. 1045, 1992.

[24] Kohn W. Nobel Lecture: Electronic structure of matter—wave functions and density functionals*. *Reviews of Modern Physics* October 1999.

.

3. Transport theory

3.1. Introduction

Theoretical and experimental studies of molecular electronics have been conducted [1][2]. That understanding the electron transport characteristics of nanoscale devices is one of the notable difficulties. When molecules (or other small structures) connect to the electrodes in this situation, phase-coherent transport can occur due to the molecules' energy levels. Because of the scattering processes that occur within the lead molecule, the contact strength between the molecule and the metal electrode is crucial in defining the transport parameters, as was described in Chapter 1. Therefore, Green's functional form is the most popular theoretical approach for examining scattering processes in these systems.

A key objective of Section 3.2 is to provide background knowledge for evaluating the Landauer formula. The Landauer equation can be used to explain the flow of electrical current because the energy of an electron moving through a nanoscale device is conserved. As a result, it is clear how the characteristics of electron transport relate to the transmission coefficient of electrons flowing from one conductor to the next across the scatterer. To calculate the transmission coefficient $T(E)$ for scattering, the computation of the transmission and reflection amplitudes introduced in Section 3.3 must first be solved. The Green's function approach for various transport systems is then presented in Section 3.4. Using a one-dimensional system as an example, one can easily determine a molecular compound's transmission coefficient $T(E)$. By using a one-dimensional system in which an electron with energy E flows from one electrode to the other, it is possible to derive the transmission coefficient $T(E)$ of a

molecular composition.

3.2. The Landauer equation

In terms of the scattering range represented by a Fermi distribution and the transmission coefficient of the connected electrodes, Landauer's equation [3][4] is a theoretical standard model for characterising the transport phenomena of non-interacting electrons. As seen in Figure 3.1, the system is presumed to be composed of two ideal ballistic electrodes connected to two electron reservoirs and a scattering region.

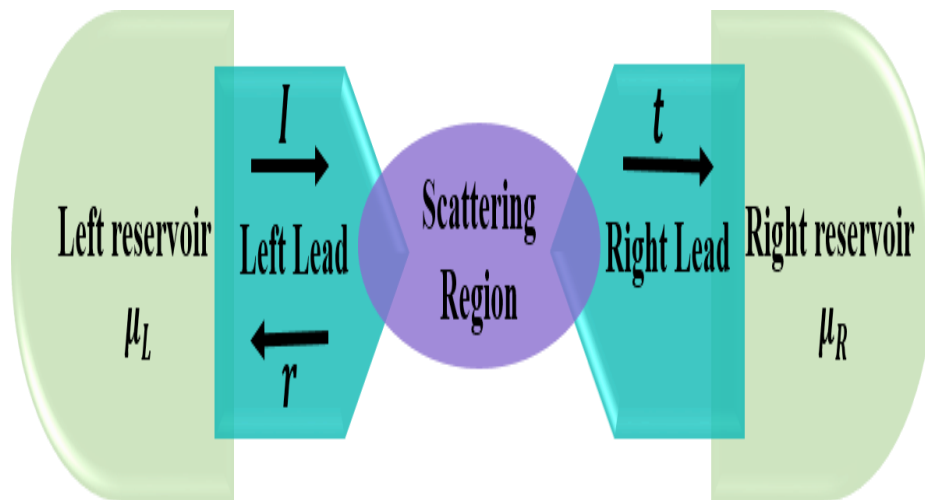


Fig (3.1): A scattering region linked to two electrodes, which are, in turn, connected to two reservoirs exhibiting chemical potential μ_L and μ_R . In the system, r is the amplitude of the transmitted wave and t is the amplitude of the wave that is reflected as a result of the left-side incident wave.

These reservoirs provide the system with electrons and due to their slightly different chemical potentials ($\mu_L - \mu_R > 0$), electrons are driven from the left to the right

reservoir. The current (I) in such a system at absolute zero (T = 0 K) results from electrons travelling to the left in the absence of scattering regimes and is in the energy range δE , $\delta I = ev_g \delta n$, $\delta n = \frac{\partial n}{\partial E} \delta E$. This is the number of electrons that move left for every unit of the energy interval δE . Group velocity is denoted by v_g .

The net current of the electrons is carried in the energy range $\delta E = \mu_L - \mu_R$ if the left- and right-hand electrons are emitted from the reservoir and this results in:

$$\delta I = ev_g \frac{\partial n}{\partial E} \delta E = ev_g \frac{\partial n}{\partial E} (\mu_L - \mu_R) \quad (3.1)$$

The terms are defined as follows: e represents the charge of an electron, v_g is group velocity, and n is the density of states (DOS).

$$\frac{\partial n}{\partial E} = \frac{\partial n}{\partial k} \frac{\partial k}{\partial E} = \frac{\partial n}{\partial k} \frac{1}{\hbar v_g} \quad (3.2)$$

This is a simplified formula for the dimension where $\frac{\partial n}{\partial k} = \frac{1}{2\pi} * 2$ for spin and group

velocities $v_g = \frac{1}{\hbar} \frac{dE}{dk}$ From 3.2:

$$\frac{\partial n}{\partial E} = \frac{2}{v_g \hbar} \quad (3.3)$$

Hence, formula 3.3 becomes

$$\delta I = \frac{2e}{\hbar} (\mu_L - \mu_R) \quad (3.4)$$

If δV is the voltage equivalent to the difference in chemical potential,

then $(\mu_L - \mu_R) = e\delta V$, obtaining:

$$\delta I = \frac{2e^2}{h} \delta V \quad (3.5)$$

According to Equation 3.5, the conductance of a perfect one-dimensional wire with an open channel and no scattering region is given by:

$$G_0 = \frac{2e^2}{h} \quad (3.6)$$

This is approximately $77.5\mu S$ (or $12.9k\Omega$ resistor). The transmitted current will be lowered by a factor of $T = |\vec{t}|^2$ and the reflected current will be $R = |\vec{r}|^2$ if the system has a scattering area. This results in a rightward flow of current through the spreader.

$$\delta I = \frac{2e^2}{h} T \delta V \quad (3.7)$$

Hence, after dividing the voltage difference:

$$G = \frac{\delta I}{\delta V} = \frac{2e^2}{h} T \quad (3.8)$$

This is the Landauer equation which incorporates conductance G and transfer probability T and evaluates it using the reservoir's Fermi energy for a one-dimensional system operating at absolute zero [16]. Specifically, Landauer's equation at finite temperature yields the net current flowing from the left electrode L to the right electrode R as

$$I = \frac{2e}{h} \int_{-\infty}^{+\infty} dE T(E) [f_L(E) - f_R(E)] \quad (3.9)$$

The charge, Planck's constant, transmission coefficient ($T(E)$) for the energetic electron E to go from one line to another within the molecule, and the Fermi distribution function (FDF) are the key ingredients in the formula above, where.

$$f_{L,R}(E) = \left(1 + e^{\frac{E - \mu_{L,R}}{k_B T}} \right)^{-1} \quad (3.10)$$

In this expression $\mu_{L,R}$ represent the left and right reservoirs' chemical potentials, respectively. The Boltzmann constant, k_B , is 8.62×10^{-5} eV/K. When the voltage V is symmetrically applied to the left and right reservoirs, the chemical reaction potentials will be:

$$\mu_L = E_F + \frac{eV}{2} \text{ and } \mu_R = E_F - \frac{eV}{2}. \text{ So, } I=0 \text{ when } f_L(E) = f_R(E) \quad (3.11)$$

This is because the only factors contributing to the net current are the variations in distributions. Therefore, the current is expressed as follows at absolute zero temperature and finite voltage:

$$I = \frac{2e}{h} \int_{E_F - \frac{eV}{2}}^{E_F + \frac{eV}{2}} dE T(E) \quad (3.12)$$

As a result, the conductance $G = I/V$ is determined by averaging $T(E)$ over an energy window

($k_B T = 25\text{meV}$ at ambient temperature) at Fermi energy. The conductivity is as follows at zero voltage and limited temperature:

$$G = \frac{1}{V} = G_0 \int_{-\infty}^{+\infty} dE T(E) \left[-\frac{df(E)}{dE} \right]_{\mu=E_F} \quad (3.13)$$

An approximately this is a thermal average of $T(E)$ over a window of energy with width $k_B T$, which at zero temperature reduce to

$$G = G_0 T(E) \quad (3.14)$$

3.3. Scattering matrix

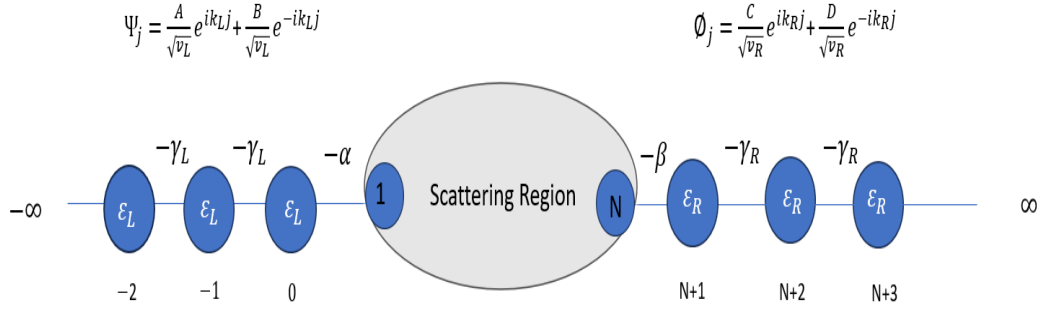


Fig (3.2): Illustrates a system comprising two distinct semi-infinite leads attached to a scattering region. This system encompasses a scattering arbitrary region with N sites ($j = 1, 2, \dots, N$), connected to one-dimensional leads from both left and right sides through matrix elements $(-\alpha, -\beta)$. The left lead encompasses sites ($j = -1, -2, \dots, -\infty$), while the right lead includes sites ($j = N + 1, N + 2, \dots, \infty$). Here, $\alpha_{R,L}$ denotes on-site energy, and $-\gamma_{R,L}$ represents the nearest coupling.

Understanding the transmission coefficients that appear in the above mentioned equation requires the scattering matrix to be computed. This is discovered by first looking at the solution of the time-independent Schrödinger equation.

$$\Psi_j = \frac{A}{\sqrt{v_r}} e^{ik_r j} + \frac{B}{\sqrt{v_r}} e^{-ik_r j} \quad (3.15)$$

where v_r is the group velocity of the left electrode, A and B are the amplitudes of the two incoming and outgoing waves moving from left to right, respectively, and A and B are the two waves' amplitudes. The energy carried by this eigenstate's current per unit is:

$$G I_{left} = |A|^2 - |B|^2 \quad (3.16)$$

The Schrödinger system's solution and accompanying current per unit for the right electrode is given by:

$$\Psi_j = \frac{C}{\sqrt{v_r}} e^{ik_r j} + \frac{D}{\sqrt{v_r}} e^{-ik_r j} \quad (3.17)$$

$$I_{right} = |C|^2 - |D|^2 \quad (3.18)$$

where C and D are the two entering and outgoing waves' relative amplitudes as they travel to the right and left. This probability conservation law is satisfied for all eigenstates and the current fulfils the connection $I_l = I_r$. Thus we have:

$$|A|^2 - |B|^2 = |C|^2 - |D|^2 \quad (3.19)$$

Therefore,

$$|A|^2 + |D|^2 = |B|^2 + |C|^2 \quad (3.20)$$

The following wavefunctions of the left and right electrodes are connected because the input current is equal to the output current.

$$Ae^{ikj} + Be^{-ikj} \quad (3.21)$$

$$Ce^{ikj} + De^{-ikj} \quad (3.22)$$

The incoming and outgoing coefficients must therefore be connected via a 2x2 matrix.

The scattering matrix S (matrix components S_{ij}) satisfies the following conditions:

$$\begin{bmatrix} B \\ C \end{bmatrix} = \begin{bmatrix} S_{11} & S_{12} \\ S_{21} & S_{22} \end{bmatrix} \begin{bmatrix} A \\ D \end{bmatrix} \quad (3.23)$$

$$B = S_{11}A + S_{12}D \quad (3.24)$$

$$C = S_{21}A + S_{22}D \quad (3.25)$$

It makes sense to use Equation 3.23 because B and C are the amplitudes of the incident wave which is the plane wave that carries the electrons to the scatterer. On the other hand, A and D are the amplitudes of the outgoing wave, so that equation (3.23) is of the form $|\text{out}\rangle = S|\text{in}\rangle$. To better comprehend the physical significance of the matrix elements S , it is interesting to consider the following two examples.

The reflected and transmitted amplitudes are shown by the symbols $B = r$ and $C = t$ in the first example where $A = 1$ and $D = 0$. In this equation, t is the transmitted wave's amplitude and r is the size of the wave's transmitted reflection by the wave coming from the left.

$$\begin{bmatrix} r \\ t \end{bmatrix} = \begin{bmatrix} S_{11} \\ S_{21} \end{bmatrix} \quad (3.26)$$

Because waves striking from the left cause reflection (r) and transmission (t), respectively, the physical meanings of the symbols S_{11} and S_{21} are reflection (r) and transmission. Case two: In the event that $A = 0$ and $D = 1$, the new matrix is:

$$\begin{bmatrix} B \\ C \end{bmatrix} = \begin{bmatrix} S_{12} \\ S_{22} \end{bmatrix} \quad (3.27)$$

The transmission (t') and reflection (r') amplitudes connected to the wave incident from the right are the physical meanings of the symbols S_{12} and S_{22} , respectively. The scattering matrix S is expressed in terms of transmission and reflection coefficients as follows:

$$S = \begin{bmatrix} S_{11} & S_{12} \\ S_{21} & S_{22} \end{bmatrix} = \begin{bmatrix} r & t' \\ t & r' \end{bmatrix} \quad (3.28)$$

From Eq. 3.20,

$$A^*A + D^*D = B^*B + C^*C \quad (3.29)$$

Therefore

$$(A^* \ D^*) \begin{pmatrix} A \\ D \end{pmatrix} = (B^* \ C^*) \begin{pmatrix} B \\ C \end{pmatrix} \quad (3.30)$$

The formula is then entered. 3.28 of 3.30 is written as follows:

$$(A^* \ D^*) \begin{pmatrix} A \\ D \end{pmatrix} = (A^* \ D^*) S^\dagger S \begin{pmatrix} A \\ D \end{pmatrix} \quad (3.31)$$

Because this is true for each of A , D , $S^\dagger S$, it is the identity matrix and can be written as follows:

$$\begin{bmatrix} r^* & t^* \\ t'^* & r'^* \end{bmatrix} \begin{bmatrix} r & t' \\ t & r' \end{bmatrix} = \begin{bmatrix} 1 & 0 \\ 0 & 1 \end{bmatrix} \quad (3.32)$$

According to scattering theory, the significant transport features are as follows:

$$|r^2| + |t^2| = 1 \Rightarrow R + T = 1 \quad (3.33)$$

$$|r'^2| + |t'^2| = 1 \Rightarrow R' + T' = 1 \quad (3.34)$$

∅

where the parameters T and R represent the transmission and the reflection coefficients, respectively.

3.4. Green's function

A method for obtaining the system's Green's function is presented in this section, which then allows us to compute reflection and transmission coefficients of diverse nanoscale structures. This provides a detailed description of the methods employed, starting with Green's functions for diverse nanoscale systems. Sections 3.4.1 and 3.4.2 discuss the formalism of Green's function for a straightforward discrete grid in one dimension. The Dyson equation is then used to integrate these separable lattice Green's functions to create the overall system Green function in the following phase (Sections 3.4.3 and 3.4.4).

3.4.1. Green's function of a doubly infinite chain

The form of Green's function for a double infinite chain with on-site energies of ϵ_0 and nearest-neighbour coupling parameter of $-\gamma$ is presented in this section and can be seen in Figure 3.3 These are perfect crystalline chains that are periodic in the horizontal transport direction.

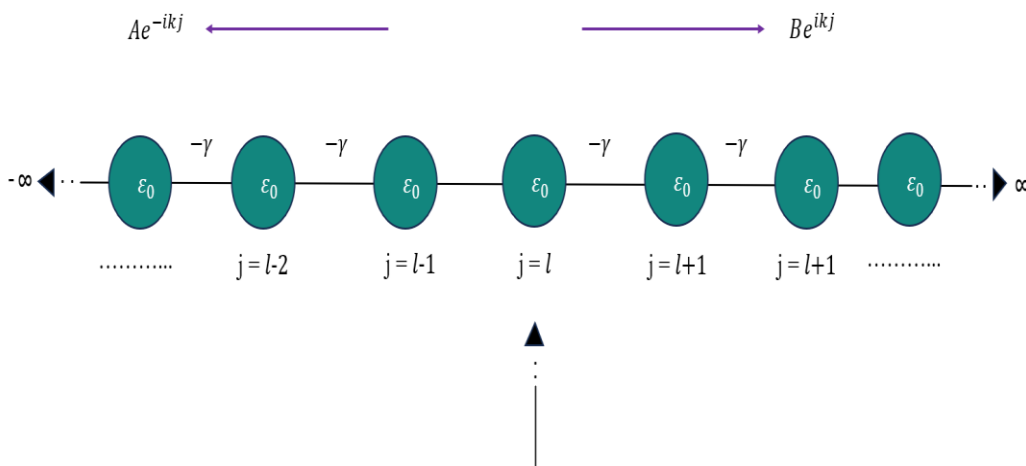


Fig (3.3): A doubly infinite chain where (ϵ_0) denotes on-site energy, and $(-\gamma)$ denotes the nearest coupling:

The time-independent Schrödinger equation for the system's wavefunction is:

$$(E - H)|\psi\rangle = 0 \quad (3.35)$$

As an alternative, the answer is the Hamiltonian's (H) Green's function of the system:

$$(E - H)G = I \quad (3.36)$$

For a finite system where H is a finite matrix, the formal solution of this equation is given by:

$$G = (E - H)^{-1} \quad (3.37)$$

For fixed l , the Green's function matrix element (G_{jl}), can be viewed as representing the wavefunction at point j resulting from a source at point l .

$$(E - H) G_{jl} = \delta_{jl} \quad (3.38)$$

δ_{jl} is called the Kronecker delta and is 1 if $j = l$ and 0 otherwise. The Green's function for a doubly infinite system can be written as:

$$\epsilon_0 G_{jl} - \gamma G_{j+l} - \gamma G_{j-1,l} + \delta_{jl} = E G_{jl} \quad (3.39)$$

The solution can be simply presented as follows:

$$G_{jl} = \begin{cases} Ae^{ikj} & j \geq l \\ Be^{-ikj} & j \leq l \end{cases} \quad (3.40)$$

The amplitudes of the two waves emanating from the left and right are represented by the arbitrary constants A and B , respectively. Equation (1) is satisfied by this response.

3.39 The Green's function must continue at the same location when $j = l$.

$$G_{jl} = \begin{cases} Ae^{ikj} \\ Be^{-ikj} \end{cases} \quad \begin{matrix} A = \alpha e^{-ikj} \\ B = \alpha e^{ikj} \end{matrix} \quad (3.41)$$

Therefore, substituting Eq. 3.41 to Eq. 3.39 yields:

$$(\epsilon_0 - E)\alpha - \gamma\alpha e^{ik} - \gamma\alpha e^{ik} = -1 \quad (3.42)$$

$$\gamma\alpha(2\cos k - 2e^{ik}) = -1 \quad (3.43)$$

$$\alpha = \frac{1}{2i\gamma\sin k} \quad (3.44)$$

$$\alpha = \frac{1}{i\hbar v} \quad (3.45)$$

In this expression, $\hbar v(E) = 2\gamma\sin k(E)$, where $v(E)$ is the group velocity. Combining the formula's two results (formula 3.45 and 3.41) gives the double infinite chain's Green's function [5][6].

$$G_{jl} = \psi_j^l = \frac{e^{ik(E)|j-l|}}{i\hbar v(E)} \quad (3.46)$$

Thus, as illustrated in Figure 3.2, G_{jl} is the delayed Green's function reflecting the waves resulting from source at $j=l$.

This equation pertains to the commonly known retarded Green's function.

More generally,

$$G_{jl} = \psi_j^l = \frac{e^{ik(E)|j-l|}}{i\hbar v(E)} + Ae^{ikj} + Be^{-ikj} \quad (3.47)$$

3.4.2. Green's function of a semi-infinite one-dimensional chain

To obtain the Green's function of the semi-infinite chain, the Green's function is used along with the double infinite chain issue and the requisite boundary conditions.

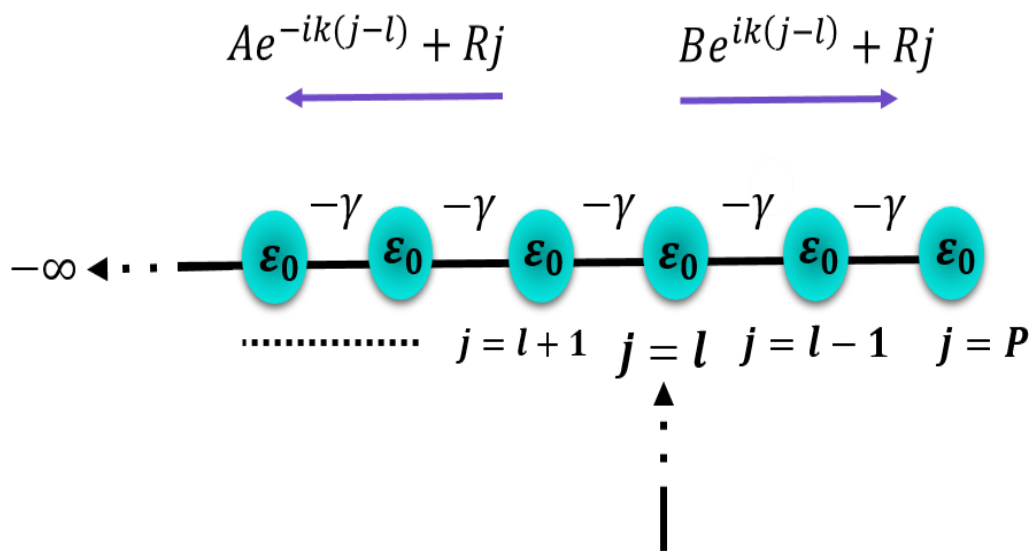


Fig (3.4): The semi-infinite linear chain with potential energy ϵ_0 and coupling $-\gamma$ ending at position P.

At location P, this infinite chain must come to an end. The constraint $\psi_{p+1}^l = 0$ is produced as a result of the fact that Green's function vanishes at position $P + 1$ and that no points exist between $P + 1$ and $P+1 > 0$.

For such a system, there will be a reflected wave $R_j = Ae^{-ikj}$. In light of this, the generic Green's function at G_{P+1} is expressed as:

$$G_{P+1} = \frac{e^{ik(P+1-l)}}{i\hbar v} + Ae^{-ik(P+1)} = 0 \quad (3.48)$$

This yield:

$$A = -e^{ik[2(P+1)-l]} \quad (3.49)$$

So, the general delayed Green's function for a semi-infinite linear chain is:

$$g_{jl} = \frac{e^{ik|j-l|} - e^{-ikj(j+l)}e^{ik(2(P+1))}}{i\hbar v} \quad (3.50)$$

This satisfies $\psi_{P+1}^l = 0$ and $\psi_j^{P+1} = 0$.

$$g_{P+1,l} = \frac{e^{ik|(P+1)-l|} - e^{-ikj(P+1)}e^{-ikl}}{i\hbar v} = 0,$$

because the absolute value will vanish as the Green's function vanishes at site P .

The Green's function ending at point P with a source of l is:

$$g_{jl} = \frac{e^{ik|j-l|} - e^{-ikj(j+l)}e^{ik(2(P+1))}}{i\hbar v} \quad (3.51)$$

From the boundary conditions where $l = P$:

$$g_{p,p} = \frac{1-e^{2ik}}{i2\gamma\text{sink}} = \frac{e^{ik}(e^{ik} - e^{-ik})}{i2\gamma\text{sink}} \quad (3.52)$$

$i2\text{sink}$ terminates at the dominator when $(e^{-ik} - e^{ik}) = i2\text{sink}$. This shows that the

Green's function on the terminal site p is:

$$g_{p,p} = -\frac{e^{ik}}{\gamma} \quad (3.53)$$

This is known as the ‘surface Green's function’ for semi-infinite chains.

3.4.3 One-dimensional scattering region.

For a system with two one-dimensional tight binding semi-infinite leads coupled by a scatter, the goal of this section is to derive the complete Green's function. According to Figure 3.5, both leads have the same on-site energy (ϵ_0) and hopping elements ($-\gamma$) .

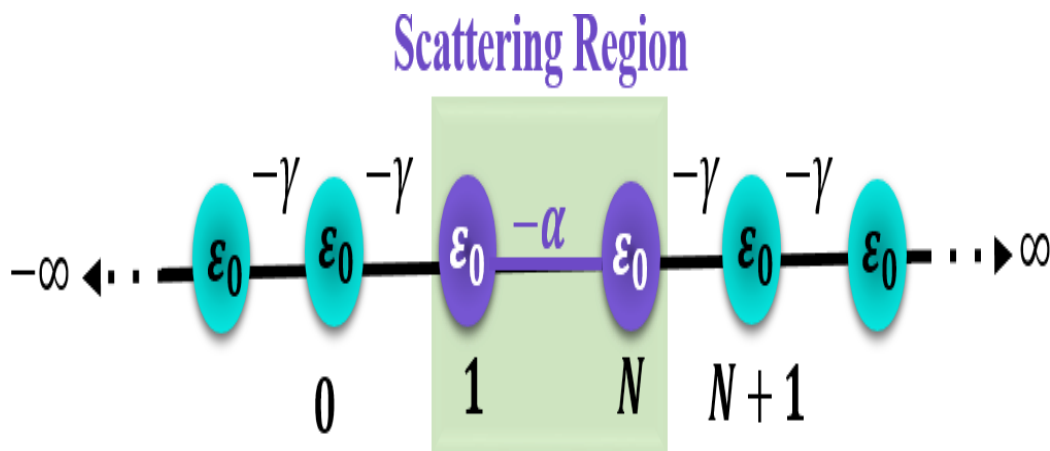


Fig (3.5): A one-dimensional scattering region attached to one-dimensional leads using a tight-binding model.

This infinite system's Hamiltonian is represented as an infinite matrix as follows:

$$H = \begin{pmatrix} \bullet & \bullet & 0 & 0 & 0 & 0 & 0 & 0 \\ \bullet & \bullet & -\gamma & 0 & 0 & 0 & 0 & 0 \\ 0 & -\gamma & \varepsilon_o & -\gamma & 0 & 0 & 0 & 0 \\ 0 & 0 & -\gamma & \varepsilon_o & -\alpha & 0 & 0 & 0 \\ 0 & 0 & 0 & -\alpha & \varepsilon_o & -\gamma & 0 & 0 \\ 0 & 0 & 0 & 0 & -\gamma & \varepsilon_o & -\gamma & 0 \\ 0 & 0 & 0 & 0 & 0 & -\gamma & \bullet & \bullet \\ 0 & 0 & 0 & 0 & 0 & 0 & \bullet & \bullet \end{pmatrix} = \begin{pmatrix} H_L & V_c \\ V_c^\dagger & H_R \end{pmatrix} \quad (3.54)$$

For the left lead and right lead in this matrix, H_L and H_R are their respective Hamiltonians and V_c is the coupling matrix that connects them. Thus, it is not possible to directly solve the following equation to get the Green's function of this issue because it is a matrix with infinite elements.

$$G = (E - H)^{-1} \quad (3.56)$$

It is useful to look at the Green's function g of the decoupled two semi-infinite leads:

$$g = \begin{pmatrix} -\frac{e^{ik}}{\gamma} & 0 \\ 0 & -\frac{e^{ik}}{\gamma} \end{pmatrix} = \begin{pmatrix} g_L & 0 \\ 0 & g_R \end{pmatrix} \quad (3.57)$$

Then Dyson's equation can be utilised to obtain Green's function after accounting for the interaction:

$$G = (g^{-1} - V)^{-1} \quad (4.58)$$

The interaction between the two leads is described by the operator V in the following form:

$$V = \begin{pmatrix} 0 & \alpha \\ \alpha & 0 \end{pmatrix} \quad (4.59)$$

Subsequently, by resolving Dyson's equation, Green's function for this system is revealed:

$$G = \frac{1}{\gamma^2 e^{-2ik} - \alpha^2} \begin{pmatrix} -\gamma e^{-ik} & \alpha \\ \alpha & -\gamma e^{-ik} \end{pmatrix} \quad (4.60)$$

The Fisher-Lee relation can be used to determine the transmission (\vec{t}) and reflection (\vec{r}) amplitudes after obtaining the Green's function for this system. This connects the scattering amplitudes of a scattering problem to Green's function. Fisher-Lee relationships are provided by:

$$r = i\hbar v G_{0,0} - 1 \quad (4.61)$$

$$t = i\hbar v G_{0,N+1} e^{ik} \quad (4.62)$$

The same process can be used to obtain these coefficients for particles travelling from the right. These coefficients' amplitudes correspond to particles impacting from the left. These coefficients provide the following definition of probability:

$$R = |r|^2 \quad (3.63)$$

$$T = |t|^2 \quad (3.64)$$

Finally, by constructing the full scattering matrix and using the Landauer formula, it is possible to calculate the zero-bias conductance of the junction.

3.5 conclusion

This chapter delves into the examination of electron transport in nanoscale structures, employing a quantum transport theory based on the time-independent Schrödinger equation. The approach is applied to diverse one-dimensional crystalline models, and their eigenvalue problems are solved using a tight-binding model (TBM). Through this, common quantum properties, such as eigenfunctions and eigenvalues of the Hamiltonian matrix, are investigated.

Additionally, the concept of quantum system is explained using the time-dependent Schrödinger equation. To illustrate these concepts further, the scattering theory is introduced with a focus on a doubly infinite chain one-dimensional structure. This provides insights into the relationship between the scattering matrix and transport properties.

To estimate the electrical conductance through the scattering region connected to two electrodes, the Landauer formula is employed. Moreover, the Green's function formalism is utilized to calculate the transmission coefficient for various simple transport regimes and their generic transport characteristics.

Bibliography:

- [1] C. Joachim and M. A. Ratner, "Molecular electronics: Some views on transport junctions and beyond," *Proc. Natl. Acad. Sci. U. S. A.*, vol. 102, no. 25, pp. 8801–8808, 2005.
- [2] Xiang D, Wang X, Jia C, Lee T, Guo X. Molecular-Scale Electronics: From Concept to Function. *Chem Rev* 2016; 116:4318-4440.
- [3] R. Landauer, "Spatial variation of currents and fields due to localized scatterers in metallic conduction," *IBM J. Res. Dev.*, vol. 1, no. 3, pp. 223–231, 1957.
- [4] M. Büttiker, Y. Imry, R. Landauer, and S. Pinhas, "Generalized many-channel conductance formula with application to small rings," *Phys. Rev. B*, vol. 31, no. 10, p. 6207, 1985.
- [5] S. Datta, *Electronic transport in mesoscopic systems*. Cambridge University Press, 1997.
- [6] E. N. Economou, *Green's functions in quantum physics*, vol. 7. Springer Science & Business Media, 2006.
- [7] G. Breit and E. Wigner, "Capture of slow neutrons," *Phys. Rev.*, vol. 49, no. 7, p. 519, 1936.
- [8] S.-H. Ke, W. Yang, and H. U. Baranger, "Quantum-interference-controlled molecular electronics," *Nano Lett.*, vol. 8, no. 10, pp. 3257–3261, 2008.
- [9] R. Stadler, "Quantum interference effects in electron transport through nitrobenzene with pyridil anchor groups," *Phys. Rev. B*, vol. 80, no. 12, p. 125401, 2009.
- [10] T. A. Papadopoulos, I. M. Grace, and C. J. Lambert, "Control of electron transport through Fano resonances in molecular wires," *Phys. Rev. b*, vol. 74, no. 19, p. 193306,

2006.

[11] C. Lambert, “Basic concepts of quantum interference and electron transport in single molecule electronics,” *Chem. Soc. rev.*, vol. 44, no. 4, pp. 875–888, 2015.

[12] J. C. Cuevas and E. Scheer, *Molecular electronics: an introduction to theory and experiment*. World Scientific, 2010.

[13] C. A. Stafford, D. M. Cardamone, and S. Mazumdar, “The quantum interference effect transistor,” *Nanotechnology*, vol. 18, no. 42, p. 424014, 2007.

[14] C. M. Finch, V. M. Garcia-Suarez, and C. J. Lambert, “Giant thermopower and figure of merit in single-molecule devices,” *Phys. Rev. B*, vol. 79, no. 3, p. 33405, 2009.

[15] C. J. Lambert, H. Sadeghi, and Q. H. Al-Galiby, “Quantum-interference-enhanced thermoelectricity in single molecules and molecular films,” *Comptes Rendus Phys.*, vol. 17, no. 10, pp. 1084–1095, 2016.

[16] C. J. Lambert, *Quantum Transport in Nanostructures and Molecules*. IOP Publishing, 2021.

[17] H. Sadeghi, S. Sangtarash, and C. J. Lambert, “Oligoynes Molecular Junctions for Efficient Room Temperature Thermoelectric Power Generation,” *Nano Lett.*, vol. 15, no. 11, pp. 7467–7472, 2015.

[18] Lin L, Jiang J, Luo Y. Elastic and inelastic electron transport in metal–molecule(s)–metal junctions. *Physica E: Low-dimensional Systems and Nanostructures* 2013; 47:167-187.

[19] A. Kambili, G. Fagas, V. I. Fal’ko, and C. J. Lambert, “Phonon-mediated thermal conductance of mesoscopic wires with rough edges,” *Phys. Rev. B-Condensed Matter*, vol. 60, no. 23, pp. 593–596, 1999.

[20] Scheer E, Cuevas JC. *Molecular electronics: an introduction to theory and experiment*. World Scientific; 2017.

[21] M. Famili, I. Grace, H. Sadeghi, and C. J. Lambert, “Suppression of Phonon Transport in Molecular Christmas Trees,” *ChemPhysChem*, vol. 18, no. 10, pp. 1234–1241, 2017.

4. Quantum interference in polycyclic aromatic molecules

4.1 Introduction

One of the key challenges in the field of molecular electronics is to gain a deeper understanding of the fundamental behaviour of electron transport through single-molecule junctions. To expand our knowledge, multiple experimental methods have been developed to establish contact with individual molecules. It has become increasingly apparent in recent years that the electronic properties of a molecular junction are determined by the whole system, including the metal-molecule-metal combination. A single-molecule junction comprises three constituents, specifically the molecular bridge, the two electrodes and the two anchors. An anchor is employed to bind the molecule to the electrodes. The essential charge-transport features of a junction are significantly influenced by the electronic connection between its individual components [6]. This raises an important question: what occurs when an isolated single molecule is brought into contact with metal (e.g., gold) electrodes? An isolated molecule contains a set of discrete energy levels, which are known as frontier orbitals (e.g., the HOMO and LUMO), whereas metal electrodes consist of a band structure that includes a continuous range of states, with a precisely defined Fermi energy. When these two components are brought into proximity, they interact with each other, resulting in various physical effects. For example, there is a transfer of charge between the two systems, which means that donating or withdrawing electrons from the molecule affects both the energy levels of the molecule and the contact. As a result of this charge transfer, the highest occupied molecular orbital (HOMO) and the lowest unoccupied molecular orbital (LUMO) may be displaced upwards or downwards, causing a more pronounced or less pronounced

slope in the transmission function at the Fermi level [7]. The chemical bonds in the anchor group, which chemically bind the molecules to the

electrodes, also influence the position of the molecular orbitals in relation to the electrodes' Fermi level. The aim of this chapter is to resolve the following paradox: why does meta connectivity show destructive quantum interference in a tight binding model, but in certain cases, does not show DQI in a DFT calculation on the same system? To answer this question, a family of molecules is selected to study the difference between meta and para connectivity with two different types of linkers, such as thiol (-SH) and methyl sulphide (-SMe), which couple different molecules to Au electrodes.

4.2 Quantum interference

Quantum interference (QI) effects have attracted significant interest in the area of charge transport at the single-molecule level owing to their exceptional potential to modulate the charge transport across molecular materials and devices at a phase-coherent level in experimental studies [8]-[10]. I can either increase or decrease conductance in molecular systems, a phenomenon known as constructive (CQI) or destructive (DQI) quantum interference, respectively [11]. Since 1988, extensive theoretical and experimental research has been carried out on QI. To illustrate QI, a simple setup can be utilised, consisting of a benzene ring connected to electrodes via para and meta connectivity (see Figure 4.1) within a tight binding model. In this instance, a quantum interference effect arises when electrons of energy E move through various paths from one point to another

in the ring and when they reach the point of exit, they can interfere constructively or destructively.

4.3 Tight binding calculation

The tight-binding model (TBM) or the linear combination of atomic orbitals (LCAO) method represents an approach to compute electronic band structures by employing a set of wave functions derived from the superposition of wave functions of isolated atoms situated at each atomic site. In the TBM, it is posited that electrons can interact with their nearest neighbor sites^{1–3}. In actuality, atomic wave functions exhibit an exponential decay as the distance increases. Consequently, it is a judicious approximation to account solely for the nearest neighbor interaction in describing the system. The equation representing the time-dependent Schrödinger equation is provided as follows:

$$H_{(x)}\Psi_{(x,t)} = i \hbar \frac{\partial}{\partial t} \Psi_{(x,t)} \quad (4.1)$$

In this expression, Ψ represents the wave function of the quantum system, \hbar is the reduced Planck constant ($\frac{h}{2}$), and H corresponds to the Hamiltonian, defined as follows:

$$H_{(x)} = \frac{-\hbar^2}{2m} \nabla^2 + V_{(x)} \quad (4.2)$$

We assume the wave function as a product of spatial and temporal terms:

$$\Psi_{(x,t)} = \Phi_{(x)}\theta_{(t)} \quad (4.3)$$

The Schrödinger equation transforms into a pair of ordinary differential equations:

$$\frac{1}{\theta_{(t)}} \frac{d}{dt} \theta_{(t)} = -\frac{iE}{\hbar} \quad (4.4)$$

And

$$H \Phi_{(x)} = E \Phi_{(x)} \quad (4.5)$$

The solution to equation (4.1) is

$$\Psi_{(x,t)} = \Phi_{(x)} e^{\frac{-iEt}{\hbar}} \quad (4.6)$$

The most general solution is a linear combination of these solutions:

$$\Psi_{(x,t)} = \sum_j \Psi_j \Phi_{j(x)} e^{\frac{-iEt}{\hbar}} \quad (4.7)$$

The wave function $\Psi(x)$ can be expressed as a linear superposition of the form:

$$\Psi_{(x)} = \sum_j \Psi_j \Phi_{j(x)} \quad (4.8)$$

$\Phi_{j(x)}$ is a localized basis function on a particular site j , Ψ_j and is the time-independent amplitude of the wave function on site j , and the probability of finding an electron on site j is $|\Psi_j|^2$. The Hamiltonian matrix elements can be expressed as:

$$H_{ij} = \langle \Phi_{i(x)} | H | \Phi_{i(x)} \rangle = \int dx \Phi_{i(x)}^* H \Phi_{j(x)} \quad (4.9)$$

The following section describes the model of chain of atoms, with a single orbital on each atom. Since the electrons interact with its nearest neighbour sites, all terms $\langle \Phi_{i(x)} | H | \Phi_{i(x)} \rangle$ with $|i - j| > 1$ are small, and therefore neglected.

Selecting a specific atom situated at site j , the time-dependent Schrödinger equation is subsequently expressed as follows:

$$i \hbar \frac{\partial \Psi_j}{\partial t} = \varepsilon_j \Psi_j + H_{j,j-1} \Psi_{j-1}(t) + H_{j,j+1} \Psi_{j+1}(t) \quad (4.10)$$

Where $\varepsilon_j = H_{jj}$ is the onsite energy of atomic orbital j .

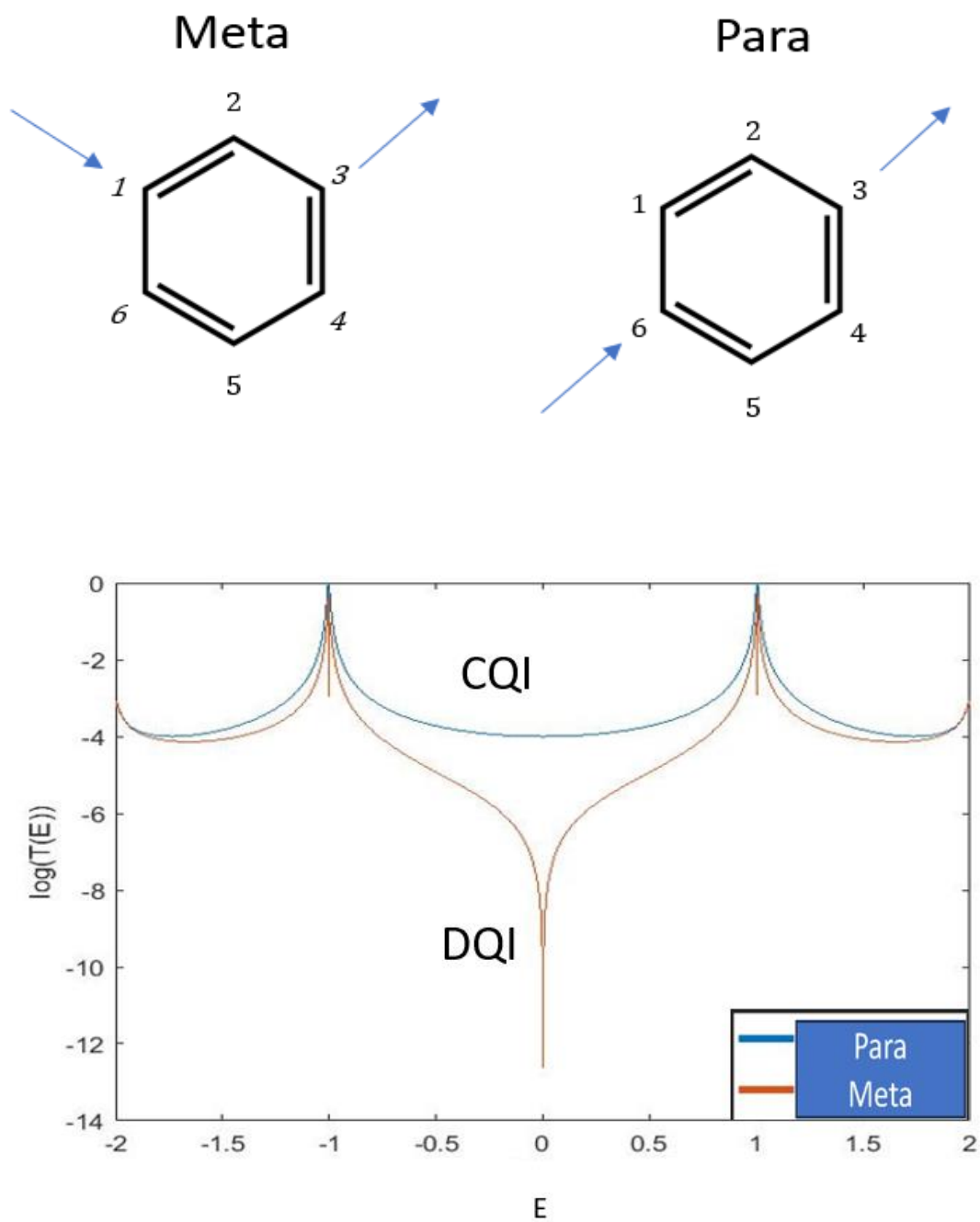


Fig (4.1): TBM constructive and destructive transmission curves of the benzene ring shown in the above panel with para and meta connectivity, respectively.

The top panel of Figure 4.1 shows the different connectivity of benzene. Meta connectivity is defined by injecting electrons at atom number 1 and collecting electrons at atom number 3, whereas para connectivity is defined by injecting electrons at atom

number 1 and collecting electrons at atom number 4. The bottom panel of figure 4.1 shows that within a TMB, meta connectivity shows DQI, whereas para connectivity shows CQI. In the tight binding case, it is possible to explore certain concepts. Here we are looking at the effect of connectivity to the electrode. When considering the meta connectivity compared with the para connectivity, the transmission coefficient is quite different. In the meta case, there is a dip in the middle of the HOMO-LUMO gap, which is a signature of DQI but there is no dip in the para case. This is a prediction from TB theory which now compare with DFT. Although, TBM has been shown to pick up the main features of the DFT [12,16], we now show that in this case, DFT does not show DQI with meta connectivity.

4.4 DFT calculation

In this section, computations are performed on benzene with meta- and para-connectivity using various linkers between the benzene core and the anchor groups. The calculations were conducted using SIESTA, a software program designed for density functional theory (DFT) calculations. DFT is a method that solves the many-body Schrödinger equation by transforming it into a non-interacting electron problem. Initially, the molecules undergo relaxation by calculating the wavefunction and energies for a specific configuration. The atomic positions are adjusted iteratively to minimise the total energy of the system, with subsequent energy and wavefunction calculations performed for the updated coordinates. This iterative process continues until the forces acting on each atom fall below a certain tolerance threshold (0.01 eV/Å). For each molecule, several wavefunctions are presented around Fermi energy. For most of the molecules, the transmission properties are mainly determined by the HOMO and LUMO, because the Fermi energy lies in between them [12]-[16].

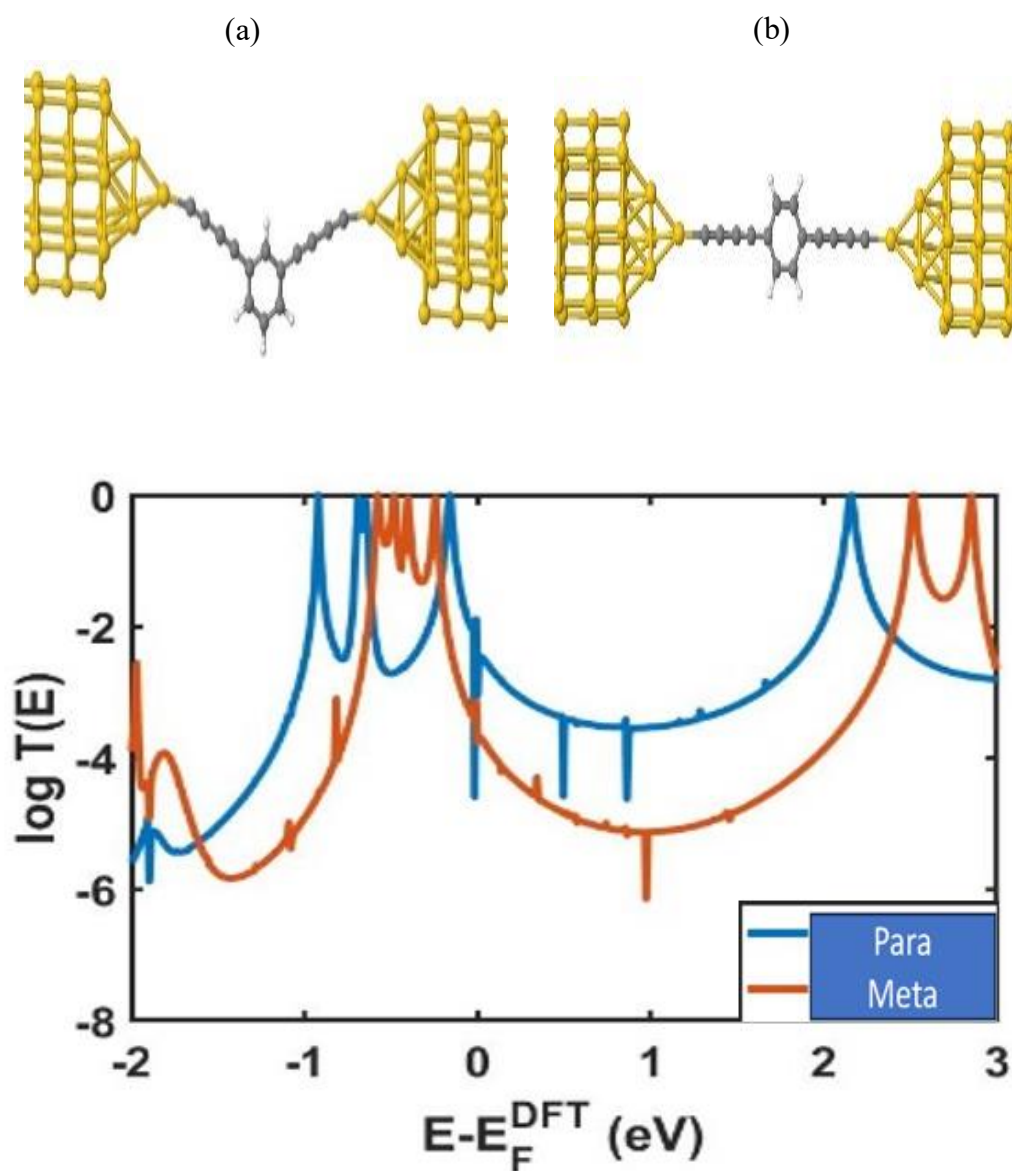


Fig (4.2): DFT-based transmission functions for Benzene with two triple bonds (a) meta connectivity (b) para connectivity.

The top panel of Figure 4.2 shows how benzene is linked to the electrode in a junction via meta and para connectivities. There are certain agreements and disagreements with the TB results in Figure 4.1. The blue curves have the same qualitative behaviours. Also,

the red curves are lower than the blue curves. However, surprisingly, the red curve from DFT does not show a sharp DQI feature near the middle of the HOMO-LUMO gap. To solve this mystery, I shall examine a series related molecules with different types of linkers connected to the central core. In the case of oligoynes linkers formed from a chain of carbon atoms connected by triple bonds. It is important to note that triple bonds have sigma bond in addition to P_y and P_z bonds.

The studied molecular cores are as follows:

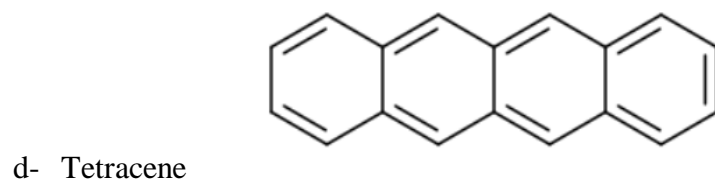
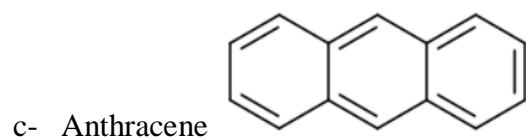
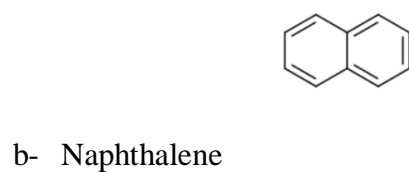
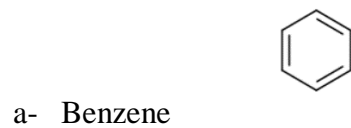


Fig (4.3) The chemical structures of the (a) benzene, (b) naphthalene, (c) anthracene and (d) tetracene.

4.5 Theory of room-temperature QI effects.

Before computing transmission coefficients, it is useful to explain a simple orbital product rule. Transmission of electrons whose energy resides inside the energy gap between the HOMO and LUMO is mediated by tunnelling and the appearance of DQI or CQI can be understood qualitatively by examining the inter-orbital QI between the HOMO and LUMO. To understand why this is the case, note that if the coupling between the molecule and the electrode is weaker, the effect of QI on transport properties can be predicted by examining the Green's function $G(E_F)$ for the isolated molecule. The transmission amplitude of an electron with energy E_F from site i to j is then proportional

$$\text{to } |G_{i,j}(E_F)|^2, \text{ where } G_{i,j}(E_F) = \sum_{n=1}^N \left(\frac{\phi_i^n \phi_j^n}{E_F - \epsilon_n} \right)$$

In this expression, ϕ_i^n is the amplitude of the n^{th} molecular orbital (MO) on site i and ϵ_n is the corresponding MO energy level. If the Fermi energy is located within the HOMO-LUMO gap, then as a first approximation, one can retain only HOMO and LUMO states in the above sum, because they correspond to the smallest denominators and the largest values of $\frac{1}{E_F - \epsilon_n}$. Furthermore, for a qualitative discussion, it is useful to consider the case where E_F is placed in the middle of the HOMO-LUMO gap.[17]-[22], in which case we obtain

$$G_{i,j}(E_F) \approx \frac{\phi_i^{\text{HOMO}} \phi_j^{\text{HOMO}} - \phi_i^{\text{LUMO}} \phi_j^{\text{LUMO}}}{\Delta}$$

where Δ is one half of the HOMO-LUMO gap.

Clearly, if $\phi_i^{HOMO} \phi_j^{HOMO} = \phi_i^{LUMO} \phi_j^{LUMO}$, then $G_{i,j}(E_F) \approx 0$ and DQI occurs. More generally, we can say that if the HOMO product $\phi_i^{HOMO} \phi_j^{HOMO}$ has the same sign as the LUMO product $\phi_i^{LUMO} \phi_j^{LUMO}$, then there will be a tendency for the HOMO product to cancel the LUMO product and $G_{i,j}(E_F)$ will be smaller than the case where the products have opposite signs. In other words, if the HOMO product $\phi_i^{HOMO} \phi_j^{HOMO}$ has the same sign as the LUMO product $\phi_i^{LUMO} \phi_j^{LUMO}$, then DQI is a possibility, whereas CQI is more likely when the products have opposite signs.

For a molecule whose structure is invariant under a 180° rotation about a vertical axis, its molecular orbitals are either symmetric or anti-symmetric under such a rotation. If the HOMO and LUMO have opposite symmetries, then CQI is likely, whereas if they have the same symmetry, DQI is likely. This is the case for the molecules shown below.

To understand why the HOMO and LUMO have opposite symmetries, consider starting from two decoupled carbon chains, each with their individual MOs. Now select one MO from each chain, lying closest to the HOMO-LUMO gap of the molecule. These ‘chain MOs’ form a two-level system, which are coupled by the central core of the molecule. If the coupling is denoted Δ , then the HOMO-LUMO gap of the two-level system is 2Δ and the HOMO and LUMO of the molecule are bonding and anti-bonding combinations of the ‘chain MOs’. Consequently, the HOMO and LUMO have opposite symmetries. Furthermore, the coupling Δ between the chains is expected to become weaker as the number of rings in the central core increase and therefore as shown in the table below, the HOMO-LUMO gap (2Δ) decreases as the number of rings increases.

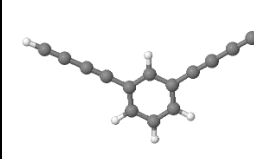
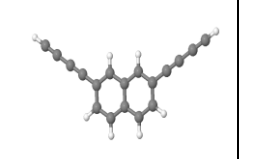
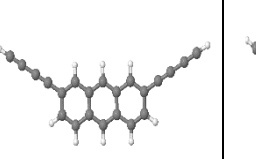
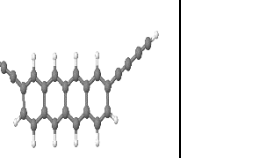
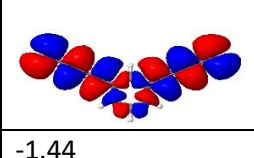
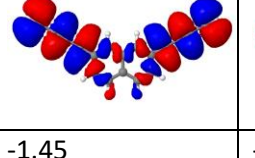
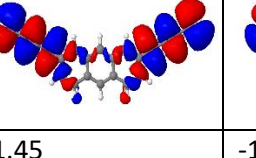
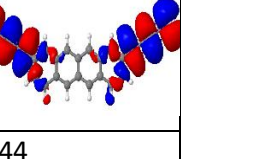
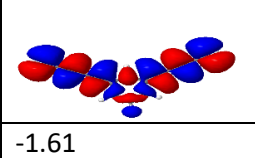
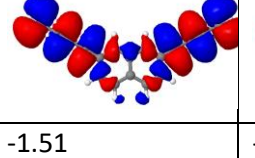
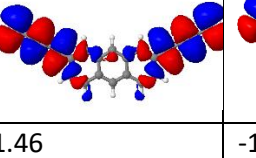
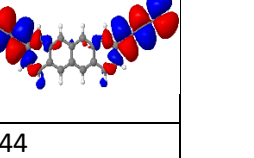
	Benzene	Naphthalene	Anthracene	Tetracene
Structur es				
LUMO				
E(eV)	-1.44	-1.45	-1.45	-1.44
LUMO				
E(eV)	-1.61	-1.51	-1.46	-1.44

Fig (4.4): Frontier molecular orbitals of the four studied molecules with their eigenvalues obtained from DFT, where red represents to positive, and blue indicates negative regions of the wave functions.

The product rule enables molecules to be identified which may exhibit DQI rather than CQI. Regarding the orbital product rule, here an example of the HOMOs and LUMOs of these two molecules, where red indicates positive amplitude and blue a negative amplitude. The orbital product rule tells us that it is necessary to look at the signs of those amplitudes at the very end of the molecules. The p orbital is parallel to the plane of benzene, and this is why orbitals are picked out.

Looking at the left molecule (Benzene), two is apparent that the energy level difference between 1.61 and 1.44 is approximately $2\Delta = 0.17\text{eV}$. With regards to the next molecule, the difference between 1.51 and 1.45 is $2\Delta = 0.06\text{eV}$. Therefore, the energy level

splitting for that molecule is much smaller and, therefore, the coupling between two alkyne chains is becoming weaker. Finally, with regards to the right one (the last molecule, Tetracene), they are almost decoupled and the difference between them is zero.[12]-[14].

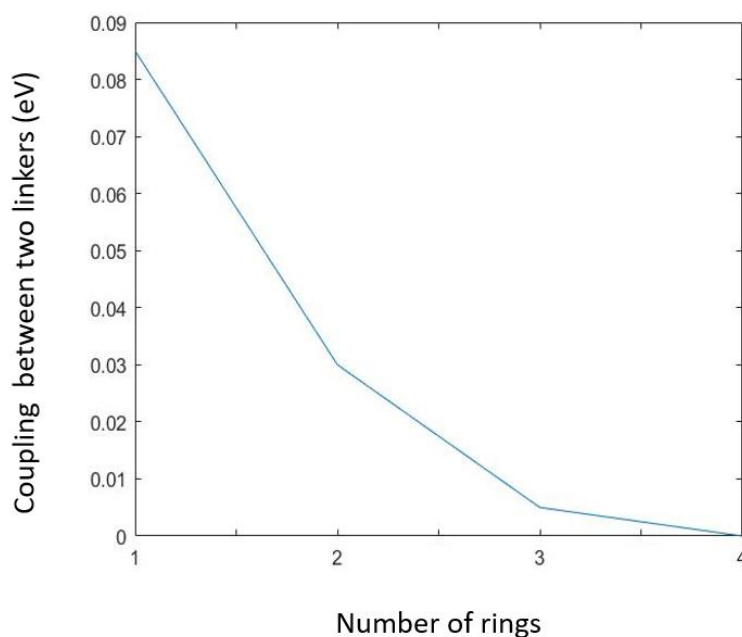


Fig (4.5) Correlation between the coupling of two linkers (measured in electron volts) and the number of rings.

The two-level model is associated with the HOMO-LUMO gap (Highest Occupied Molecular Orbital - Lowest Unoccupied Molecular Orbital) gap. As per the two-level model, the connection between the two sides can be associated with the energy disparity between the bonding and anti-bonding energy levels divided by two. The diminishing coupling with an increasing number of rings in the central core is depicted in Figure 4.6. This trend is evident in the molecular orbitals displayed in Figure 4.5, where there is a

significant amplitude on the benzene core but a notably smaller amplitude in the central cores of the other molecules.

$$\Delta = \frac{\text{bonding energy} - \text{anti bonding energy}}{2}$$

4.6 Frontier molecular orbitals and Green's function.

HOMO and LUMO for the naphthalene molecule are depicted in Figure 4.6 [17]. The molecular orbitals of a molecule can form various paths for the flow of electricity, depending on their connectivity to external electrodes.

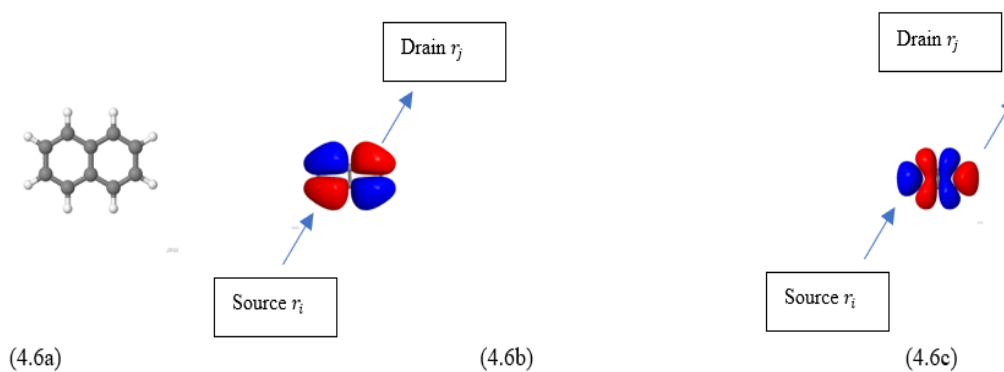


Fig (4.6): Frontier molecular orbitals. (4.6a) A lattice representation and frontier molecular orbitals of Naphthalene; (4.6b) HOMO wave function for Naphthalene; (4.6c) LUMO wave function for Naphthalene.

The above product rule describes the effect of "inter-orbital QI" provides insight into the connection between molecular orbitals and quantum interference. As an example, Figure 4.6 shows that, the HOMO product $\psi^{HOMO}(r_1) \psi^{HOMO}(r_2)$ (i.e. $-*-$) is positive, whereas the LUMO product $\psi^{LUMO}(r_1) \psi^{LUMO}(r_2)$ (i.e. $-*+$) is negative, so this connectivity exhibits CQI and allows for high electrical conductance, which depends on the amplitude of the wave function at the source and drain. Despite the simplicity of this product rule, its qualitative predictions have been successfully validated against experimental data [25].

4.7 Transmission coefficient

In this section, the transmission coefficients $T(E)$ for the above molecule with different anchors and linkers are computed using DFT. The steps for calculating the transmission coefficient are as follows. First, the molecule is relaxed using SIESTA. Finally, the $T(E)$ for molecules with different anchors are computed, and CQI or DQI features are identified for para and meta connectivities.

4.7.1 Transmission coefficient for the benzene core with different linkers connected to gold electrodes:

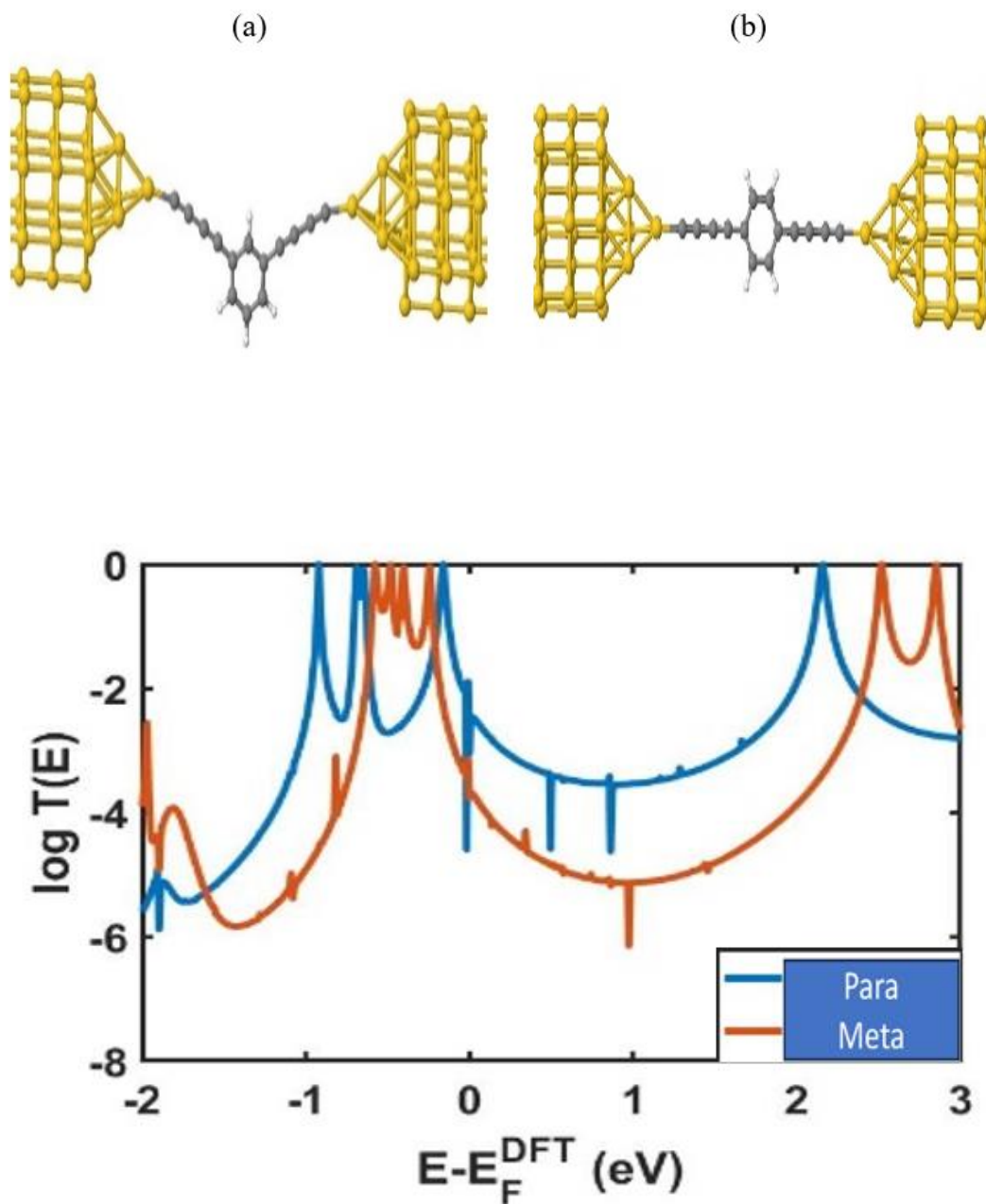


Fig (4.7) DFT-based transmission functions for Benzene with two triple bonds (a) meta connectivity (b) para connectivity.

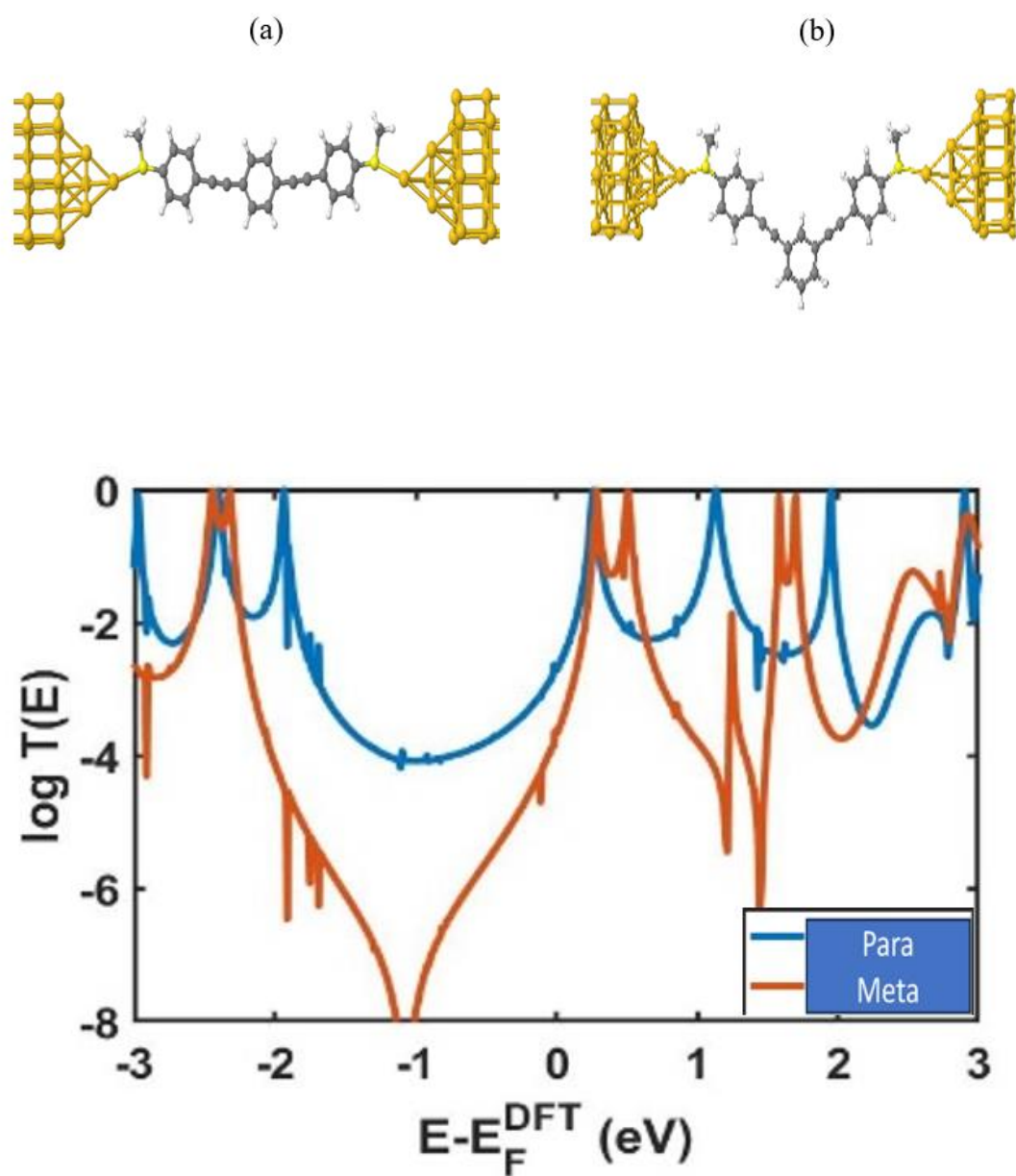


Fig (4.8) DFT-based transmission functions for Benzene connected to the gold via SMe-anchor at different connectivities (a) meta connectivity (b) para connectivity.

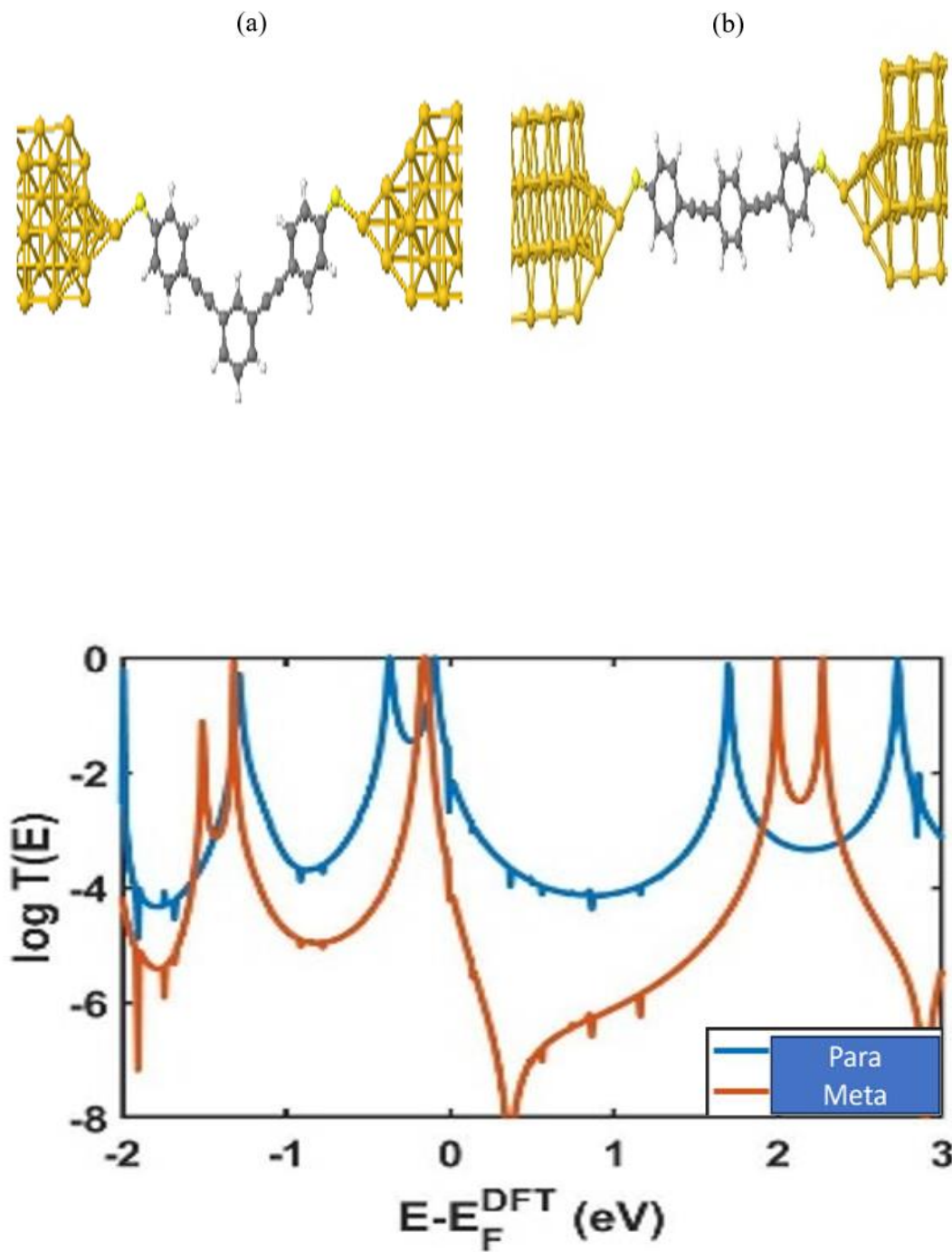


Fig (4.9) DFT-based transmission functions for Benzene connected to the gold via Sulphur (S)-anchor at different connectivities (a) meta connectivity (b) para connectivity.

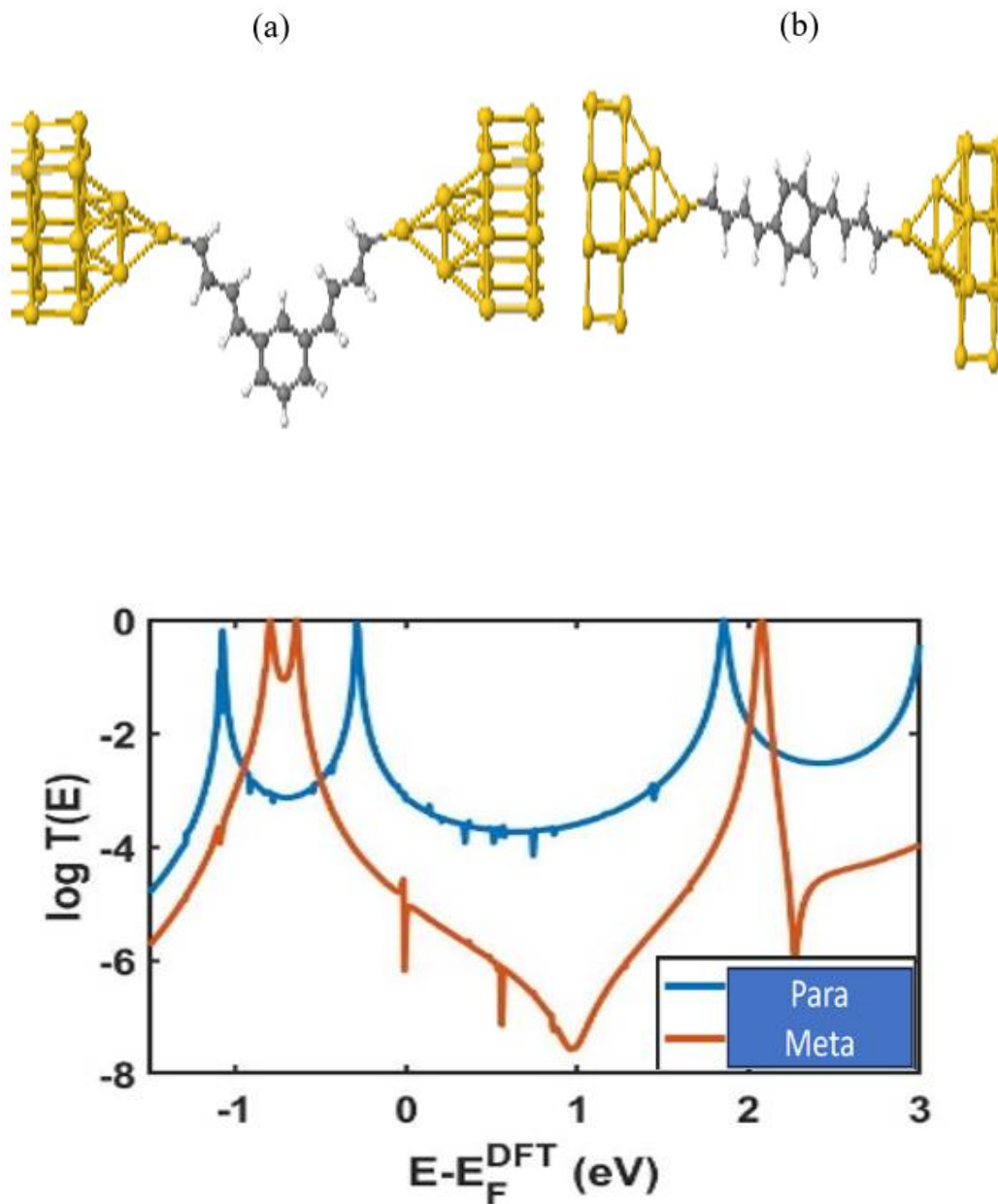


Fig (4.10) DFT-based transmission functions for Benzene connected to the gold via double-bonded alkene chain at different connectivities (a) meta connectivity (b) para connectivity.

Figure 4.7 shows the transmission coefficients $T(E)$ for a benzene core with different linkers to gold electrodes. Surprisingly, the meta connectivity in Figure 4.7b shows no DQI dip, whereas the meta connectivities in all other cases shows a DQI dip. This suggests that the absence of the DQI dip in Figure 4.7a is associated with the presence of the oligoyne linker, which in this case is connected to the gold electrode by a gold-carbon bond. This leads us to the conjecture that the absence of a DQI dip is associated with the fact that the oligoyne possesses two pi systems. One of these is associated with p_z orbitals, which couple to the p_z system of the benzene ring and the other consists of p_y orbitals, which are orthogonal to the p_z system of the benzene ring, but could couple to the sigma orbitals of the benzene ring. If the p_z system exhibits a DQI dip, transmission through the p_y system creates a parallel transmission path which hides the dip.

Changing to SME and sulfur linkers containing an extra benzene rings, as in Figures 4.8b and 4.9b, means that the p_y orbitals of the oligoynes couple only weakly to the p_z system of the benzene rings in the linkers and therefore their ability to create a parallel transport path is diminished and the DQI dip is revealed. In other words, the two benzenes in the linkers act like p_y filters such that only transport via the p_z system is relevant. This conceptual framework is further evidenced by Figure 4.10b, in which the linkers are formed from double-bonded alkene chains, which only contain a p_z system. In this case, the DQI dip is clearly evident.

4.7.2 Transmission coefficient for the benzene with an increasing number of central rings:

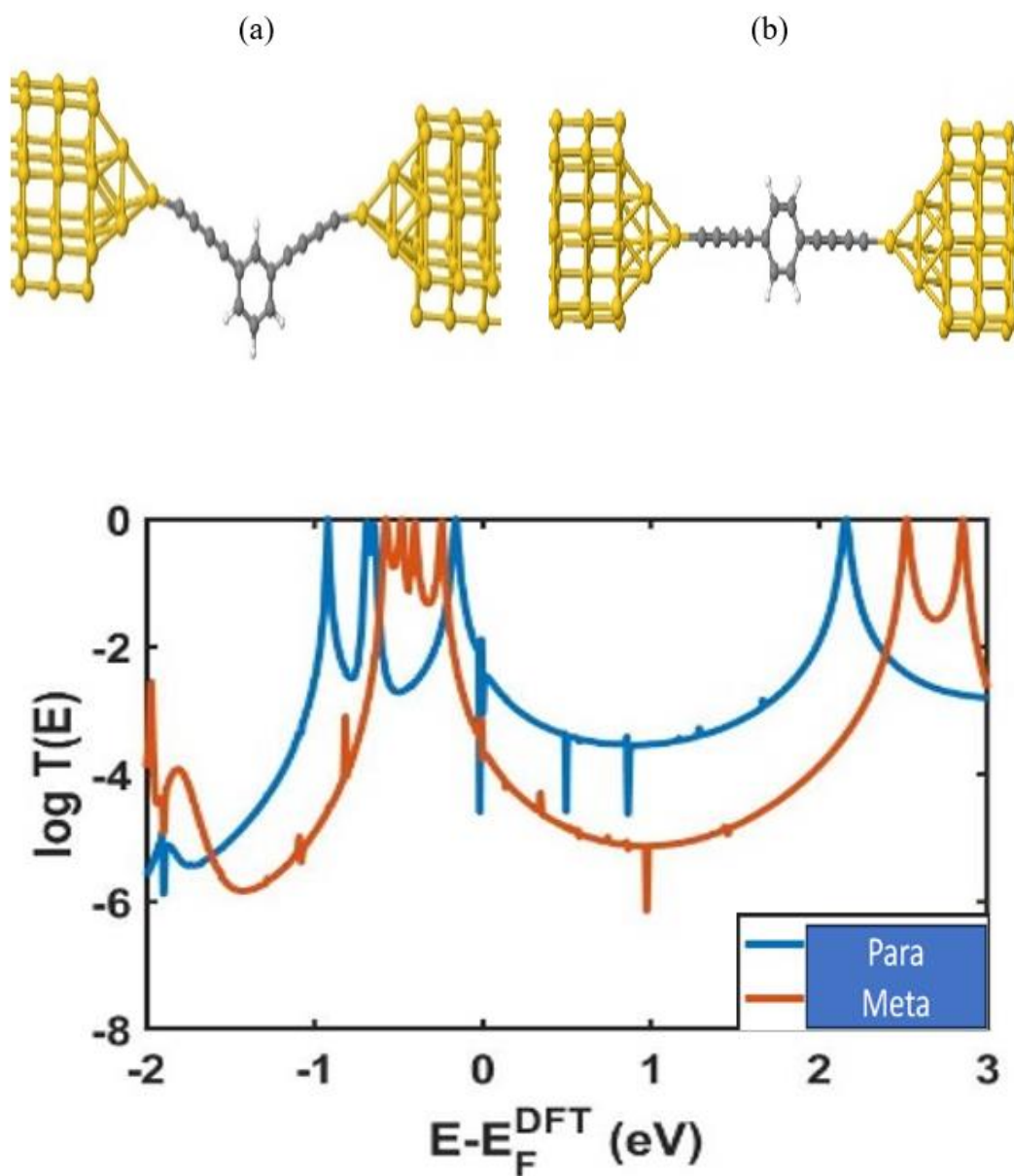


Fig (4.11) DFT-based transmission functions for Benzene with two triple bonds (a) meta connectivity (b) para connectivity.

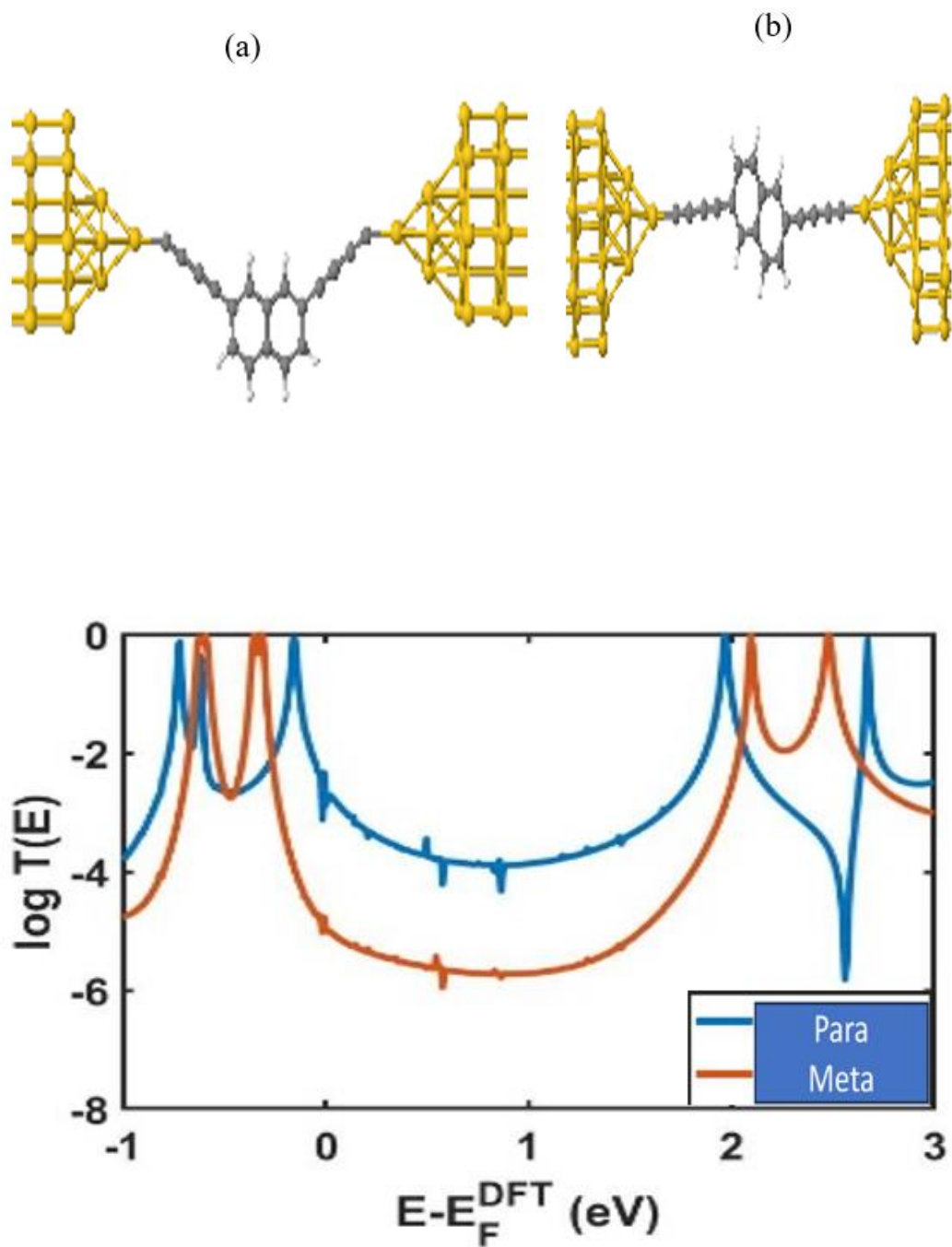


Fig (4.12) DFT-based transmission functions for Naphthalene with two triple bonds (a) meta connectivity (b) para connectivity.

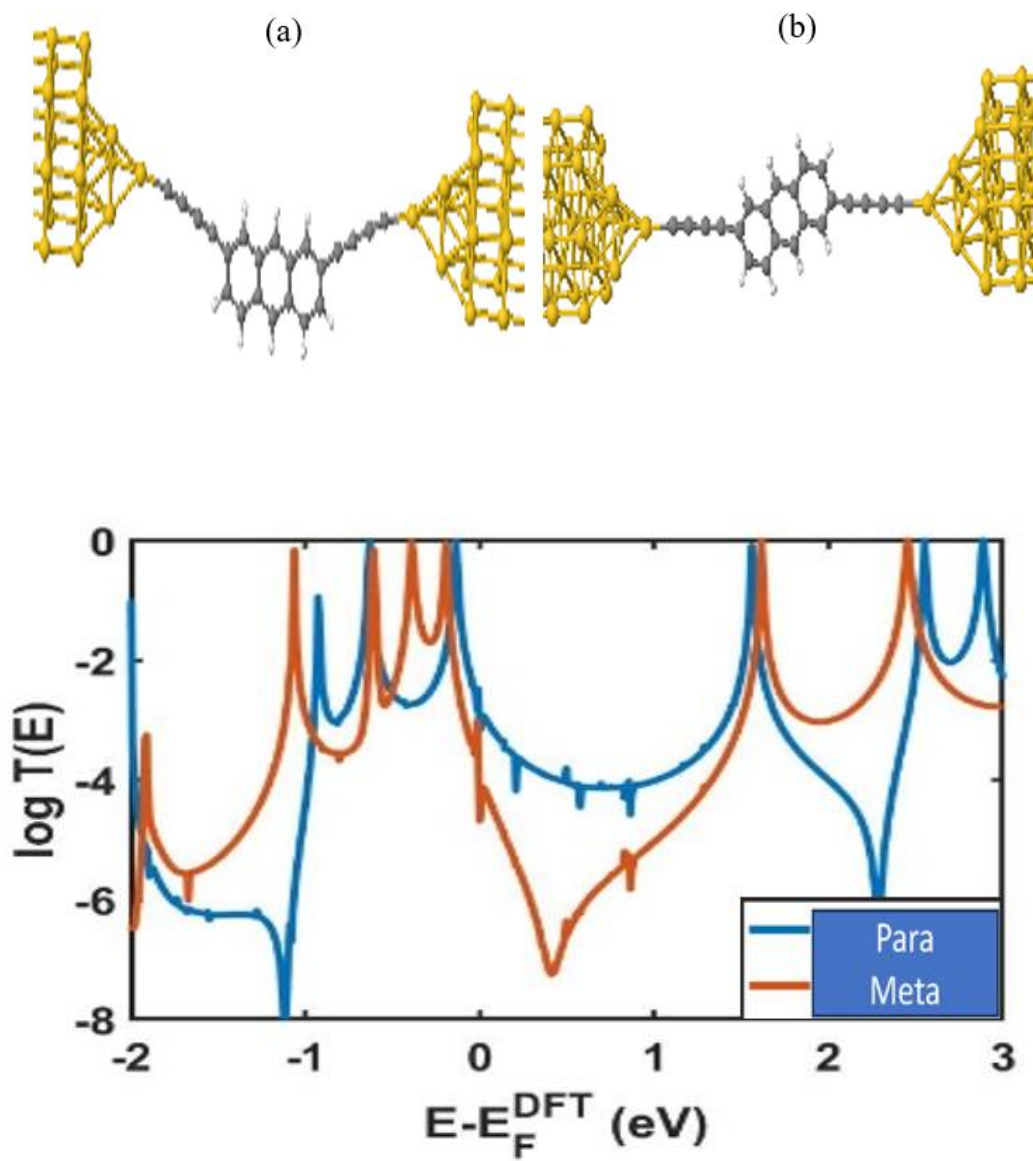


Fig (4.13) DFT-based transmission functions for Anthracene with two triple bonds (a) meta connectivity (b) para connectivity.

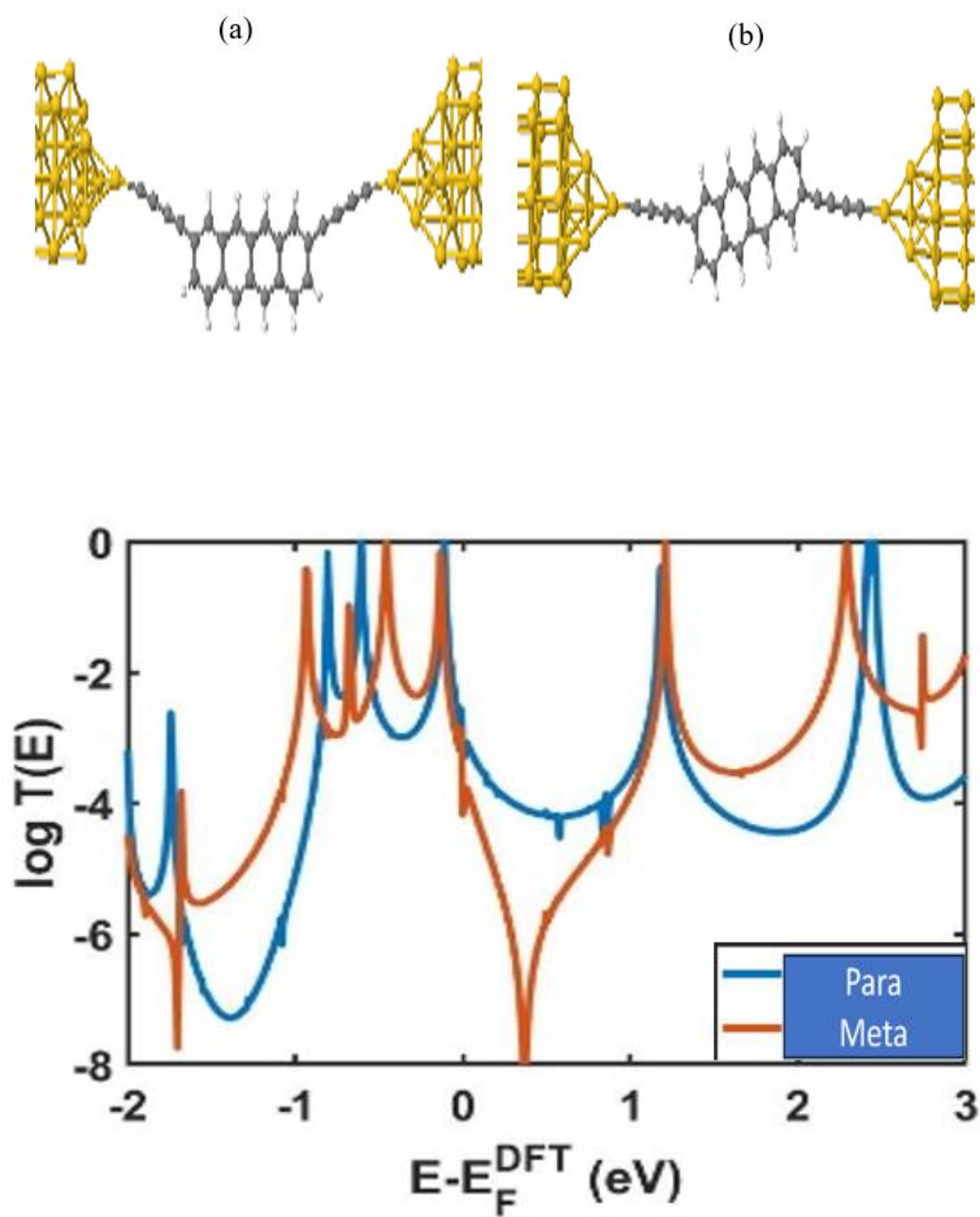


Fig (4.14) DFT-based transmission functions for Tetracene with two triple bonds
(a) meta connectivity (b) para connectivity.

Transmission through the sigma system of the central rings is expected to decrease with the length of the core is increased, so if the absence of a DQI dip is due to the p_y system of the oligoyne linkers coupling to the sigma system, then the effect of this parallel transmission path should decrease as the number of rings is increased. This is clearly shown in Figure 4.11b, where a DQI dip is not present for the shorter cores in Figures 4.11b and 4.12b, but is clearly visible for the longer cores of Figures 4.13b and 4.14b.

On the other hand, since both the p_z and p_y MOs of oligoyne linkers are delocalized along the length of the oligoyne and do not decay with length, we expect the p_y system to play a significant role even when the length of the oligoyne is increased. This feature is clearly evidenced by the absence of a DQI dip in all the transmission coefficients of Figure 4.15.

4.7.3 Transmission coefficients for the benzene cores with oligoyne linkers of different lengths

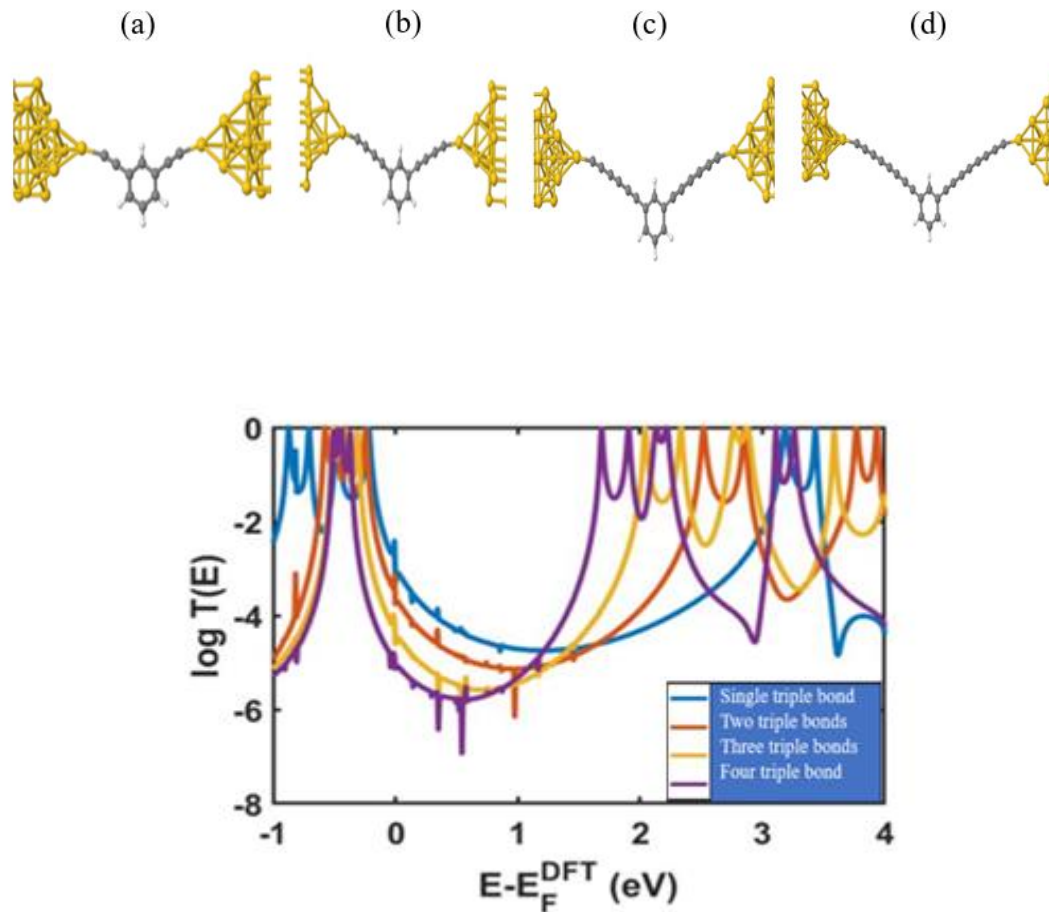


Fig (4.15) Transmission coefficients $T(E)$ for the benzene cores with oligoyne linkers of different lengths (a) single triple bond (b) two triple bonds (c) three triple bonds (d) four triple bonds.

Enhancing the length considerably has a notable dampening effect on sigma transport. Even with an increased length of the triple bond, the absence of Destructive Quantum Interference (DQI) suggests that the contribution does not originate from sigma transport.

4.7.4 Transmission coefficients for the benzene with an increasing number of central rings connected to gold via SMe-anchor:

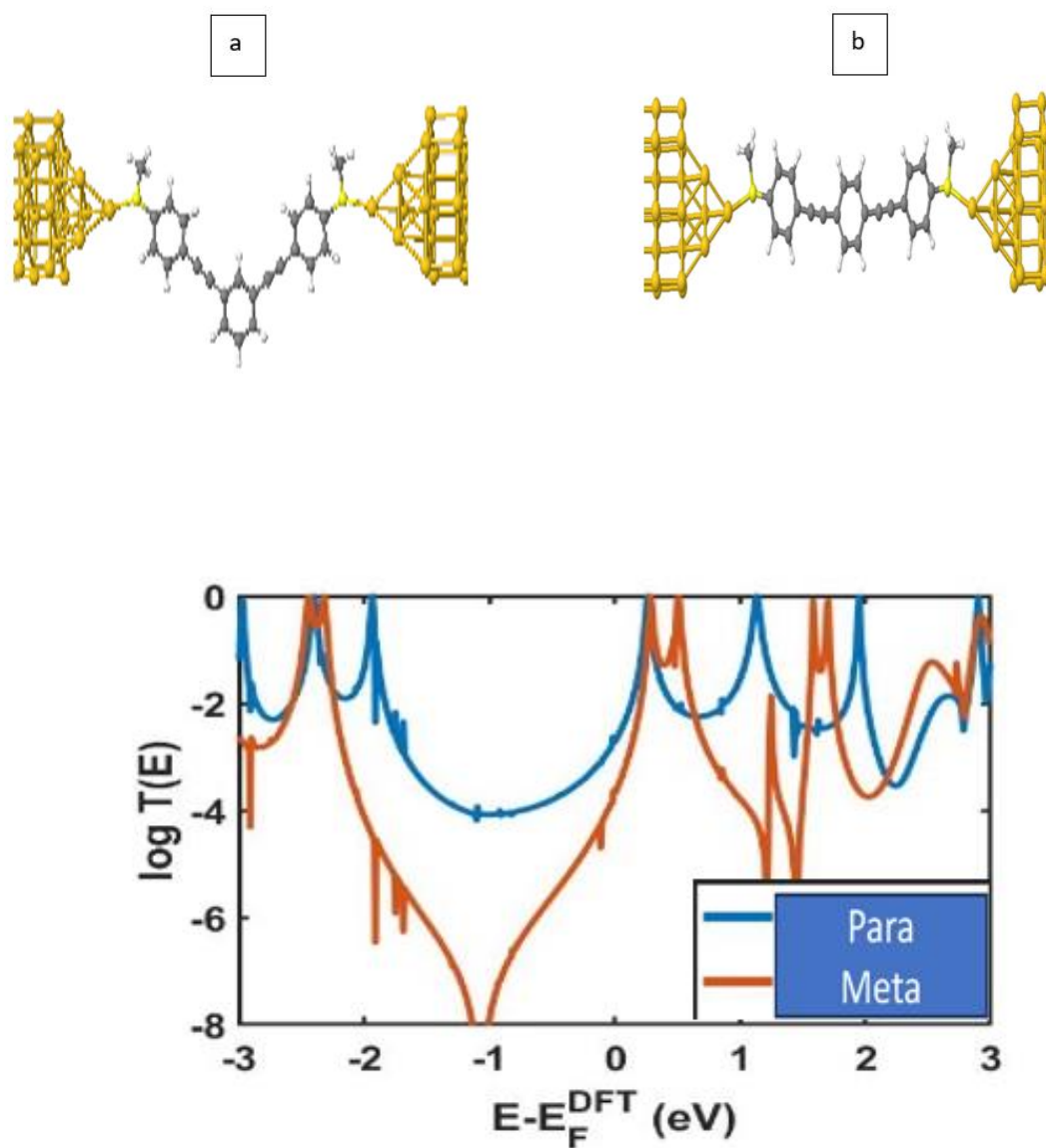
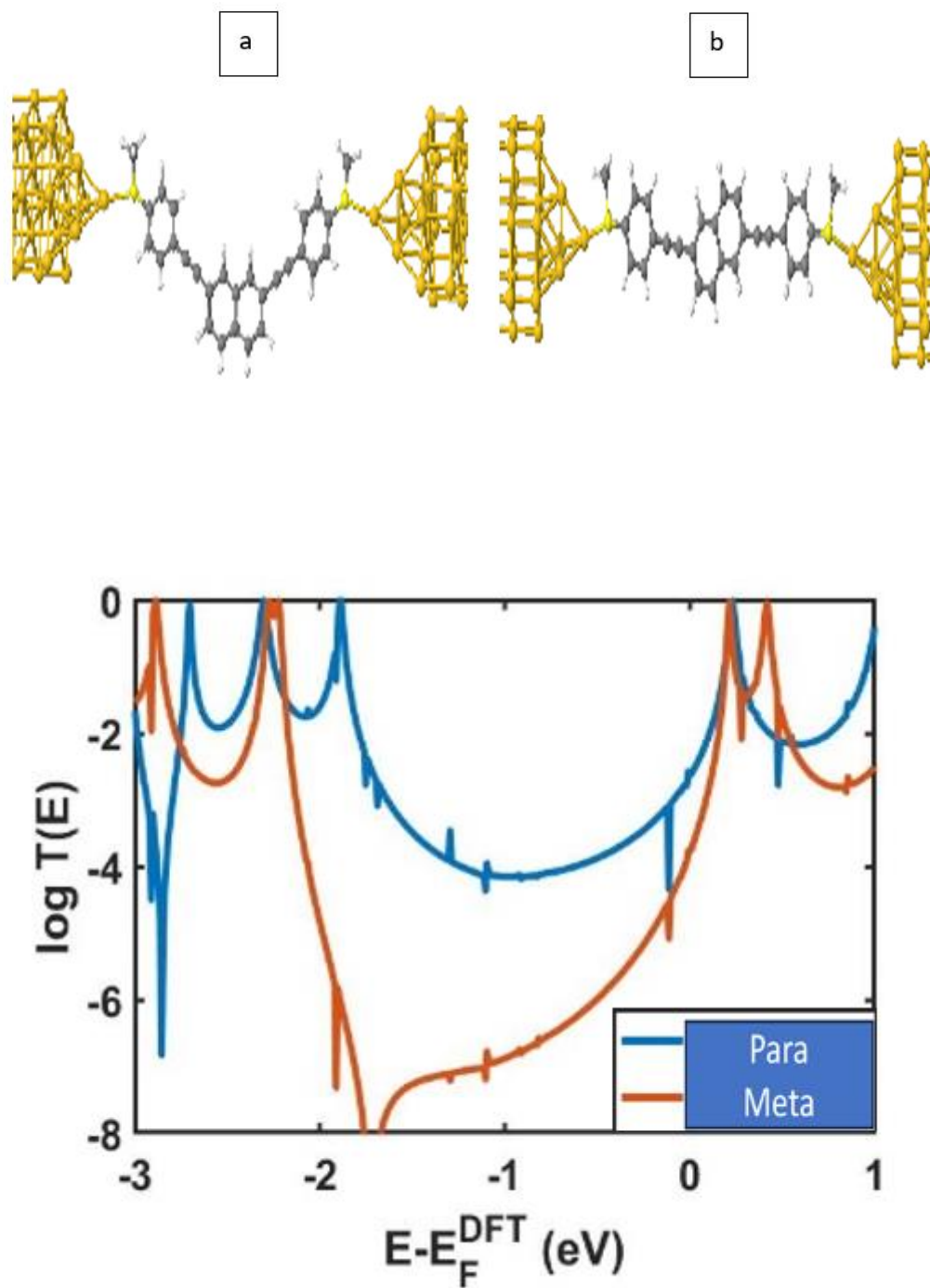


Fig (4.16) DFT-based transmission functions for Benzene connected to the gold via SMe-anchor at different connectivities (a) meta connectivity (b) para connectivity.



Fig(4.17) DFT-based transmission functions for Naphthalene connected to the gold via SMe-anchor at different connectivities (a) meta connectivity (b) para connectivity.

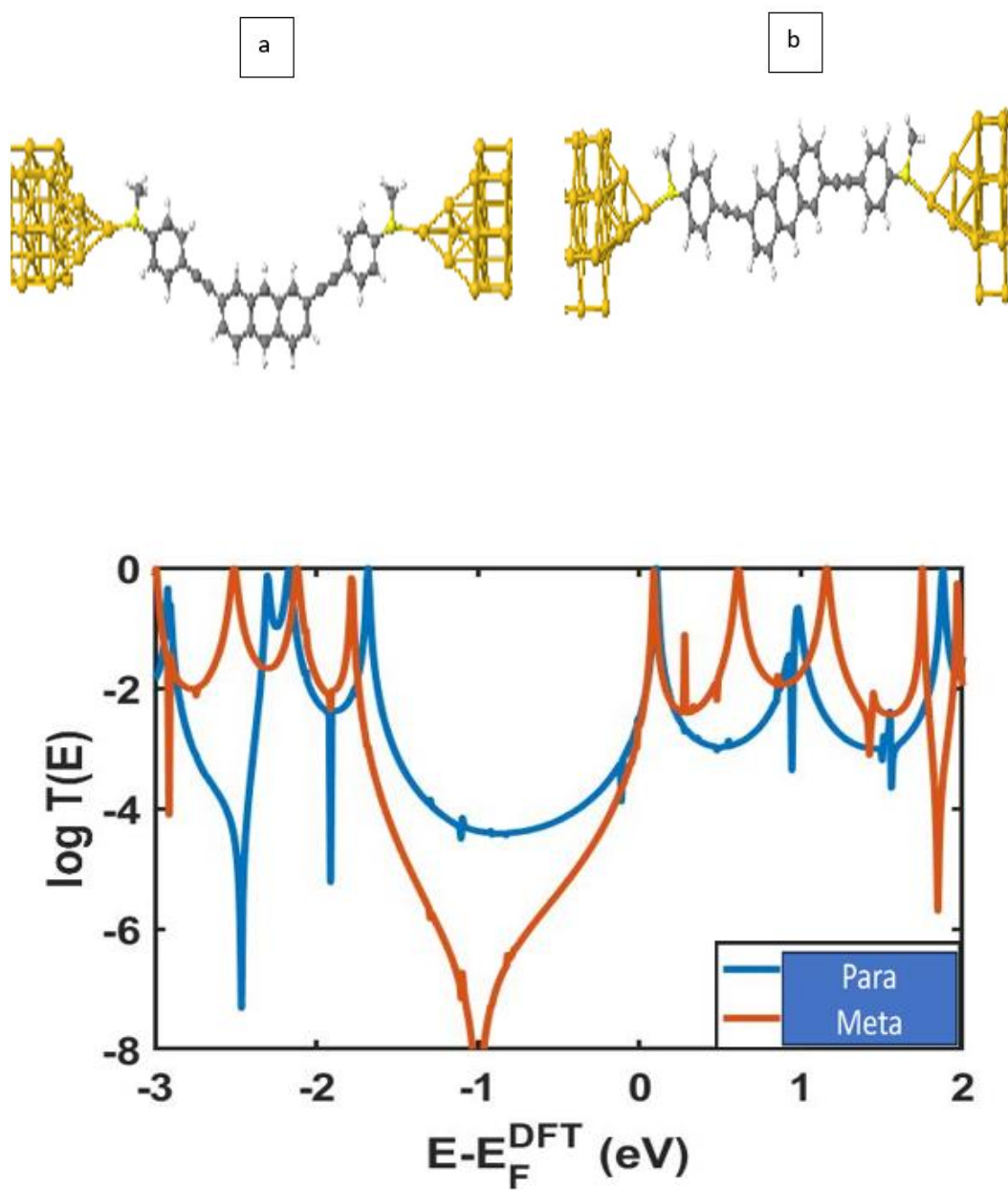


Fig (4.18) DFT-based transmission functions for Anthracene connected to the gold via SMe-anchor at different connectivities (a) meta connectivity (b) para connectivity.

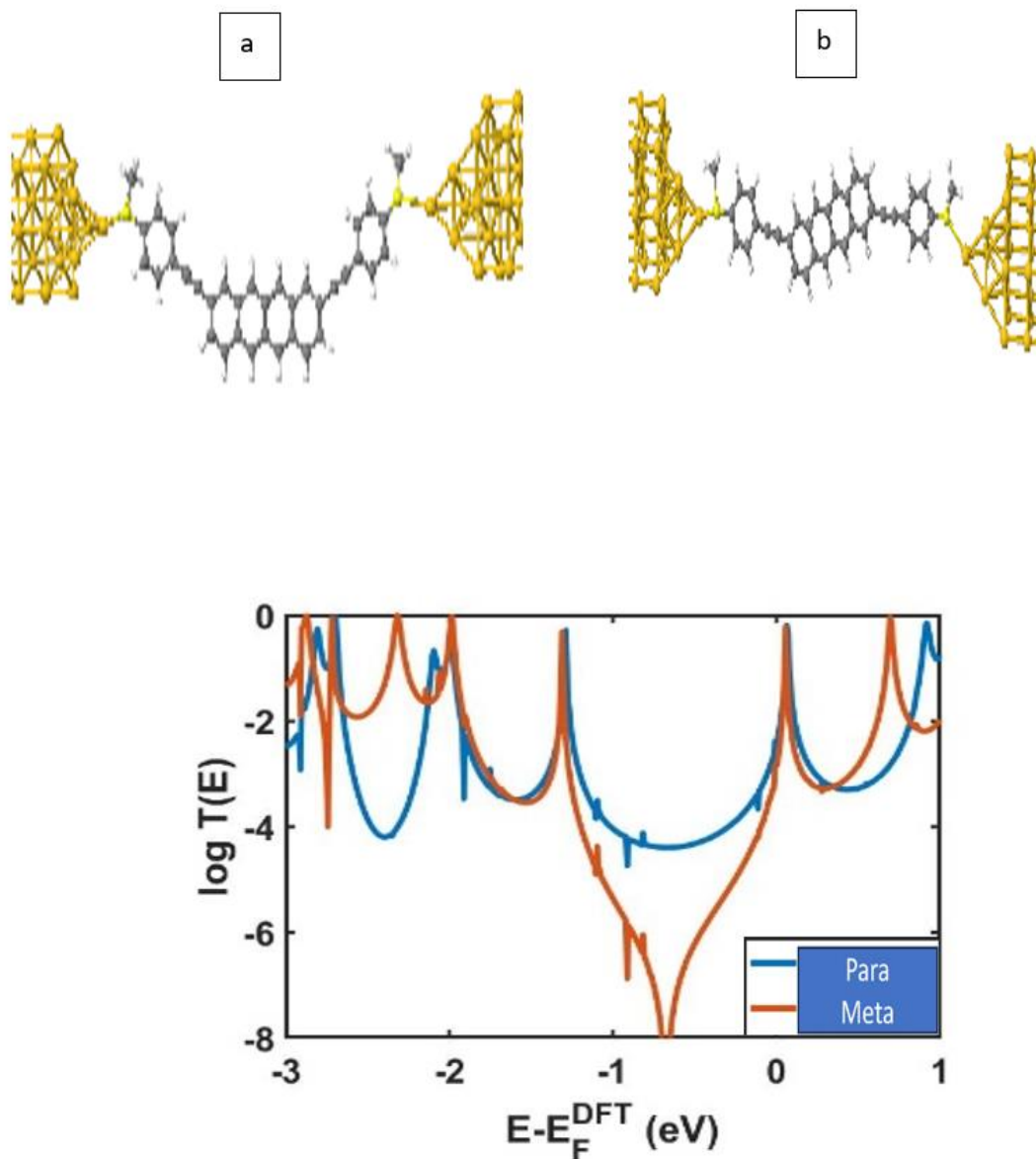


Fig (4.19) DFT-based transmission functions for Tetracene connected to the gold via SMe-anchor at different connectivities (a) meta connectivity (b) para connectivity.

Expanding the central ring with SME linkers demonstrates a consistent observation of Destructive Quantum Interference (DQI) in all instances. By filtering out the p_y orbitals, we can bring to light the existence of DQI.

What causes the appearance of a dip in the HOMO-LUMO gap when the linker is altered? When switching to a different linker, the π orbital becomes perpendicular to the benzene molecule. Both benzene structures function as linkers, connecting the central ring to the electrode. Despite the electrode sending a distinct type of P orbital, the benzene acts as a filter. Following the filtration process involving the phenyl ring, only the p_z orbital remains. Consequently, Destructive Quantum Interference (DQI) becomes apparent. This process resembles the purification of quantum interference. The presence of influences from other π orbitals would obscure the observation of DQI.

4.8. Conclusion

In this work, I investigated charge transport through molecular junctions with gold electrodes using density functional theory (DFT). The DFT results show that there are two approaches to attain Destructive Quantum Interference (DQI). One of the strategies is to extend the length of the central rings. The second strategy is to utilize different types of linkers to prevent the inclusion of p_y orbitals in the linkers.

This chapter suggests that a tight-binding theory based on a single level per atomic site will predict the qualitative features of a DFT calculation or a laboratory study of transport through related molecular cores, provided the linkers contain only a single pi system. This is illustrated in Figure (4.17-4.20), where each linker contains only a single pi system. Alternatively, if more than one pi system is present in the linkers, the tight binding model should be increased in complexity by assigning more than one level to each atomic site.

Bibliography:

- [1] Tour, J.M., 2003. Molecular electronics: commercial insights, chemistry, devices, architecture and programming. World Scientific.
- [2] Ratner, M.A., 2002. Introducing molecular electronics. *Materials today*, 5(2), pp.20-27.
- [3] Tans, S.J., Devoret, M.H., Dai, H., Thess, A., Smalley, R.E., Geerligs, L.J. and Dekker, C., 1997. Individual single-wall carbon nanotubes as quantum wires. *Nature*, 386(6624), pp.474-477.
- [4] Xiao, X., Xu, B. and Tao, N.J., 2004. Measurement of single molecule conductance: Benzenedithiol and benzenedimethanethiol. *Nano letters*, 4(2), pp.267-271.
- [5] McCreery, R.L., Yan, H. and Bergren, A.J., 2013. A critical perspective on molecular electronic junctions: there is plenty of room in the middle. *Physical Chemistry Chemical Physics*, 15(4), pp.1065-1081.
- [6] Su, T.A., Neupane, M., Steigerwald, M.L., Venkataraman, L. and Nuckolls, C., 2016. Chemical principles of single-molecule electronics. *Nature Reviews Materials*, 1(3), pp.1-15.
- [7] Cui, L., Miao, R., Jiang, C., Meyhofer, E. and Reddy, P., 2017. Perspective: Thermal and thermoelectric transport in molecular junctions. *The Journal of Chemical Physics*, 146(9), p.092201.
- [8] Baer, R. and Neuhauser, D., 2002. Phase coherent electronics: a molecular switch based on quantum interference. *Journal of the American Chemical Society*, 124(16), pp.4200- 4201.
- [9] Cardamone, D.M., Stafford, C.A. and Mazumdar, S., 2006. Controlling quantum

transport through a single molecule. *Nano letters*, 6(11), pp.2422-2426.

[10] Guédon, C.M., Valkenier, H., Markussen, T., Thygesen, K.S., Hummelen, J.C. and Van Der Molen, S.J., 2012. Observation of quantum interference in molecular charge transport. *Nature nanotechnology*, 7(5), pp.305-309.

[11] Liu, J., Huang, X., Wang, F. and Hong, W., 2018. Quantum interference effects in charge transport through single-molecule junctions: detection, manipulation, and application. *Accounts of Chemical Research*, 52(1), pp.151-160.

[12]. Lambert, C.J., 2015. Basic concepts of quantum interference and electron transport in single- molecule electronics. *Chemical Society Reviews*, 44(4), pp.875-888.

[13]. Lambert, C.J. and Liu, S.X., 2018. A magic ratio rule for beginners: a chemist's guide to quantum interference in molecules. *Chemistry–A European Journal*, 24(17), pp.4193-4201.

[14] Lambert, C.J. and Raimondi, R., 1998. Phase-coherent transport in hybrid superconducting nanostructures. *Journal of Physics: Condensed Matter*, 10(5), p.901.

[15] Geng, Y., Sangtarash, S., Huang, C., Sadeghi, H., Fu, Y., Hong, W., Wandlowski, T., Decurtins, S., Lambert, C.J. and Liu, S.X., 2015. Magic ratios for connectivity-driven electrical conductance of graphene-like molecules. *Journal of the American Chemical Society*, 137(13), pp.4469-4476.

[16] Arfken, G., Weber, H. H. and Harris, F. (2013). *MATHEMATICAL METHODS FOR PHYSICISTS*. 7th ed. ELSEVIER.

[17] A. P. Sutton, 1993. *Electronic structure of materials*. Oxford University Press, USA.

[18] Xiang D, Jeong H, Lee T, Mayer D. Mechanically controllable break junctions for molecular electronics. *Adv Mater* 2013; 25:4845-4867.

[19] Van der Waals Density Functional for General Geometries. PHYSICAL REVIEW LETTERS 2004; 92.

[20] José M Soler EA, Julian D Gale, Alberto García, Javier Junquera, Pablo Ordejo n and Daniel Sa´nchez-Portal. The SIESTA method for ab initio order-N materials simulation. JOURNAL OF PHYSICS: CONDENSED MATTER 2002.

[21] Zhao S, Deng ZY, Albalawi S, Wu Q, Chen L, Zhang H, Zhao XJ, Hou H, Hou S, Dong G, Yang Y, Shi J, Lambert CJ, Tan YZ, Hong W. Charge transport through single-molecule bilayer-graphene junctions with atomic thickness. Chemical Science 2022; 13:5854-5859.

[22] Naher M, Milan DC, Al-Owaedi OA, Planje IJ, Bock S, Hurtado-Gallego J, Bastante P, Abd Dawood ZM, Rincon-Garcia L, Rubio-Bollinger G, Higgins SJ, Agrait N, Lambert CJ, Nichols RJ, Low PJ. Molecular Structure-(Thermo)electric Property Relationships in Single-Molecule Junctions and Comparisons with Single- and Multiple-Parameter Models. J Am Chem Soc 2021; 143:3817-3829.

[23] C. J. Lambert, Quantum Transport in Nanostructures and Molecules. IOP Publishing, 2021.

[24] H. Sadeghi, S. Sangtarash, and C. J. Lambert, "Oligoyne Molecular Junctions for Efficient Room Temperature Thermoelectric Power Generation," Nano Lett., vol. 15, no. 11, pp. 7467–7472, 2015.

5. Quantum interference-controlled conductance enhancement in stacked graphene-like dimers

5.1 Introduction

Research has shown that when two monomers are placed in series, to form a dimer, the electrical conductance is decreased compared to that of the monomer. However, in the study [1,3], conflicting results were observed. For instance, when two anthanthrene monomers are pi stacked and the resulting dimer studied using a scanning tunneling microscopic break junction, the conductance is found to increase by a factor of 25 compared to the monomer. Interestingly the conductance of the dimer is found to be lower than that of the monomer when the connectivity of external electrodes to the monomer core is changed. This feature has been proven both theoretically and experimentally [4,5]. Therefore, it is clear that charge transfer between molecules can be optimized and modified if synthetic control of connectivity to the molecular core is combined with stacking between the monomers.

Pi stacking is of great importance in chemistry, biology, and organic optoelectronic. Charge transfer between molecules can improve the efficiency of organic optoelectronics such as field-effect devices [8,9] photovoltaic devices [6,7] and light-emitting materials. Electron transport through vertically stacked two-dimensional (2D) van der Waals (vdW) heterostructures is only possible through stacking interactions. Furthermore, by adopting a variety of stacking configurations, one can alter a variety of properties, depending on the AA, AB, or twisted–angle stacking configuration of bilayer graphene [8-10].

The presence of conjugated central units in anthanthrene and pyrene suggests that these graphene-like molecules can be used as a model to study inter-molecular charge transport and quantum state regulation via stacking. Their connection to external electrodes is advantageous since they can be fabricated with atomic accuracy through chemical synthesis, Thus it is easy to switch intramolecular quantum interference (QI) between CQI and DQI by adjusting the connectivity. Indeed, the study of QI effects in monomer-molecules and dimers is now possible experimentally using monomer-molecule junctions [10-15].

Unlike in the past, where experiments show that QI can be used to regulate the flow of charge and energy through monomer-molecules, lately it was confirmed that these quantum effects can be translated into self-assembled molecular layers (SAMs) hence ushering the new era of designing 2D organic materials, whose room temperature transport properties are governed by quantum interference [16-18].

The presence of intermolecular interactions is a major feature that is not featured in monomer–molecule junctions. Therefore, there is a need for clarification about the interplay between QI and stacking interactions, in order to achieve the goal of utilizing quantum–enhanced SAMS in real devices [20-22].

The following study shows that even at room temperature, this interplay can lead to highly non-classical behavior in electron transport properties [18,19].

5.2 Studied molecules:

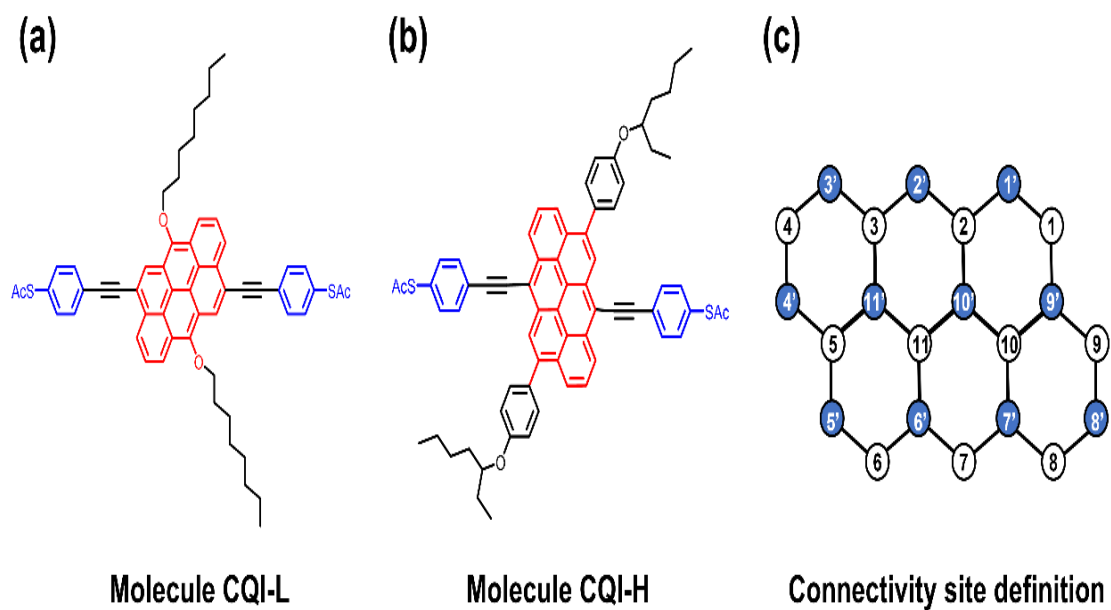


Fig (5.1): Molecular structures. (a, b) Structures of molecules Constructive Quantum interference- Low Conductance (CQI-L) and Destructive Quantum Interference- High Conductance (CQI-H). (c) Sketch of an anthanthrene core with connectivity site definition.

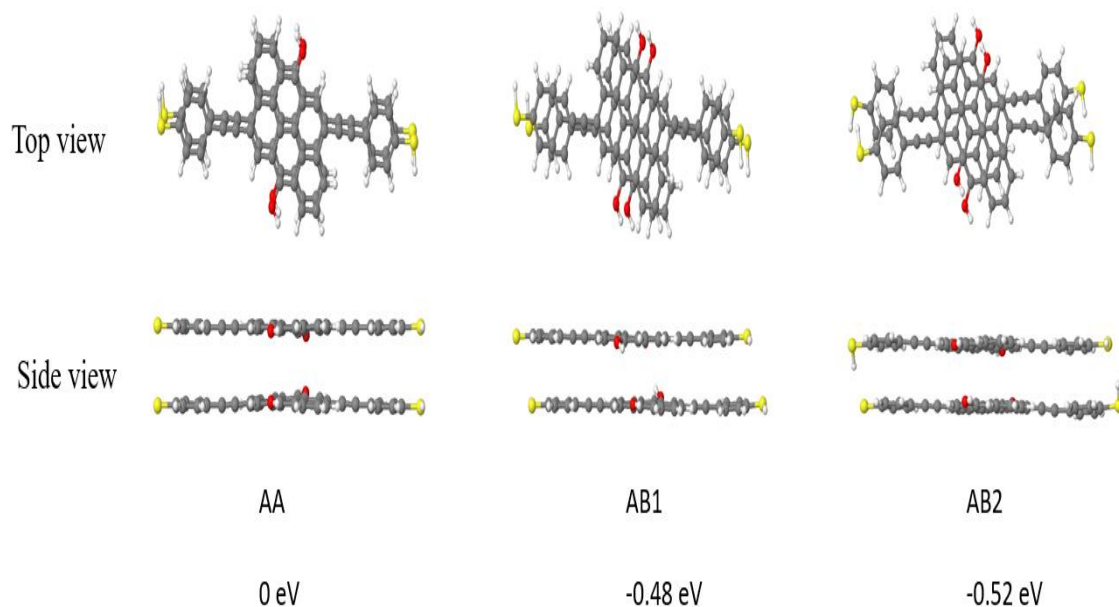


Fig (5.2): Top and side views of the three archetypal stacking patterns for the molecule CQI-L.

5.3 Finding and discussing:

Exploring the orbital interactions of these monomers when coupled in various stacking configurations is intriguing. The impact of stacking them together is noteworthy. In the case of AA stacking, the transition from Constructive Quantum Interference (CQI) to Destructive Quantum Interference (DQI) occurs. This transformation is substantiated in my calculations, where the product rule indicates that HOMO and LUMO possess opposite symmetries, resulting in observable destructive quantum interference.

Transmission in Density Functional Theory (DFT): In AA stacking, a noticeable dip is observed, indicating a correspondence to Destructive Quantum Interference (DQI) within the HOMO-LUMO gap. Interestingly, in the cases of AB2 and AB1, the electrical conductance of AB2 surpasses that of AB1. When the monomers are significantly separated, each maintains isolated orbitals, and all orbitals are doubly degenerate. As they come closer, treating the degenerate pairs as a two-level system reveals that the splitting between the two levels serves as a measure of the coupling between them.

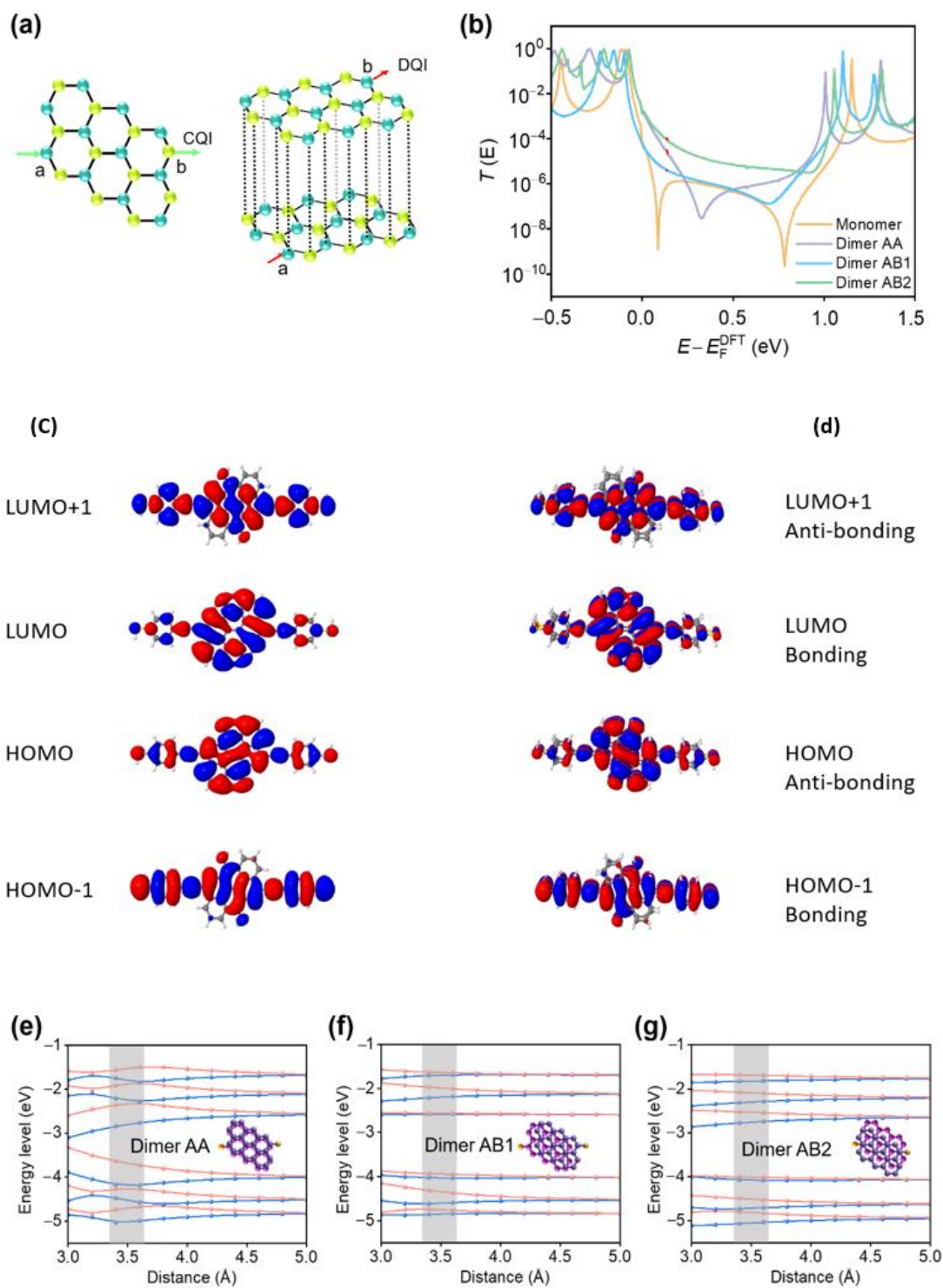


Fig. 5.3: The mechanism underlying a stacked dimer's increased conductance. (a) Monomer and dimer anthanthrenes' transport characteristics. (b) Transmission coefficients for the CQI-L monomer and dimers with AA, AB1 and AB2 stacking. (c) The CQI-L monomer's frontier molecular orbitals, including HOMO-1,

HOMO, LUMO, and LUMO+1. (d) Dimerization induces HOMO and LUMO splitting into pairs of bonds and antibonds. (e-g) HOMO-2 to LUMO+2 energy level evolution for the AA, AB1 and AB2 stacking as a function of the vertical distance between the two monomers.

Examination from a theoretical perspective of dimers' increased conductivity. Room-temperature QI between the systems of the pi stacked monomers is the cause of this distinctly non-classical behavior. The bipartite nature of the anthanthrene core is what essentially drives QI effects in the monomers. Carbon atoms can be thought of as "green" or "yellow" sites, with "green" sites connecting to "yellow" sites only and vice versa, as illustrated in the left panel of (Fig. 5.3a), in a straightforward Hückel (i.e. tight-binding) description of charge transfer across the system. CQI may result from an electron being injected through a "green" site (such as site a) and collected via a "yellow" site (such as site b). [20, 27, 37, and 38]. We explore a basic tight binding model with only nearest-neighbor couplings to emphasize the interaction between QI and stacking interactions. The 'yellow' and 'green' sites in the right panel of (Fig. 5.3a) show that the AA stacked dimer is still a bipartite lattice in this instance. Due to the fact that the collecting and injecting sites are both "green," the route shown by the red arrows from site an of the lower monomer to site b of the upper monomer now relates to DQI. As a result, it is anticipated that for AA stacking, the conductance of the dimer will be less than that of the monomer [26,27]. There are other stacking configurations that can be used in a real experiment, and AA stacking is not always preferred. Since our experimental measurements and DFT modeling show that the anthanthrene dimer's most-probable conductance is a factor of 25 higher than that of the monomer, even though this straightforward example is useful for illuminating the interaction between QI and

stacking interactions, it is not a good representation of those results. The transmission coefficient $T(E)$ representing electrons of the energy E traveling through the molecular junctions depicted in (Fig. 5.3b) was estimated using DFT in conjunction with the quantum transport code Gollum [31] to shed light on the cause of this substantially non-classical conductance rise. Three paradigmatic stacking patterns were taken into consideration to characterize the transmission through the dimer; these are designated as AA, AB1 and AB2 in (Figure 5.2). The resulting transmission coefficients close to the center of the HOMO-LUMO gap are sensitive to the type of stacking mode, as illustrated in (Fig. 5.3b). The dimer's (green curve) mid-gap transmission coefficient for AB2 stacking is substantially higher than the monomer's (yellow curve). In contrast to AA stacking, where it may be greater or lower depending on the energy E , AB1 stacking almost exactly matches that of the monomer. At room temperature, AA is extremely rare, and the conductance of AB2 stacked dimers dominates the Boltzmann distribution weighted conductance (Fig. 3f). This is because the ground states of fully relaxed AB1 and AB2 stacking are less energetic than AA stacking by 0.48 eV and 0.52 eV, respectively (Fig. 5.2).

We start by thinking about the monomer in order to comprehend the geometry of these curves. An orbital product rule [39,40] states that each molecular orbital's contribution to charge transport is influenced by the color of the orbitals on sites a and b, which are coupled to the electrodes. The lowest unoccupied molecular orbit (LUMO) for the monomer depicted in Fig. 3c has different signs (A) at the two ends, resulting in CQI, as indicated by the flat mid-gap transmission curve (yellow in Fig. 5.3b), while the highest occupied molecular orbit (HOMO) is the same color denoted by (S) at the two ends (a and b). However, because LUMO+1 and LUMO have dissimilar symmetries

(i.e., distinct colors at the two ends), they interact negatively at energies in the HOMO-LUMO gap immediately beneath LUMO, causing an anti-resonance in the yellow curve.

To grasp the shapes of the dimer transmission curves, let's begin with the scenario of AA stacking. In this case, the transition from Constructive Quantum Interference (CQI) in a monomer to Destructive Quantum Interference (DQI) in the dimer occurs, as illustrated in the case of stacked benzenes discussed in section 8 of the Supplementary Information. This transition results in a transmission dip at $E-E_F^{\text{DFT}}=0.3$ eV in the purple curve in Fig. 5.3b. The mechanism behind this shift can be elucidated by examining the molecular orbitals of the dimer. As two monomers approach each other and the distance between them diminishes, the π - π interaction induces the formation of pairs of bonding and anti-bonding orbitals in the dimer. As depicted in Fig.5.3d, the new Lowest Unoccupied Molecular Orbital (LUMO) and the new Highest Occupied Molecular Orbital (HOMO) of the dimer both exhibit the same color (S) at the injecting and collecting ends (indicated by blue circles), giving rise to DQI in the dimer.

As a function of the vertical distance between the monomers, (Figs. 5.3e–5.3g) depict the evolution of the dimer's energy levels for each of the three archetypal stacking configurations. This demonstrates how the pairs of degenerate energy levels—one from each monomer—split when the distance shrank from 5 Å to 3 Å. The inter-monomer coupling matrix and the unit matrix are virtually equivalent for AA stacking. As a result, only the coupling between an orbital on one monomer and its partner orbital on the other monomer is non-zero since monomer orbitals are orthogonal. As a result, monomer levels transform into pairs of dimer levels, and the AA-stacked dimer's spectrum only displays a minimal level repulsion. The LUMO+1, LUMO+2, LUMO+3, and LUMO+4 are located, respectively, at 3.6 Å. Despite the high couplings between each pair of the

energy levels, the DQI feature in the HOMO-LUMO gap in (Fig. 5.3b) lowers the conductance for AA stacking. Even at the ideal distance of roughly 3.5 Å, (Figure 5.3f) for the AB1-stacked dimer demonstrates that the HOMO and LUMO are practically degenerate, showing a very weak coupling between the two HOMOs and two LUMOs in the dimer. As a result, in the blue transmission curve of (Fig. 5.3b), the DQI characteristics that were immediately below the LUMO and immediately above the HOMO (in the yellow curve) are no longer visible. The HOMOs are weakly coupled and the LUMOs are highly coupled for the AB2-stacked dimer, in contrast (Fig. 5.3g). As a result, the DQI dip is eliminated since the weakly linked HOMOs barely affect the transport. The green transmission curve in (Fig. 5.3b), on the other hand, has a greater value due to the stronger coupling between the LUMOs.

5.4 Transmission function calculations of the molecule CQI-L

based on AB2 stacking:

Shifting top molecule down:

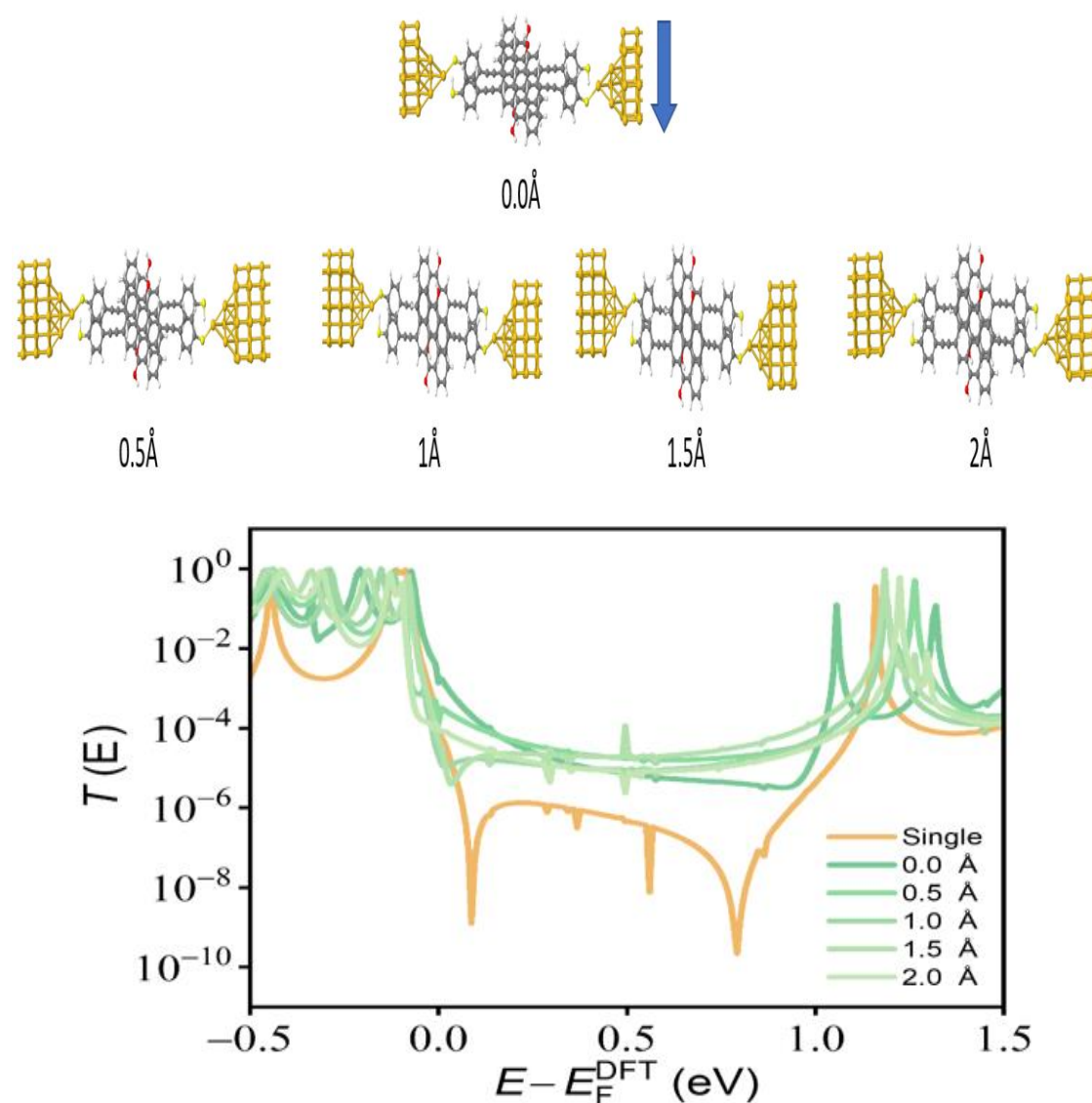


Fig. 5.4: Transmission functions $T(E)$ based on AB2 stacking of the molecule CQI-L corresponding to the different top molecule shifts (down: 0.0 Å, 0.5 Å, 1.0 Å, 1.5 Å and 2.0 Å, respectively).

Shifting top molecule up:

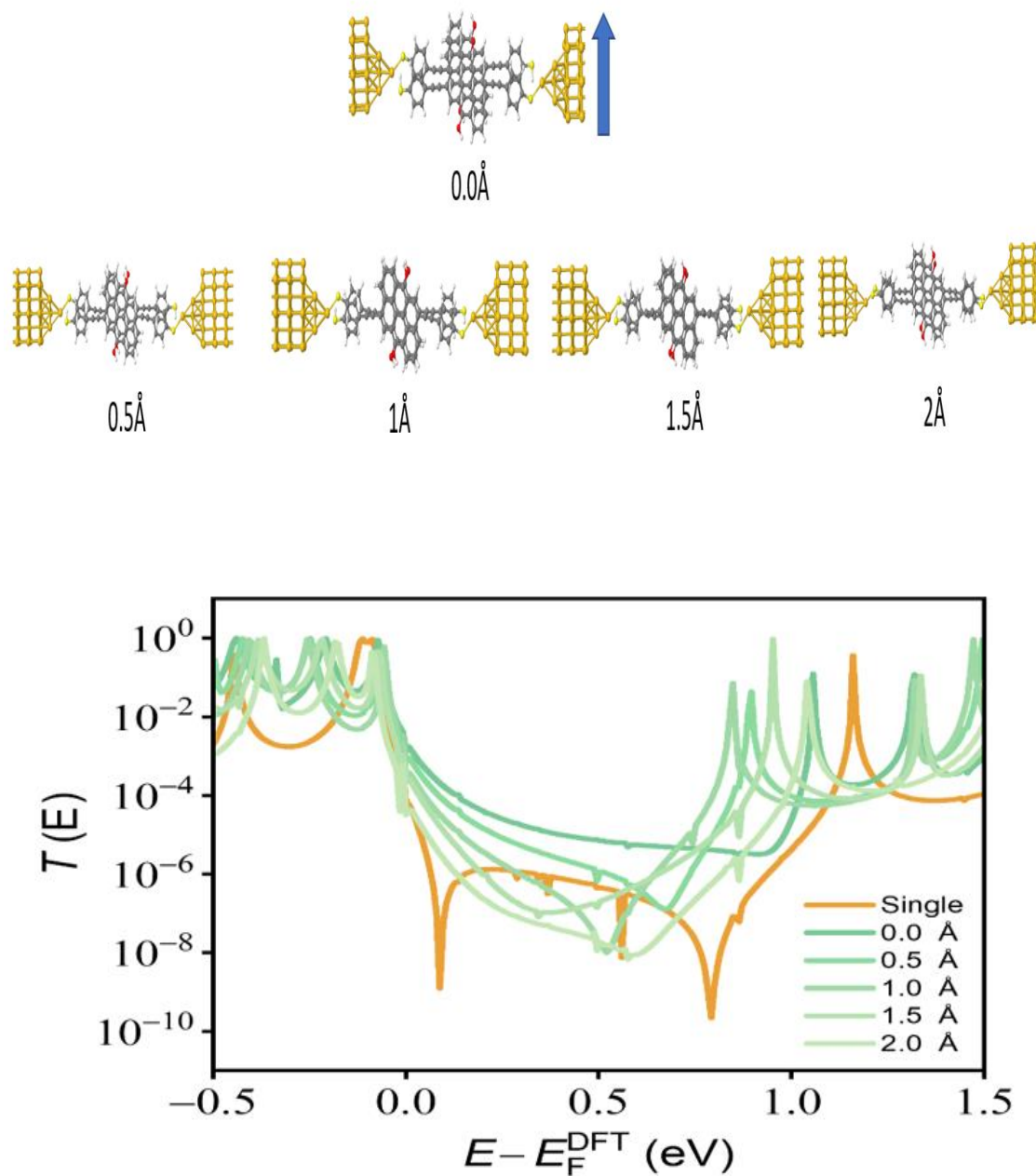


Fig. 5.5: Transmission functions $T(E)$ based on AB2 stacking of the molecule CQI-L corresponding to the different top molecule shifts (up: 0.0 Å, 0.5 Å, 1.0 Å, 1.5 Å and 2.0 Å, respectively).

Shifting top molecule left:

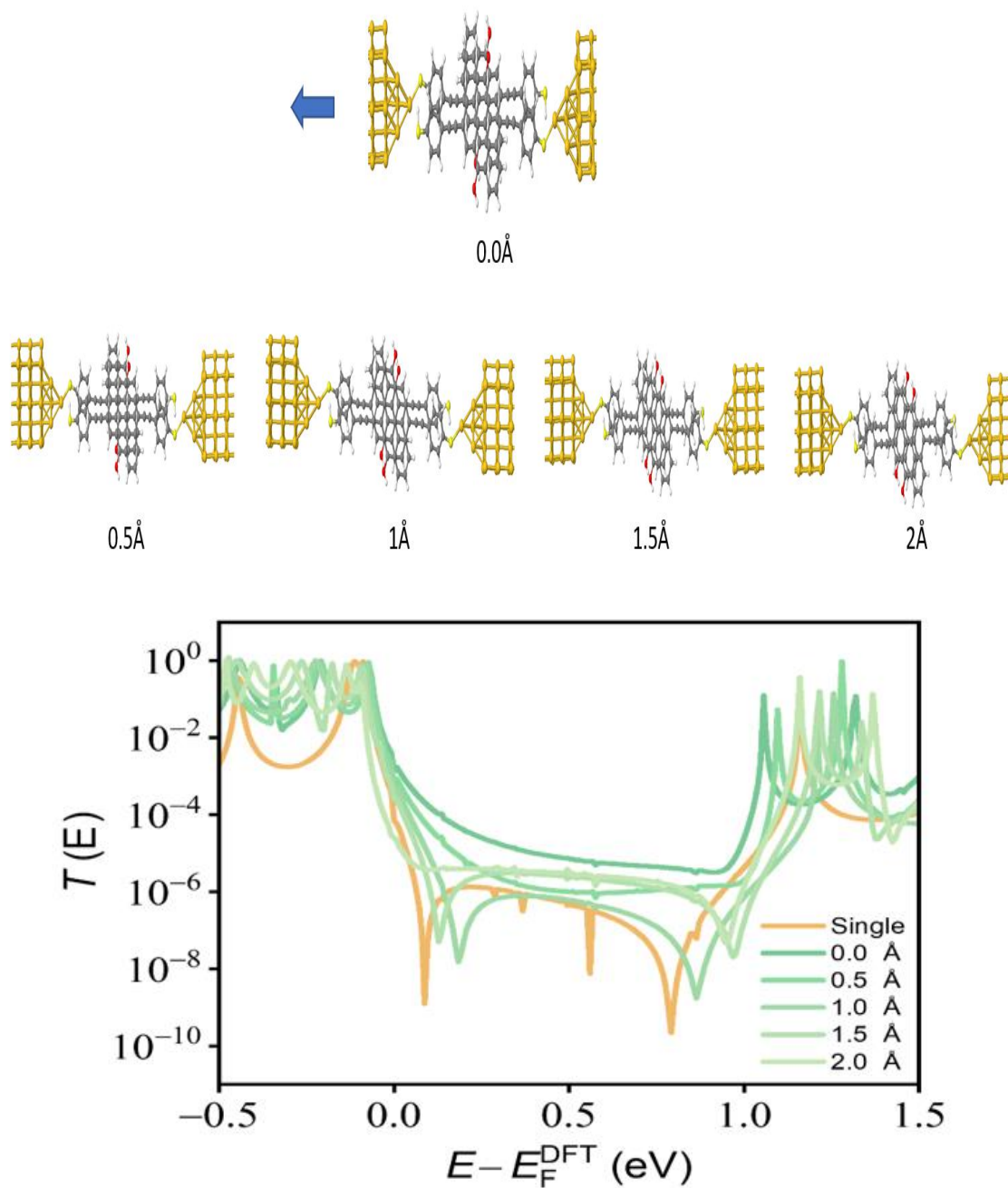


Fig. 5.6: Transmission functions $T(E)$ based on AB2 stacking of the molecule CQI-L corresponding to the different top molecule shifts (left: 0.0 Å, 0.5 Å, 1.0 Å, 1.5 Å and 2.0 Å, respectively).

Rotating top molecule:

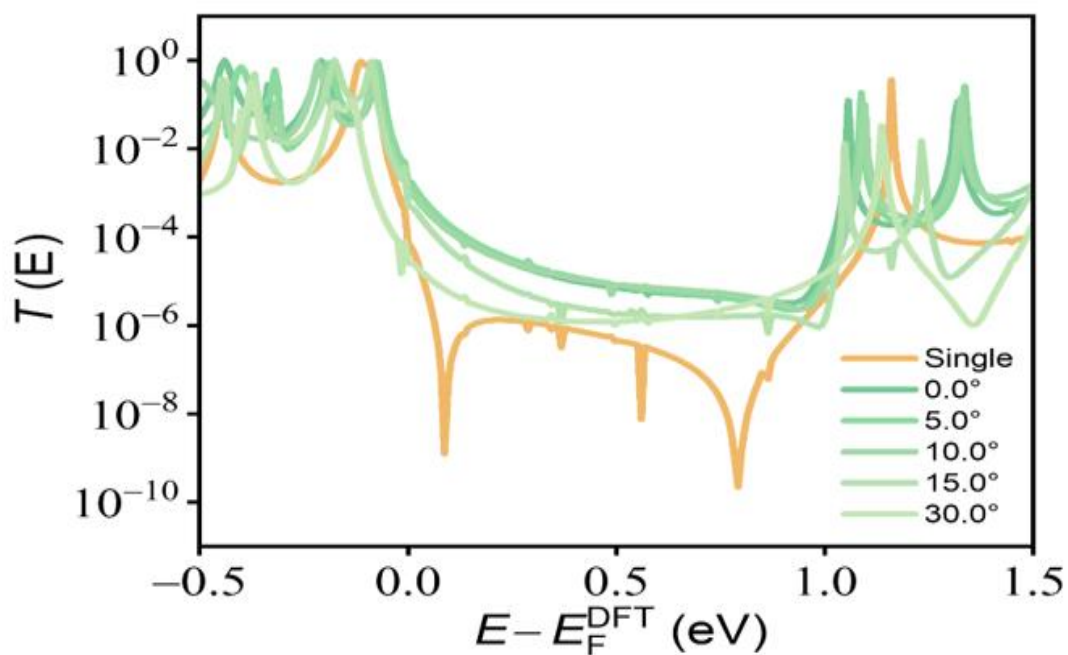
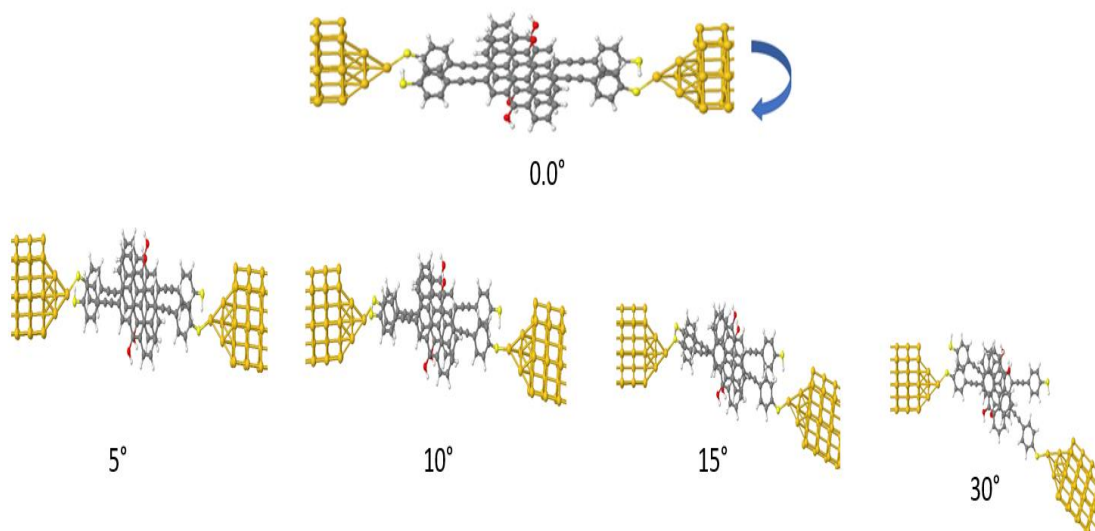


Fig. 5.7 Transmission functions $T(E)$ based on AB2 stacking of the molecule CQI-L corresponding to the different top molecule rotations (0.0° , 5.0° , 10.0° , 15.0° and 30.0° , respectively).

The robustness of the dimer state with high conductance is remarkable. This phenomenon is not confined to AB2 stacking and is able to persist even when the top monomer is shifted or rotated. As illustrated in (Fig. 5.4-5,7), the higher conductance of the dimer can remain even when the shifting distance is up to 2.0 Å or the degree of rotation is up to 15.0°. This finding indicates the strong stability of the dimer state with high conductance. It is worth noting that this robustness might be attributed to the interactions between the two monomers, such as the Van der Waals force between them. As a result, the dimer state can maintain its high conductance even when the two monomers are slightly displaced or rotated. As the interelectrode distance changes, the two dimers can slide relative to each other resulting in a single trace from a high-to-low conductance state. However, due to the limitation of the device, the conductance of an AA stacked dimer is much lower than that of a monomer, so the AA stacking cannot be detected beyond this limitation. The transition between high and low conductance states is an important process to consider in materials science. This transition is considered to be a change from AB2 stacking to AB1 stacking. In AB2 stacking, adjacent layers of molecules are stacked in alternating directions, while in AB1 stacking, adjacent layers are stacked in the same direction. This transition is critical in determining the properties of the material, as it affects the electronic structure and band gap of the material. Additionally, this transition is thought to be responsible for changes in the optical and electrical properties of the material. As a result, understanding the mechanism of the transition is important for designing materials with desired properties.

5.5 Transmission function calculations of the molecule CQI-H

based on AB2 stacking:

Rotating top molecule:

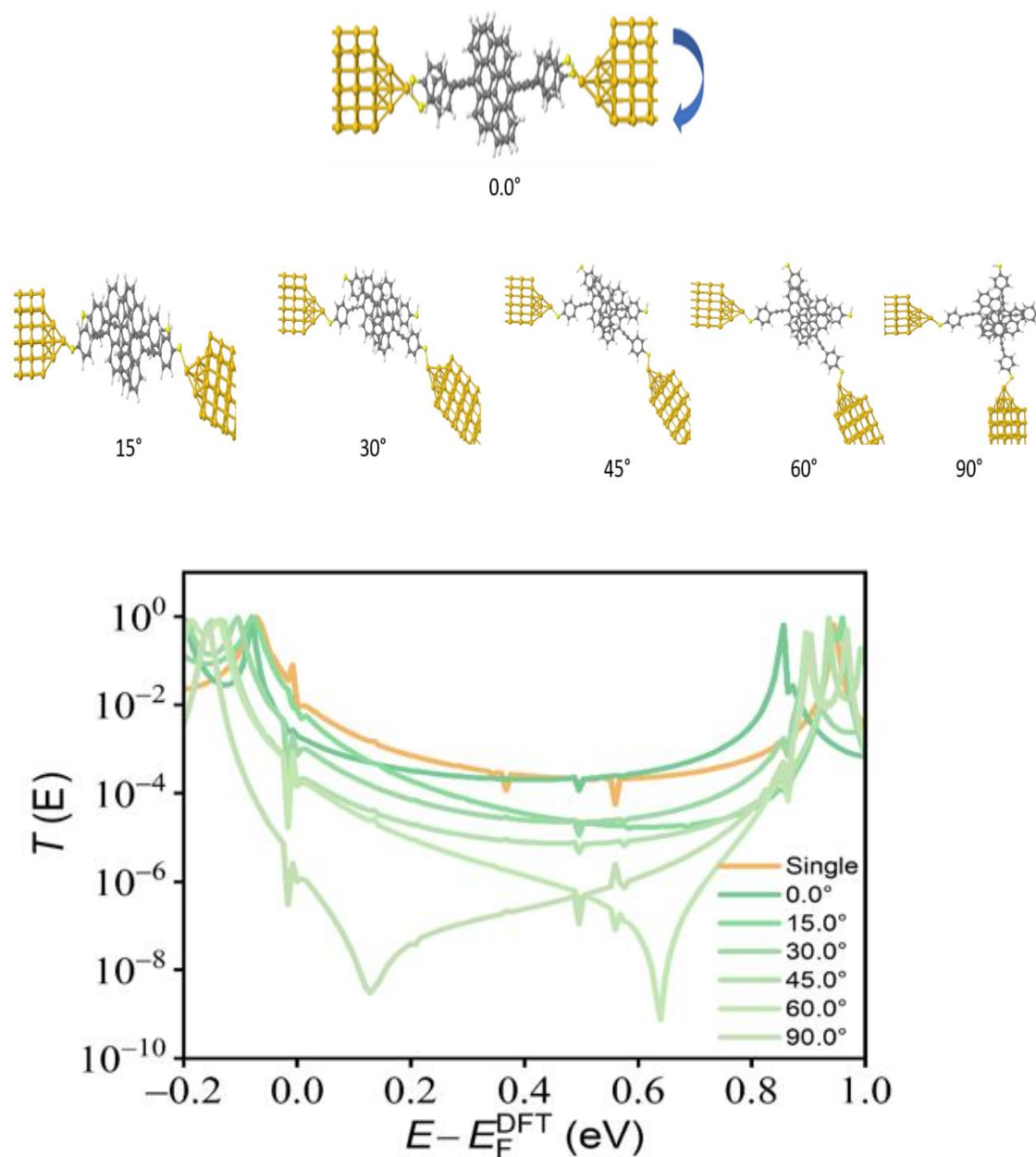


Fig. 5.8 Transmission functions $T(E)$ for AB stacking of the molecule CQI-H corresponding to the different top molecule rotations (0.0° , 15.0° , 30.0° , 45.0° , 60.0° and 90.0° , respectively).

Shifting the top molecule to the right:

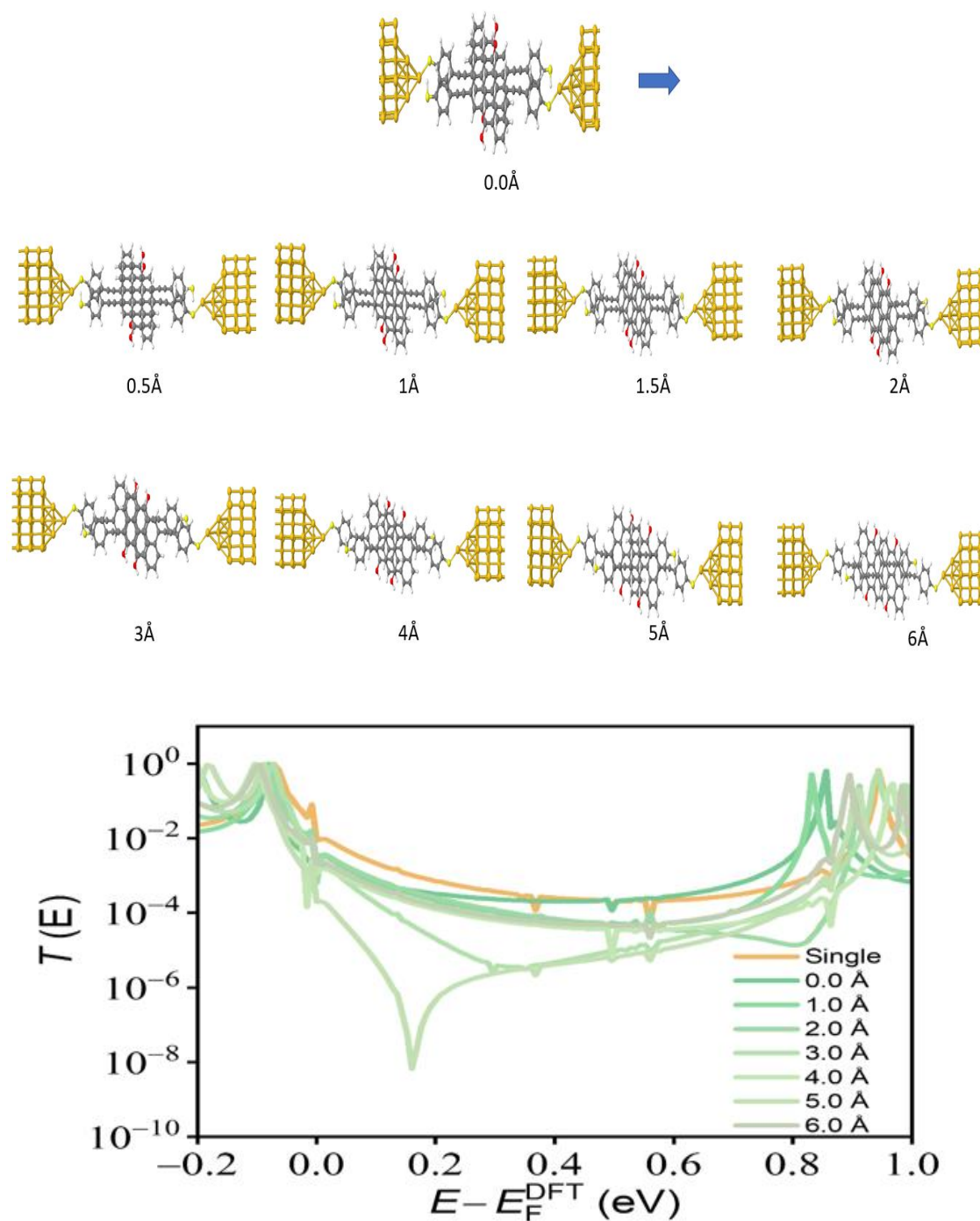


Fig. 5.9 Transmission functions $T(E)$ for AB stacking of the molecule CQI-H corresponding to the different top molecule shifts (right: 0.0 Å, 1.0 Å, 2.0 Å, 3.0 Å, 4.0 Å, 5.0 Å and 6.0 Å, respectively).

5.6 Comparison of DFT results with experimental results for molecule CQI-L

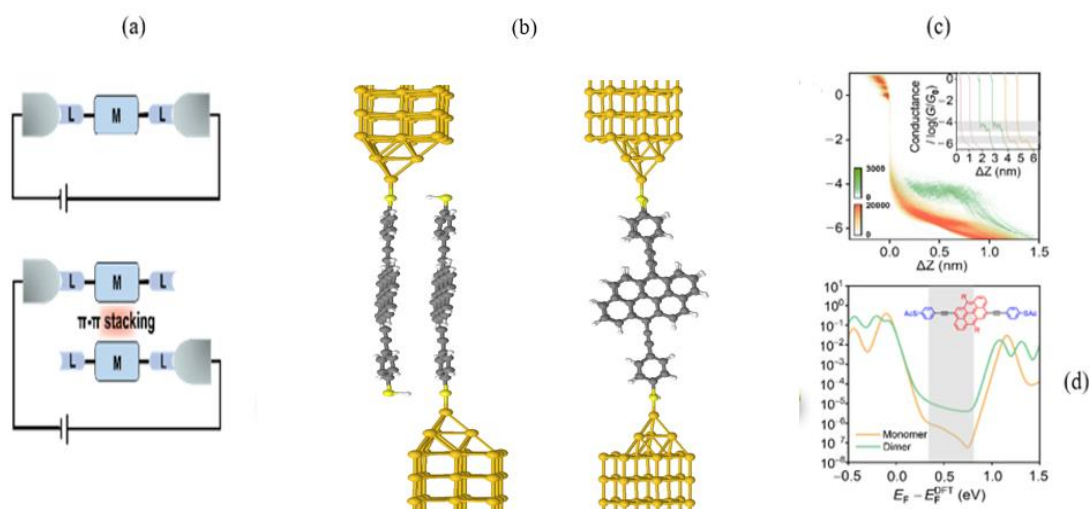


Fig. (5.10) Charge transmission between monomer and dimer molecules as seen in Circuits with monomers (top) and dimers (bottom) are shown schematically in (a). (b) monomer molecule and dimer theoretical transmission spectra. (c) Junction conductance-displacement histograms built from around 4500 individual traces with a bias of 0.1 V. (d) Transmission coefficients regarding the conductance of the monomer (yellow) and dimer (green) of CQI-L molecules.

For organic molecules resembling graphene, the passage of electrical current from one monomer to another in a dimer via pi-pi stacking is seen in (Figures 5.10a) (lower) and (5.10b) (right). The electrical conductance of two identical conductors connected in series is typically lower than that of a monomer conductor (Fig. 5.10a), which is consistent with the idea that two-series resistors typically have lower electrical conductance than a monomer resistor. Accordingly, earlier research showed that a dimer's conductance is typically lower than that of the corresponding monomer, even

when quantum effects are present [3,25,27]. Noting how closely related the conductance mechanism of traditional electrical circuits and the charge transport mechanism of the dimer different. Using a combination of the scanning tunneling microscope break junction (STM-BJ) technique [28-30] and density functional theory (DFT) [31], we examine charge transport through a graphene-like dimer in (Fig. 5.3b). We find that, depending on the QI pattern and stacking configuration, the dimer's conductance can be up to 25 times greater than that of the monomer. Even though other dimer systems also exhibit quantum interference, the conductance of the dimer is typically lower than that of the monomer. For instance, periodic decreases in dimer conductance brought on by mechanically regulated quantum interference have been observed [26] for an oligo-phenylene-ethynylene (OPE3) pi-conjugated molecular system. Our system's anomalous conductance rise also differs from conductance superposition in monomer-molecule circuits with parallel paths [32].

The selected monomer is shown as CQI-L (a constructive QI molecule with a comparatively low conductance) in (Fig. 5.3b) left and is depicted in the inset of (Figs. 5.3d) and 1. Its acetylthiol terminal groups [19], which connect the molecule to external electrodes, are attached to an anthanthrene core, which resembles graphene. As illustrated in (Fig. 5.3d), this CQI-L monomer exhibits CQI as demonstrated in a prior study [20], but with a comparatively low (L) conductance when current is injected and collected via the triple bonds attached to the anthanthrene core. The conductance of a molecular junction is repeatedly measured as a function of tip-substrate displacement using the STM-BJ approach to produce conductance versus displacement traces. In a 1,2,4-trichlorobenzene (TCB) solution, the molecular connections are specifically generated and broken As a result, it is possible for one monomer to bridge the space between the two points or for two separate monomers to bind to different tips, allowing

current to flow from one electrode to the other by pi-pi stacking. The junctions' typical individual traces under 0.1 V of bias are shown in (Fig. 5.10c), inset. It is possible to see the conductance features below G_0 at particular molecular values as well as the features at integer multiples of G_0 ($G_0 = 2 e^2/h$). The pink traces represent the tunneling degradation following the breakage of an Au atomic contact in a pure solvent, whereas the conductance plateaus corresponding to the molecular conductance are detected in solution with the target molecules. To create the conductance histograms, hundreds to thousands of such conductance traces are utilized. A chemical named CQI-L is shown in two-dimensional (2D) conductance-displacement histograms in (Figure 5.10c). The Lorentzian fitting peak can be seen as a low conductance peak at $\sim 2.0 \times 10^{-6} G_0$ (≈ 0.16 nS). This is in line with the conductance that a monomer CQI-L molecule would most likely have, according to earlier research [19]. A second conductance peak, which is more than 25 times greater than the conductance of the monomer, can be seen in addition to this monomer conductance peak at $\sim 5.0 \times 10^{-5} G_0$ (≈ 3.9 nS) (Fig. 5.10c). This improvement is in line with what we predicted theoretically, as illustrated in (Fig. 5.10d). Theoretical simulations shown in (Fig. 5.3d), which plots the conductance versus the Fermi energy E_F (relative to the DFT-predicted Fermi energy E_F^{DFT}) for the monomer (yellow curve) and dimer (green curve), the high conductance state of the molecule CQI-L can therefore be attributed to -stacked dimers (Fig. 5.10b right).

5.7 Comparison of DFT results with experimental results for molecule CQI-H:

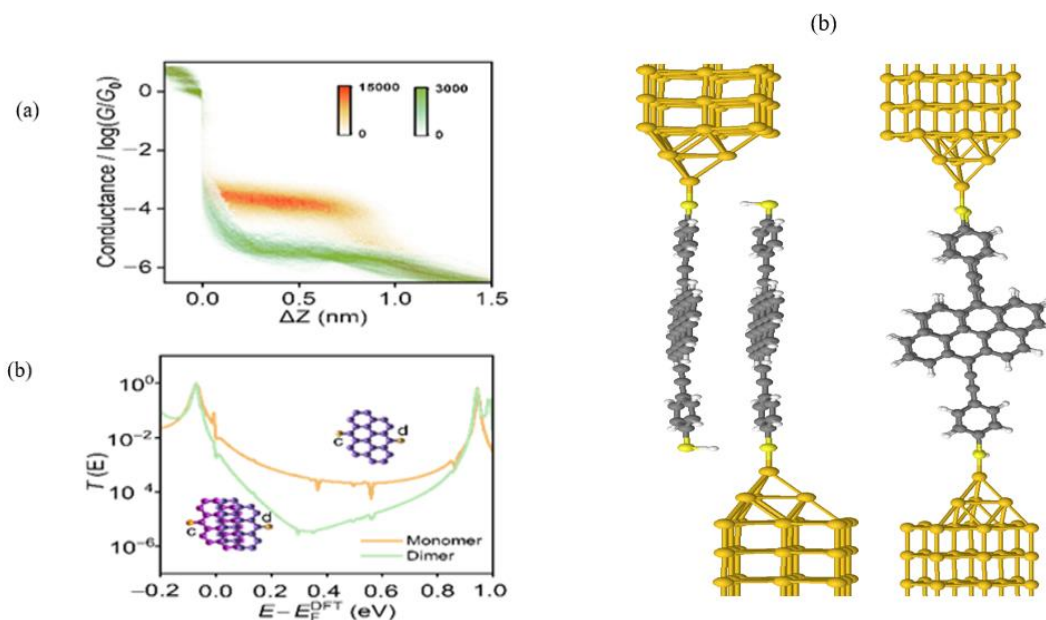


Fig. 5.11: Charge transport of a comparative molecule CQI-H. (a) 2D conductance-displacement histograms for CQI-H at a bias of 0.1 V. The number of counts normalized to the number of curves seen in the histograms is displayed on the color wheel. (b) using the molecule CQI-H as a model, a diagram is shown to show monomer-molecule and dimer connections. (c) monomer molecule and dimer theoretical transmission spectra.

Comparative system's charge transport. By adjusting the connection of the anthanthrene core to the electrodes, it is possible to manage the above-increased conductance of the dimer in comparison to the monomer. Consider the monomer in (Fig. 5.11c) (left), where the triple bonds connect to the locations denoted by the letters c and

d, to demonstrate this property. According to Ref. [20], (Fig. 5.1a-5.1b), this monomer (labeled CQI-H and a constructive QI molecule with a comparatively high conductance) demonstrates CQI and has a greater (H) conductance than the CQI-L monomer of (Fig. 5.1b) (left). In accordance with the theoretical transmission coefficient of (Fig. 5.11b), as well as other studies [20], In contrast to the molecule CQI-L, a second conductance peak that is roughly 40 times smaller than the monomer conductance arises at $\sim 2.5 \times 10^{-6} G_0$ (≈ 0.20 nS), (Fig. 5.11a). In this instance, the dimer conductance is anticipated to be lower than the monomer conductance, as shown by comparison with the mid-gap theoretical transmission curve of the dimer (green curve in Fig. 5.11b). Once more, as the bias voltage is raised, the ratio of the low conductance rises, demonstrating that the high conductance results from the monomer state. This is more proof that the dimer is responsible for the low conductance of the molecule CQI-H and it is in line with the theoretical model in (Fig. 5.11b), which shows that the lower conductance dimer has a longer molecular length than a monomer-molecule. Theoretical calculations reveal that the dimers of the molecule CQI-H with various stacking configurations do not generally exhibit the higher conductance than the monomer due to the lower conductance of the dimer.

5.8 Transmission function calculations of the molecule CQI-L

connecting to the electrodes on both sides:

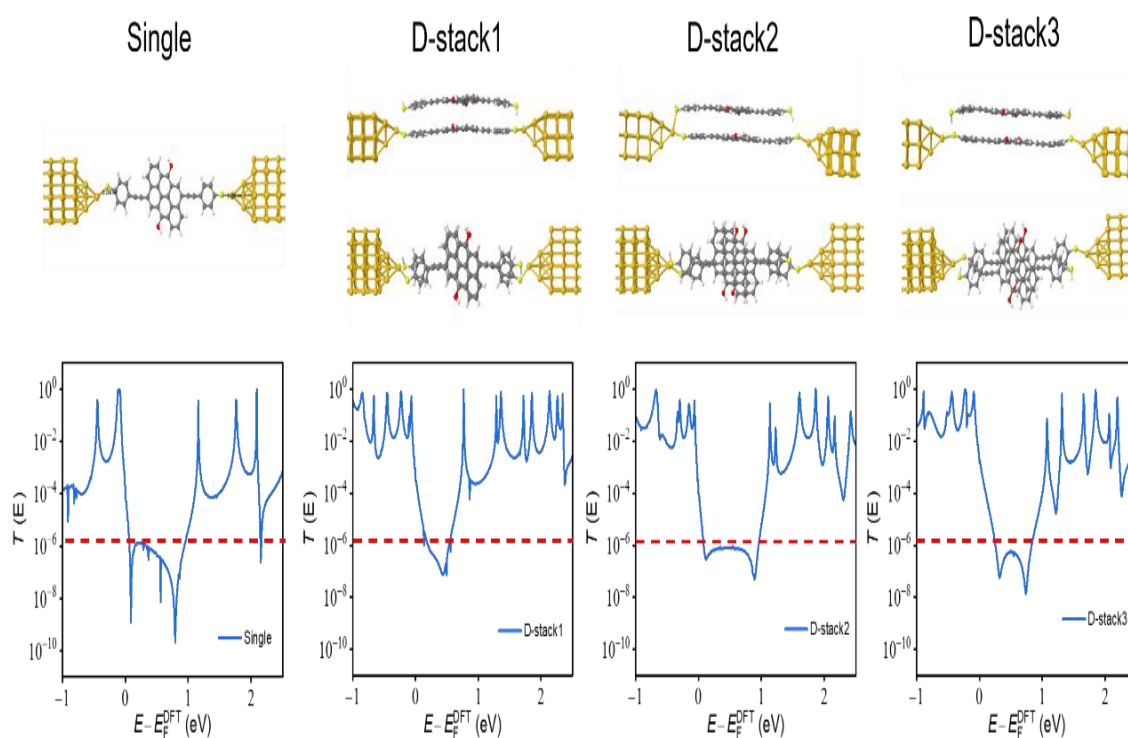


Fig. 5.12: The transmission spectra of the molecule CQI-L, connected to the electrodes on both sides, are examined in the presence of another interacting molecule.

If the monomer connects with electrodes, the scenario changes when another molecule stacks onto the monomer. However, these transmissions or configurations remain constant, as the upper molecule interacts very weakly with the electrode. Consequently, it makes only a minimal contribution to the electrode.

5.9 Conclusion

In conclusion, we have given a combined experimental and theoretical investigation of charge transport in stacked graphene-like dimers and shown that the interaction between room-temperature quantum interference and stacking controls their highly non-classical electrical conductance. The electrical conductance of the dimer for the molecule CQI-L can be 25 times greater than that of the monomer thanks to the most energetically favorable stacking interactions. In contrast, the conductance of the dimer is around 40 times less for the molecule CQI-H than that of the monomer. This demonstrates unequivocally that logical control of connectivity to molecular cores combined with stacking interactions between their systems offers a general route to modify and optimize charge transfer between molecules, which will encourage vigorous research at both macroscopic and microscopic levels.

Bibliography:

- [1] Chen H, Fraser Stoddart J. From molecular to supramolecular electronics. *Nature Reviews Materials* 2021; 6:804-828.
- [2] Madhu M, Ramakrishnan R, Vijay V, Hariharan M. Free Charge Carriers in Homosorted pi-Stacks of Donor-Acceptor Conjugates. *Chem Rev* 2021; 121:8234-8284.
- [3] Li X, Wu Q, Bai J, Hou S, Jiang W, Tang C, Song H, Huang X, Zheng J, Yang Y, Liu J, Hu Y, Shi J, Liu Z, Lambert CJ, Zhang D, Hong W. Structure-Independent Conductance of Thiophene-Based Single-Stacking Junctions. *Angew Chem Int Ed Engl* 2020; 59:3280-3286.
- [4] Kim YH, Zhai Y, Lu H, Pan X, Xiao C, Gaubing EA, Harvey SP, Berry JJ, Vardeny ZV, Luther JM, Beard MC. Chiral-induced spin selectivity enables a room-temperature spin light-emitting diode. *Science* 2021; 371:1129-1133.
- [5] Tu L, Xie Y, Li Z, Tang B. Aggregation-induced emission: Red and near-infrared organic light-emitting diodes. *SmartMat* 2021; 2:326-346.
- [6] Li G, Chang W-H, Yang Y. Low-bandgap conjugated polymers enabling solution-processable tandem solar cells. *Nature Reviews Materials* 2017; 2:1-13.
- [7] Jiye Lee PJ, Philip D. Reusswig, Shane R. Yost, Nicholas J. Thompson, Daniel N. Congreve, Eric Hontz, Troy Van Voorhis, and Marc A. Baldo. Singlet Exciton Fission Photovoltaics. *Acc. Chem. Res.* 2013.
- [8] Chen H, Zhang W, Li M, He G, Guo X. Interface Engineering in Organic Field-Effect Transistors: Principles, Applications, and Perspectives. *Chem Rev* 2020; 120:2879-2949.
- [9] Li P, Jia C, Guo X. Molecule-Based Transistors: From Macroscale to Single Molecule. *Chem Rec* 2021; 21:1284-1299.

- [10] Wang P, Jia C, Huang Y, Duan X. Van der Waals Heterostructures by Design: From 1D and 2D to 3D. *Matter* 2021; 4:552-581.
- [11] Novoselov K, Mishchenko A, Carvalho A, Castro Neto A. 2D materials and van der Waals heterostructures. *Science* 2016; 353:aac9439.
- [12] Liu Y, Huang Y, Duan X. Van der Waals integration before and beyond two-dimensional materials. *Nature* 2019; 567:323-333.
- [13] Wu Q, Sadeghi H, Garcia-Suarez VM, Ferrer J, Lambert CJ. Thermoelectricity in vertical graphene-C(60)-graphene architectures. *Sci Rep* 2017; 7:11680.
- [14] S. Zhao QW, J. Pi, J. Liu, J. Zheng, S. Hou, J. Wei, R. Li, H. Sadeghi, Y. Yang, J. Shi, Z. Chen, Z. Xiao, C. Lambert, W. Hong,. Cross-plane transport in a single-molecule two-dimensional van der Waals heterojunction. *SCIENCE ADVANCES* 2020.
- [15] Stepanov P, Das I, Lu X, Fahimniya A, Watanabe K, Taniguchi T, Koppens FH, Lischner J, Levitov L, Efetov DK. Untying the insulating and superconducting orders in magic-angle graphene. *Nature* 2020; 583:375-378.
- [16] Zondiner U, Rozen A, Rodan-Legrain D, Cao Y, Queiroz R, Taniguchi T, Watanabe K, Oreg Y, von Oppen F, Stern A. Cascade of phase transitions and Dirac revivals in magic-angle graphene. *Nature* 2020; 582:203-208.
- [17] Nuckolls KP, Oh M, Wong D, Lian B, Watanabe K, Taniguchi T, Bernevig BA, Yazdani A. Strongly correlated Chern insulators in magic-angle twisted bilayer graphene. *Nature* 2020; 588:610-615.
- [18] Rozen A, Park JM, Zondiner U, Cao Y, Rodan-Legrain D, Taniguchi T, Watanabe K, Oreg Y, Stern A, Berg E. Entropic evidence for a Pomeranchuk effect in magic-angle graphene. *Nature* 2021; 592:214-219.

- [19] Famili M, Jia C, Liu X, Wang P, Grace IM, Guo J, Liu Y, Feng Z, Wang Y, Zhao Z. Self-assembled molecular-electronic films controlled by room temperature quantum interference. *Chem* 2019; 5:474-484.
- [20] Geng Y, Sangtarash S, Huang C, Sadeghi H, Fu Y, Hong W, Wandlowski T, Decurtins S, Lambert CJ, Liu S-X. Magic ratios for connectivity-driven electrical conductance of graphene-like molecules. *Journal of the American Chemical Society* 2015; 137:4469-4476.
- [21] Valkenier H, Guédon CM, Markussen T, Thygesen KS, van der Molen SJ, Hummelen JC. Cross-conjugation and quantum interference: a general correlation? *Physical Chemistry Chemical Physics* 2014; 16:653-662.
- [22] Guédon CM, Valkenier H, Markussen T, Thygesen KS, Hummelen JC, Van Der Molen SJ. Observation of quantum interference in molecular charge transport. *Nature nanotechnology* 2012; 7:305-309.
- [23] Xiang D, Wang X, Jia C, Lee T, Guo X. Molecular-scale electronics: from concept to function. *Chemical reviews* 2016; 116:4318-4440.
- [24] Lambert CJ. *Quantum Transport in Nanostructures and Molecules: An introduction to molecular electronics*. IoP Publishing; 2021.
- [25] Wu S, González MT, Huber R, Grunder S, Mayor M, Schönenberger C, Calame M. Molecular junctions based on aromatic coupling. *Nature nanotechnology* 2008; 3:569-574.
- [26] Frisenda R, Janssen VA, Grozema FC, Van Der Zant HS, Renaud N. Mechanically controlled quantum interference in individual π -stacked dimers. *Nature chemistry* 2016; 8:1099-1104.

- [27] Solomon GC, Herrmann C, Vura-Weis J, Wasielewski MR, Ratner MA. The chameleonic nature of electron transport through π -stacked systems. *Journal of the American Chemical Society* 2010; 132:7887-7889.
- [28] Liu J, Zhao X, Zheng J, Huang X, Tang Y, Wang F, Li R, Pi J, Huang C, Wang L. Transition from tunneling leakage current to molecular tunneling in single-molecule junctions. *Chem* 2019; 5:390-401.
- [29] Bai J, Daaoub A, Sangtarash S, Li X, Tang Y, Zou Q, Sadeghi H, Liu S, Huang X, Tan Z. Anti-resonance features of destructive quantum interference in single-molecule thiophene junctions achieved by electrochemical gating. *Nature Materials* 2019; 18:364-369.
- [30] Tang C, Chen L, Zhang L, Chen Z, Li G, Yan Z, Lin L, Liu J, Huang L, Ye Y. Multicenter-bond-based quantum interference in charge transport through single-molecule carborane junctions. *Angewandte Chemie* 2019; 131:10711-10715.
- [31] Ferrer J, Lambert CJ, García-Suárez VM, Manrique DZ, Visontai D, Oroszlany L, Rodríguez-Ferradás R, Grace I, Bailey S, Gillemot K. GOLLUM: a next-generation simulation tool for electron, thermal and spin transport. *New Journal of Physics* 2014; 16:093029.
- [32] Vazquez H, Skouta R, Schneebeli S, Kamenetska M, Breslow R, Venkataraman L, Hybertsen M. Probing the conductance superposition law in single-molecule circuits with parallel paths. *Nature Nanotechnology* 2012; 7:663-667.
- [33] Adak O, Rosenthal E, Meisner J, Andrade EF, Pasupathy AN, Nuckolls C, Hybertsen MS, Venkataraman L. Flicker noise as a probe of electronic interaction at metal–single molecule interfaces. *Nano letters* 2015; 15:4143-4149.

- [34] Garner MH, Li H, Chen Y, Su TA, Shangguan Z, Paley DW, Liu T, Ng F, Li H, Xiao S. Comprehensive suppression of single-molecule conductance using destructive σ -interference. *Nature* 2018; 558:415-419.
- [35] Tang Y, Zhou Y, Zhou D, Chen Y, Xiao Z, Shi J, Liu J, Hong W. Electric field-induced assembly in single-stacking terphenyl junctions. *Journal of the American Chemical Society* 2020; 142:19101-19109.
- [36] Kamenetska M, Koentopp M, Whalley A, Park Y, Steigerwald M, Nuckolls C, Hybertsen M, Venkataraman L. Formation and evolution of single-molecule junctions. *Physical review letters* 2009; 102:126803.
- [37] Sangtarash S, Huang C, Sadeghi H, Sorohhov G, Hauser Jr, Wandlowski T, Hong W, Decurtins S, Liu S-X, Lambert CJ. Searching the hearts of graphene-like molecules for simplicity, sensitivity, and logic. *Journal of the American Chemical Society* 2015; 137:11425-11431.
- [38] Markussen T, Stadler R, Thygesen KS. The relation between structure and quantum interference in single molecule junctions. *Nano letters* 2010; 10:4260-4265.
- [39] Lambert CJ, Liu SX. A magic ratio rule for beginners: a chemist's guide to quantum interference in molecules. *Chemistry—A European Journal* 2018; 24:4193-4201.
- [40] Yoshizawa K. An orbital rule for electron transport in molecules. *Accounts of chemical research* 2012; 45:1612-1621.
- [41] Soler JM, Artacho E, Gale JD, García A, Junquera J, Ordejón P, Sánchez-Portal D. The SIESTA method for ab initio order-N materials simulation. *Journal of Physics: Condensed Matter* 2002; 14:2745.

6. Conclusions and Future works

6.1. Conclusions

In this thesis, electrical properties diverse molecular devices have been thoroughly examined through several methodologies. Chapter 2 introduces the application of density functional theory and the Green's function scattering formalism to analyze these properties. Furthermore, in Chapter 3, a straightforward tight-binding approach is employed to explore the underlying concepts.

In the chapter 4, it is proposed that a tight-binding theory, which involves a single level per atomic site, can effectively capture the qualitative aspects of both DFT calculations and laboratory studies concerning transport through related molecular cores. This holds true as long as the linkers solely consist of a single pi system. On the other hand, when the linkers possess more than one pi system, the tight-binding model needs to be enhanced in complexity by assigning multiple levels to each atomic site. This adjustment is necessary to accurately account for the additional intricacies introduced by multiple pi systems in the linkers.

In chapter 5, I conducted a comprehensive investigation, combining experimental and theoretical approaches, to explore charge transport in stacked graphene-like dimers. My findings reveal that the interplay between room-temperature quantum interference and stacking interactions plays a pivotal role in governing their profoundly non-classical electrical conductance. For the specific molecule CQI-L, the electrical conductance of the dimer surpasses that of the monomer by an impressive factor of 25, thanks to the favorable stacking interactions that occur energetically. Conversely, the molecule CQI-H exhibits a dimer conductance that is approximately 40 times lower than that of the monomer. This

compelling evidence indicates that by strategically controlling the connectivity to molecular cores while considering their stacking interactions, we can create a versatile approach to modify and optimize charge transfer between molecules. These findings are expected to inspire vibrant research efforts at both macroscopic and microscopic scales.

6.2. Future works

In my research work, I delved into exploring the electrical conductance of various molecules connected to gold electrodes. Looking ahead, there are certain aspects that warrant deeper investigation. One crucial aspect involves understanding the connectivity effects on quantum transport through the polycyclic aromatic molecules, considering different aromatic rings. [1] Specifically, I am intrigued by examining the impact of substituting SMe with alternative anchor groups like amino (NH₂), direct carbon-gold (C), and thiol (S) bonds in relation to the electrodes [2,3]. These inquiries open up promising avenues for future studies. In recent developments, researchers have been exploring alternative electrode materials for molecular electronics, particularly the use of graphene electrodes. This intriguing avenue offers promising possibilities for various projects. However, it's important to address certain challenges, such as the need for novel anchor groups to ensure a coherent electron transport at the molecule-graphene interface. Nevertheless, due to graphene's exceptional properties, it presents itself as an excellent candidate for an electrode material in the field of molecular electronics.[8][15].

In the realm of molecular electronics, there remain intriguing and significant questions that require exploration. One such query pertains to how chemical modifications of molecules and electrodes can lead to profound changes in their electrical properties. Additionally, investigating the impact of alternative electrode materials on molecular electronics, like graphene, silicene , platinum and, palladium [16,17], or even

superconducting electrodes [14][15], is highly valuable, as they introduce novel interference effects. These avenues hold great promise for future research and the development of extraordinary and unprecedented molecular-scale devices. For instance, graphene stands out due to its remarkable properties and diverse potential applications, such as sensing applications [13]. Its unique characteristics, including a simplified metal-molecule interface, a wide electrochemical potential window, low electrical resistance, and well-defined redox peaks, enhance sensitivity [14]. Moreover, graphene's high thermal conductivity makes it an attractive material for managing and dissipating heat in high-density devices. In the field of nanoelectronics, another intriguing topic is the study of hybrid systems that incorporate superconducting (S) and ferromagnetic (F) materials, particularly for their relevance in spintronics applications. Spintronic devices capitalize on spin-polarized currents and magnetic fields, which both influence superconducting transport. These investigations open up exciting possibilities for advancing technology and understanding novel electronic phenomena [19].

In this particular study in Chapter 5, it would be valuable to explore the π -stacking phenomenon among these molecules in greater depth. Understanding the electron transport mechanisms and how different configurations influence quantum interference (QI) [4][6] is essential. When parallel π -stacked molecular systems exhibit weak interactions, they may display low conductance due to destructive interference. Interestingly, this reduction in conductance could potentially lead to increased thermopower. Additionally, investigating the impact of various metal ions trapped in the complex, such as Zn, Fe, Cu, Co, Ni, and Mn, is of utmost significance, as charge transport depends not only on the ligand nature but also on the type of metal ion present. The choice of metal atom can tune the molecular energy levels relative to the Fermi energy of the electrodes [7]. It would be intriguing to calculate the charge transfer of these

different metal elements and explore how the electron transfer between the metal and the molecular backbone affects transmission and Seebeck behaviors. Furthermore, the presence of palladium attached to two Cl atoms allows the application of a reduction process by removing both Cl atoms. This process might shift the position of the electrode Fermi energy closer to the Fano resonance, potentially leading to further enhancement in conductance. These investigations hold significant promise for advancing our understanding of electron transport and behavior in the studied molecular systems [7].

Finally, this thesis has focussed on QI in electronic systems. However, interference is a generic property of waves and therefore it would be interesting to explore these ideas to molecular-scale and meso-scale vibrational properties [23]. Such a study would be particularly timely, because it has only recently become possible to measure the thermal conductance of a single molecule [24].

Bibliography:

- [1] C. J. Lambert, *Quantum Transport in Nanostructures and Molecules*. IOP Publishing, (2021).
- [2] F. Chen, X. Li, J. Hihath, Z. Huang, and N. Tao, “Effect of anchoring groups on single-molecule conductance: Comparative study of thiol-, amine-, and carboxylic-acid-terminated molecules,” *J. Am. Chem. Soc.*, 128, (49), 15874–15881, (2006).
- [3] Al-Khaykane, M.K., Ismael, A.K., Grace, I. and Lambert, C.J., Oscillating Seebeck coefficients in π -stacked molecular junctions. *RSC Advances*, 8(44), 24711-24715, (2018).
- [4] Shen, P., Huang, M., Qian, J., Li, J., Ding, S., Zhou, X.S., Xu, B., Zhao, Z. and Tang, B.Z., Achieving efficient multichannel conductance in through-space conjugated single-molecule parallel circuits. *Angewandte Chemie*, 132(11), 4611-4618, (2020).
- [5] Markin, A., Ismael, A.K., Davidson, R.J., Milan, D.C., Nichols, R.J., Higgins, S.J., Lambert, C.J., Hsu, Y.T., Yufit, D.S. and Beeby, A., Conductance Behavior of Tetraphenyl-Aza-BODIPYs. *The Journal of Physical Chemistry C*, 124(12), 6479-6485, (2020).

- [6] Al-Galiby, Q.H., Sadeghi, H., Algharagholy, L.A., Grace, I. and Lambert, C., Tuning the thermoelectric properties of metallo-porphyrins. *Nanoscale*, 8(4), 2428-2433, (2016).
- [7] Lu, Y., Merchant, C.A., Drndic, M. and Johnson, A.C., In situ electronic characterization of graphene nanoconstrictions fabricated in a transmission electron microscope. *Nano Letters*, 11(12), 5184-5188, (2011).
- [8] S. Bailey, D. Visontai, C. J. Lambert, M. R. Bryce, H. Frampton, and D. Chappell, “A study of planar anchor groups for graphene-based single-molecule electronics,” *J. Chem. Phys.*, 140, 5, (2014).
- [9] Barreiro, A., Borrnert, F., Rummeli, M.H., Buchner, B. and Vandersypen, L.M., Graphene at high bias: Cracking, layer by layer sublimation, and fusing. *Nano Letters*, 12(4), 1873-1878, (2012).
- [10] X.H. Zheng, G.R. Zhang, Z. Zeng, V.M. García-Suárez, C.J. Lambert, Effects of antidots on the transport properties of graphene nanoribbons. *Phys. Rev. B* 80 (7), 075413, (2009).
- [11] Q. Wu, H. Sadeghi, V. M. García-Suárez, J. Ferrer, and C. J. Lambert, “Thermoelectricity in vertical graphene-C60-graphene architectures,” *Sci. Rep.*, 7, 11680, (2017).
- [12] M. Pykal, P. Jurečka, F. Karlický, and M. Otyepka, “Modelling of graphene functionalization,” *Phys. Chem. Chem. Phys.*, 18, (9), 6351–6372, (2016).

- [13] M. S. Artiles, C. S. Rout, and T. S. Fisher, "Graphene-based hybrid materials and devices for biosensing," *Advanced Drug Delivery Reviews.*, 63, (14-15), 1352- 1360, (2011).
- [14] C.G. Peterfalvi, L. Oroszlany, C.J. Lambert and J. Cserti, Intraband electron focusing in bilayer graphene, *New J. Phys* 14 063028 (2012).
- [15] V. M. García-Suárez, A. R. Rocha, S. W. Bailey, C. J. Lambert, S. Sanvito, and J. Ferrer, "Single-channel conductance of H₂ molecules attached to platinum or palladium electrodes," *Phys. Rev. B*, 72, (4,) 45437, (2005).
- [16] VM García-Suárez, AR Rocha, SW Bailey, CJ Lambert, S Sanvito, J Ferrer, Conductance oscillations in zigzag platinum chains. *Phys. Rev. Lett.* 95 (25), 256804, (2005).
- [17] CJ Lambert, R Raimondi, V Sweeney, AF Volkov, "Boundary conditions for quasiclassical equations in the theory of superconductivity," *Phys. Rev. B* 55 (9), 6015, (1997).
- [18] M. Eschrig, A. Cottet, W. Belzig, and J. Linder, "General boundary conditions for quasiclassical theory of superconductivity in the diffusive limit: Application to strongly spin-polarized systems," *New J. Phys.*, 17, 8, (2015).
- [19] NR Claughton, M Leadbeater, CJ Lambert, Theory of Andreev resonances in quantum dots. *J. Phys.: Condensed Matter* 7 (46), 8757 (1995).

[20] N. L. Plaszkó, P. Rakyta, J. Cserti, A. Kormányos, and C. J. Lambert , Quantum interference and non-equilibrium Josephson current in molecular Andreev interferometers. *Nanomaterials* 10 1033 (2020).

[21] P. Rakyta, A. Alanazy, A. Kormányos, Z. Tajkov, G. Kukucska, J. Koltai, S. Sangtarash, H. Sadeghi, J. Cserti and C.J. Lambert, Magic number theory of superconducting proximity effects and Wigner delay times in graphene-like molecules. *J. Phys. Chem C.* 123 6812 (2019) .

[22] A Kambili, G Fagas, VI Fal'ko, CJ Lambert, Phonon-mediated thermal conductance of mesoscopic wires with rough edges. *Phys. Rev. B-Condensed Matter* 60 (23), 15593-15596 (1999).

[23] N. Mosso, H. Sadeghi, A. Gemma, S. Sangtarash, C. Lambert, and B. Gotsmann, Thermal transport through single molecule junctions. *Nanoletters* 19 (11) 7614-7622 (2019).